Cross-Layer Design and Optimization of OFDMA-based Cognitive Radio Networks

Saki, Hadi

Awarding institution:
King's College London

Cross-Layer Design and Optimization of OFDMA-based Cognitive Radio Networks

Hadi Saki

Centre for Telecommunications Research (CTR)

King's College London

A DISSERTATION PRESENTED TO THE GRADUATE SCHOOL OF KING'S COLLEGE LONDON, IN PARTIAL FULFILMENT OF THE REQUIREMENTS FOR THE DEGREE OF

Doctor of Philosophy

March 2014

When you do things from your soul, you feel a river moving in you,

a joy.

Rumi

Acknowledgements

Above all, I would like to thank my wonderful family. It is extremely difficult to express how much love I feel for my Mother, Father, brothers and my sisters. They supported me in every possible way and in every single moment during these years and they were always beside me although they were so many thousand miles away. I would like to express my gratitude to my supervisor Dr. Mohammad Shikh-Bahaie, in which his limitless patience, guidance, and support provided a conducive atmosphere for learning. His vast knowledge, and charisma were essential to the progress of my project. The consideration, support and friendship of my second supervisor, Prof. Hamid Aghvami, have been invaluable on both personal and academic life, for which I am extremely grateful. I am very much thankful to the examiners for their deep and constructive comments and suggestions. My sincere thanks to Prof. M. Dohler and Dr. O. Holland, for their valuable time. The author would like to thank Dr. P. Anker, Senior Policy advisor Frequency management at Ministry of Economic Affairsand, and Dr. A. Medeisis, Chair of COST ActionIC0950 "TERRA". Their comments and suggestions that significantly improved the quality of this research. I greatly benefited from the ACROPOLIS cognitive wireless communications summer school. My sincere thanks goes to Dr. A. Shojaeifard and Dr. J.Hwang, with whom I collaborated in some studies. I would like to express my thanks to the students and staff at the Institute of Telecommunications (IOT), in particular, Mohammad Mirtavoosi, Krishna, Merat, Nur Abdul, Mojdeh, Vahid, Hossein, Alexandre, Shabnam, Ehsan, Wataru, Helen, and Nicola.

Abstract

Increasing demand and sophistication of wireless applications require intelligent systems which, along with performing efficient and reliable adaptive operations, should be simple to implement. Cognitive radio (CR) is one such system which has the capability of adapting to its surroundings. In this thesis, the role of different layers of network in carrying out the functionalities of CR systems is investigated and cross-layer design strategies involving the physical (PHY), the media access control (MAC), and the application are proposed. This thesis makes several contributions.

Firstly, we propose novel optimal radio resource allocation (RRA) algorithms under different scenarios with deterministic and probabilistic interference violation limits based on perfect and imperfect availability of cross-link channel state information (CSI). In particular, in contrast to the 'average case' and 'worst case' estimation error scenarios in the literature, we propose a probabilistic approach to mitigate the total imposed interference on the primary service under imperfect cross-link CSI. An expression for the cumulative density function (cdf) of the received signal-to-interference-plus-noise ratio (SINR) is developed to evaluate the average spectral efficiency. Through simulation results, we investigate the achievable performance and the impact of parameters uncertainty on the overall system performance.

Secondly, we implement stochastic RRA algorithms in both hybrid- (i.e., mixed underlay and overlay) and opportunistic (i.e., overlay) access orthogonal frequency-division multiple access (OFDMA)-based CR systems. The proposed solutions allocate power and subcarrier to cognitive users over wireless fading channels in order to maximize the total transmission rate based on the probabilities of channel availability obtained through spectrum sensing. In order to protect the primary service operation from harmful intervention, stochastic transmit and interference power constrains are imposed on the cognitive users. The performance of the proposed stochastic algorithms and their advantages over the conventional hard-decision-based approaches are assessed and demonstrated through simulation results.

Finally a specific cross-layer design for multi scalable video application transmission in an interference-limited spectrum sharing system is proposed. The proposed design jointly considers the parameters from the PHY and the application layers in order to maximize the overall peak signal-to-noise ratio (PSNR). Results indicate that significant improvement in secondary receivers (SRxs) average video quality is achieved through our proposed algorithm over other state-of-the-art non-quality-aware (NQA) designs in the literature. The enhanced performance was obtained whilst guaranteeing SRx minimum quality and primary receiver (PRx) prescribed quality of service (QoS) constraints.

Table of Contents

References 147

Author's Publications

[1] **H. Saki**, A. Shojeifard, M. M. Mahyari, and M. Shikh-Bahaei, "On the Ergodic Rate of OFDMA Cognitive Radios under Imperfect Cross-Link Information," *IEEE Consumer Communications and Networking Conference (CCNC 2014), 2014 IEEE*, pp. 1-6, Jan. 2014.

[2] **H. Saki**, A. Shojeifard, and M. Shikh-Bahaei, "Cross-Layer Resource Allocation for Video Streaming over OFDMA Cognitive Radio Networks with Imperfect Cross-Link CSI," *International Conference on Computing, Networking and Communications (ICNC 2014), 2014 IEEE*, pp. 1-6, Feb. 2014.

[3] A. Shojeifard, **H. Saki**, M. M. Mahyari, and M. Shikh-Bahaei, "Cross-Layer Radio Resource Allocation for Multi-Service Networks of Heterogeneous Traffic," *International Conference on Computing, Networking and Communications (ICNC 2014), 2014 IEEE*, pp. 1-7, Feb. 2014.

[4] **H. Saki**, A. Shojeifard, and M. Shikh-Bahaei, "Stochastic Resource Allocation for OFDMA-Based Cognitive Radios with Hybrid Spectrum Access," *IEEE Wireless Communications and Networking Conference (WCNC 2014), 2014 IEEE*, pp. 1-5, Apr. 2014.

[5] J. Hwang, **H. Saki**, and M. Shikh-Bahaei, "Adaptive Modulation and Coding and Cooperative ARQ in a Cognitive Radio System," *IEEE Wireless Communications and Networking Conference (WCNC 2014), 2014 IEEE*, pp. 1-5, Apr. 2014.

[6] A. Shojeifard, **H. Saki**, M. M. Mahyari, and M. Shikh-Bahaei, "Resource Allocation and Interference Management for Adaptive Modulation and Coding-based OFDMA Cognitive Radio Networks," *IEEE International Conference on Communications (ICC 2014), 2014 IEEE*, pp. 1-6, Jun. 2014.

Submitted paper

[1] **H. Saki**, and M. Shikh-Bahaei, "Quality-Aware Resource Allocation for Scalable Video transmission over Cognitive Radio Networks," *IEEE Global Communications Conference (GLOBECOM 2014), 2014 IEEE, under review*, pp. 1-6, Jun. 2014.

[2] **H. Saki**, and M. Shikh-Bahaei, "Cross-Layer Resource Allocation for Video Streaming over Adaptive MQAM/OFDMA Cognitive Radio Networks," *IEEE Trans. Multimedia, submitted in Feb. 2014*, pp. 1-10, Feb. 2014.

[3] **H. Saki**, A. Shojeifard and M. Shikh-Bahaei, "Spectral Efficiency of Adaptive MQAM/OFDMA Cognitive Radio Networks," *IEEE Trans. Veh. Technol, Submitted in Feb. 2014*, pp. 1-15, Feb. 2014.

[4] **H. Saki**, A. Shojeifard and M. Shikh-Bahaei, "Ergodic Rate of OFDMA Cognitive Radios under Imperfect Cross-Link Knowledge," *IEEE Trans. Veh. Technol, submitted in Mar. 2014*, pp. 1-7, Mar. 2014.

[5] J. Hwang, **H. Saki**, and M. Shikh-Bahaei, "Joint Design of Adaptive Modulation and Coding and Cooperative ARQ in a Cognitive Radio System," *IEEE Trans. Wireless Commun., submitted in Feb. 2014*, pp. 1-7, Feb. 2014.

List of Figures

List of symbols

Δf ..... Spacing between subcarriers of OFDM
$\phi_k(t)$ ..... Carrier signal
K ..... Number of subcarriers
T_s ..... Symbol duration
X_k ..... Transmitted symbol
f_c ..... Carrier frequency
T ..... Orthogonality duration
$\tilde{s}(t)$ ..... OFDM output signal
$s(t)$ ..... Bandpass signal
$s_b(t)$ ..... Baseband-equivalent signal
$u_T(t)$ ..... Shaping function
$h_a(t)$ ..... Rectangular shaping function
$\epsilon(t)$ ..... Shaping error function
$y(t)$ ..... Received signal
$a_i(t)$ ..... Attenuation over path i
$\phi_i(t)$ ..... Phase shift over path i
$\tau_i(t)$ ..... Propagation delay over path i
$s(t)$ ..... transmitted signal
$\nu_i(t)$ ..... Additive white Gaussian noise
$h(t, \tau)$ ..... Impulse response mobile radio channel
γ ..... Signal-to-noise-ratio
$\bar{\gamma}$ ..... Average signal-to-noise-ratio
$f(.)$ ..... Probability density function
$\Gamma(.)$ ..... Complete Gamma function
N ..... Number of secondary receivers
M ..... Number of primary receivers
B ..... Total bandwidth
$H_{n,k}^{ss}$ ..... Channel gain from secondary transmitter to secondary receiver
$H_{n,k}^{ps}$ ..... Channel gain from primary transmitter to secondary receiver
$H_{m,k}^{sp}$ ..... Channel gain from secondary transmitter to primary receiver
$\gamma_{n,k}(t)$ ..... instantaneous received SINR
$P_{n,k}$ ..... Transmit power of the k^{th} subcarrier and n^{th} secondary receiver
σ_n^2 ..... Noise power
$\sigma_p^2 s$ .. Received power on the secondary receiver from primary transmitter
$\hat{H}_{m,k}^{sp}$ .. Channel estimation from secondary transmitter to primary receiver
$\Delta H_{m,k}^{sp}$ ..... Channel estimation error from secondary transmitter to primary receiver
$\delta_{\Delta H_{m,k}^{sp}}^2$ ..... Channel estimation error variance
$\delta_{H_{m,k}^{sp}}^2$ ..... Channel error variance
$\delta_{\hat{H}_{m,k}^{sp}}^2$ ..... Channel estimation variance
ρ .. Correlation between the estimated channel and the estimation error
I_{th}^m ..... Maximum tolerable interference at m^{th}primary receiver
$\varphi_{n,k}(\gamma_{n,k})$ ..... Time-sharing factor

ϵ^m ..... Collision probability
$\mathscr{P}(.)$ ..... Probability
$E_x(.)$ ..... Expectation
P_t ..... Total average power
$\xi^b_{n,k}$ Instantaneous BER of the k^{th} subcarrier of the n^{th} secondary receiver
$M_{n,k}$ ..... MQAM constellation size of the k^{th} subcarrier of the n^{th} SU
$F_{\gamma_{n,k}}(\Gamma)$ ..... Cumulative distribution function of received SINR
$f_{\gamma_{n,k}}(\Gamma)$ ..... Probability density function of received SINR
$Q(.)$ ..... Q function
λ_k ..... Lagrange multiplier
μ ..... Lagrange multiplier
η ..... Lagrange multiplier
τ_1^i ..... Subgradient step size
τ_2^i ..... Subgradient step size
pr ..... Worst case bound
$\mathscr{P}^f_{n,k}$ ..... False-alarm probability
$\mathscr{P}^d_{n,k}$ ..... Detection probability
$\mathscr{P}(\mathscr{H}^i_{n,k})$ ..... Probability that the band is idle
$\mathscr{P}(\mathscr{H}^b_{n,k})$ ..... Probability that the band is busy
$\epsilon_{n,k}$ ..... Decision threshold
R ..... Transmission rate
$P^I_{n,k}$ ..... Transmit power when the band is detected as idle
$P^B_{n,k}$ ..... Transmit power when the band is detected as busy
$\varphi^I_{n,k}$ ..... Time-sharing factor when the band is detected as idle
$\varphi^B_{n,k}$ ..... Time-sharing factor when the band is detected as busy
$I_{m,t}$ Total interference caused by secondary transmitter of the m_{th} primary receiver
L ..... Number of SVC layers
$|S|$ ..... Number of spatial layers
$|T|$ ..... Number of temporal layers
$|Q|$ ..... Number of quality layers
$PSNR^l_n$ ..... PSNR of the l^{th} layer of the n^{th} SVC secondary user
U_n ..... Total layers PSNR of the n^{th} SVC secondary user
$\Delta PSNR^l_n$ ..... PSNR increase of the n^{th} SVC secondary user by l^{th} layer
ΔR^l_n ..... Rate increase of the n^{th} SVC secondary user by l^{th} layer
$r^c_{n,k}$ ..... k^{th} subcarrier of the n^{th} secondary receiver coding rate
P_{max} ..... Maximum possible power
π ..... Ordered normalized minimum required rate set
R^t_n ..... n^{th} secondary receiver maximum achivable rate
$\Re_n$ .... Normalized quality improvement set of the n^{th} secondary receiver
Φ^l_n . Normalized quality improvement of the l^{th} level of the n^{th} secondary receiver
$\mathbb{E}$ Sorted set of secondary users quality improvement in descending order
$\mathbb{Z}$ ..... Subcarrier allocation policy set
$\mathbb{PZ}$ ..... Power allocation policy set

Abbreviations

2G	2^{nd} generation
3G	3^{rd} generation
3GPP	3^{rd} generation partnership project
4G	4^{th} generation
AASE	Aggregate average spectral efficiency
AMC	Adaptive modulation and coding
AMPS	Advanced mobile phone service
ARQ	Automatic repeat request
AWGN	Additive white Gaussian noise
BER	Bit-error-rate
BICM	Bit interval coded modulation
BPSK	Binary phase shift keying
BS	Base station
cdf	Cumulative distribution function
CDMA	Code division multiple access
CFO	Carrier-frequency offset
CGS	Coarse grain scalability
CIF	Common intermediate format
CINR	Channel-to-noise-plus-interference ratio
CLT	Central limit theorem
CNR	Carrier-to-noise ratio
CP	Cyclic prefix
CR	Cognitive radio
CRC	Cyclic redundancy check
CSI	Channel state information
CSMA	Carrier sense multiple access

CU	Cognitive user
DLL	Data link layer
DSM	Dynamic spectrum management
FCC	Federal communications commission
FDM	Frequency division multiplexing
FDMA	Frequency division multiple access
FEC	Forward error correction
FFT	Fast Fourier transform
FGS	fine grain scalability
GSM	Global system for mobile communications
GPRS	General packet radio service
HF	High frequency
HPA	High power amplifier
HSA	Hybrid spectrum access
i.i.d.	Independent and identically distributed
ICS	Intermediate control server
ICI	Inter-carrier interference
IDFT	Inverse discrete Fourier transform
IFFT	Inverse fast Fourier transform
i.i.d.	Independent and identically distributed
ISI	Inter-symbol interference
JSVM	Joint scalable video model
KKT	Karush-Kuhn-Tucker
LOS	Line of sight
LTE	Long term evolution
M2M	Machine-to-machine
MAC	Medium access control
MCM	Multi-carrier modulation

MDCNLP	mixed discrete-continuous non-linear programing
MGS	Medium grain scalability
MIMO	Multiple-input multiple-output
NAL	Network abstraction layer
NMT	Nordic mobile telephony
NQA	Non-quality-aware
OFDM	Orthogonal frequency division multiplexing
OFDMA	Orthogonal frequency division multiple access
OSA	Opportunistic spectrum access
OSI	Open systems interconnection
PAPR	Peak-to-average-power ratio
pdf	Probability density function
PER	Packet error rate
PHY	Physical
PRx	Primary receiver
PSD	Power spectral density
PSNR	Peak signal-to-noise ratio
PSK	Phase shift keying
PTx	Primary transmitter
PU	Primary user
Q-R	Quality-rate
QA	Quality-aware
QAM	Quadrature amplitude modulation
QCIF	Quarter common intermediate format
QoE	Quality of experience
QoS	Quality of service
QPSK	Quadrature phase-shift keying
Ofcom	Office of communications

OSI	Open systems interconnection
ROC	Receiver operating characteristic
RRA	Radio resource allocation
RRM	Radio resource management
RTP	Real-time transport protocol
SC	Small-cell
SDC	Space diversity combining
SIR	Signal-to-interference ratio
SINR	Signal-to-interference-and-noise ratio
SMS	Short messaging services
SNR	Signal-to-noise ratio
SRx	Secondary receiver
STx	Secondary transmitter
SU	Secondary user
SVC	Scalable video coding
TACS	Total access communication system
TCP	Transport control protocol
TDM	Time division multiplexing
TDMA	Time division multiple access
UEP	Unequal error protection
UMTS	Universal mobile telecommunications system
USA	Underlay spectrum access
VNI	Visual networking index
WSD	White space devices

Chapter 1

Introduction and Overview

1.1 Evolution of Wireless Communications

In the beginning, man resorted to shouting to make himself heard beyond the immediate surroundings. Then, as now the human voice could only carry so far. Later, when people learn to master fire, they used signal fires, placing them on the hilltop or other clearly visible landmarks. In the 18th century, the optical telegraph made it possible to send coded messages for the average distance of around 10 km but could be up to three times that across the waters. Samuel Morse was originally an American artist who was to become famous for his electrical alphabet. In 1835, he presented the world first commercial telegraph. In 1867, James Clark Maxwell, a professor of Natural Philosophy at King's College London, developed the relation between electricity and magnetism, inspired by the earlier experimental work of Michael Faraday, and predicted the existence of electromagnetic waves, later discovered by Hertz in 1887. At the end of the 19th century, Italian inventor, Guglielmo Marconi invented wireless signalling [1]. By 1901, he managed to transmit a Morse-coded message across the Atlantic. In 1906 the first International Radiotelegraph Convention was signed during the International Radiotelegraph Conference (Berlin, 1906). In addition to the service regulations and final protocol, it was also decided that priority should be given to the SOS distress Morse signal (...- - -...) [2]. A real breakthrough in radio came in the same year (1906), when Lee de Forest invented triode, the first radio tube that could be used as an amplifier. Since then, on Radio

waves used in many applications, including two-way voice communications, video and voice broadcast, and point-to-point digital microwave communications. However, the cellular telephone system has been the most successful application of the wireless communications. The origin of these systems began in the 1910s, when the first wireless audio transmission was established between New York and San Francisco. The Japanese had the lead in cell technology development, where the first cellular network was established. In 1981, the first cellular license in the US was awarded, and in 1983, the cellular mobile service started by Ameritech Corporation, known as the advanced mobile phone system (AMPS). The AMPS carrier frequency was 850 MHz and was based on the frequency division multiple access (FDMA) technology. Along with it, Nordic mobile telephony (NMT) in northern Europe countries. Within a couple of years, here in the UK, Vodafone, and shortly after Cellnet, released the total access communication system (TACS). These formed a part of what is known as "first generation mobile systems" (1G), which was catered for voice services and was based on analogue transmission technology.

Over the past few years, there have been extensive research, development and expansion, in wireless communications, particularly, in the field of cellular systems. In 1987, the FCC declared the use of new technologies in the 800 MHz radio spectrum, in which resulted in the first digital cellular transmission technologies (time division multiple access (TDMA), code division multiple access (CDMA), and global system for mobile communication (GSM) tested shortly thereafter). 2^{nd} generation (2G) has been extremely successful, where GSM became the prominent standard in Europe and major part of Asia, and CDMA and GSM jointly in America. 2G networks were the first to provide short messaging service (SMS) and data. General packet radio service (GPRS) was introduced into the GSM for supporting the packet switching traffic in a GSM network. It offers higher data rates than the conventional GSM, however the enthusiasm for 3^{rd} generation (3G) and immense hype in the late 1990s was creating an evidently unstoppable demand for higher data rate and new applications. 3G networks offer faster data rates, makes them particularly suitable for modern smart-phones, many of their applications require stable high speed internet connection. The emergence of digital technologies has

changed the landscape of cellular communications. With the deployment of 3G and recently 4G communication systems, the way of communications has dramatically shifted from voice service to multimedia and data centric communications. Success of cellular technologies, together with the advanced technology in smart phones and application developments, have seized the interest and imagination of the population. As a result, there has been an exponentially growing demand for cellular mobile technologies; according to Cisco visual networking index (VNI), by the end of 2013, the number of cellular connected devices will surpass the number of people of the world. Rapid increase in the number of mobile-connected devices, along with the demand for faster and more reliable mobile connections in a growing number of mobile applications, such as video and games, show the significance and perspective of wireless communication over the next coming years.

1.2 Challenges and Design of Wireless Systems

Providing ubiquitous mobile access to an extended number of connected devices, requires a solution to several scientific and economic challenges, vary from advanced signal processing algorithms and low power semiconductor design to the scarcity of available radio resources and the deployment of wider cellular networks. In this means, any wireless system needs to overcome transmission and propagation effects that are significantly more hostile and critical compared to that for a wired system. In the early stages of wireless communications, Marconi showed that wireless waves can travel across the Atlantic and Pacific oceans. Today, the purpose of wireless communications has developed: The radio technology is not being used merely to communicate over large distances, but rather for its economic aspects, comfort and flexibility. Short-range mobile communications provide access to the fixed communication infrastructure. Essential technical bottlenecks in a wireless technology are the capacity of the wireless channel, its uncertainty and unreliability due to unfavourable time-varying, multipath propagation and critical inter and intra cell interference. Integrating digital microelectronics and signal processing developments, provided solutions to overcome the issues associated with the mobile wireless channel [3]. As

a result of the rapid developments in digital signal processing and microelectronic circuits, nowadays the problems associated with transmission over wireless channels are mostly resolved. Particularly, innovative developments including space diversity combining (SDC), adaptive antennas, spread-spectrum techniques, digital modulation schemes, multi-carrier modulation (MCM), and multiple-input multiple-output (MIMO) systems have overcome the channel impairments and consequently have had a major contribution to mobile technology growth. However the scarcity of resources (e.g., spectrum and power) is remained to be resolved. As a result of this limitation in availability of resources, intelligent and adaptive resource allocation to the users is vital for providing the best possible service quality considering the economical parameters. This is particularly crucial with the high data rates demands for the next generation mobile communication systems. The issue of allocating subcarriers, rates, power, and time slots has therefore become an active area of research. Even though the conventional layered networking approach, e.g., open systems interconnection (OSI), enjoys the advantages of simplicity, modularity, expandability, and standardization, this architecture was defined for wired networks and its inflexible and rigid design makes the layered model inefficient to overcome the wireless networks related problems. In contrast to the layered scheme, cross-layer design tends to blur such rigid boundaries to allow interaction between layers by enabling information and configuration exchange from one layer to another layer [4, 5].

Further, contrary to the conventional strict non-shared spectrum usage regulations, intelligent shared-based spectrum deployment approaches are currently have appeared as a favourable candidate in order to overcome the spectrum crunch problem [6]. In the following of this chapter, I briefly highlight the research background of the mobile networks and technical challenges, as well as remedies, are reviewed in detail. Finally, the research outline and contributions of this thesis are provided at the end of this chapter.

1.3 Fundamentals

1.3.1 Orthogonal Frequency-Division Multiplexing

Multi-carrier modulation (MCM) is a modulation technique in which multiple carriers are used for modulating the information signals (data bits), in contrast to a single carrier used in the most common single carrier modulation schemes such as binary phase-shift keying (BPSK) and quadrature phase-shift keying (QPSK). Thus multi-carrier modulation is usually defined as the principle of transmitting information by dividing the data stream into several parallel data bit streams, and by using these sub-streams to modulate several carriers. The first systems utilized MCM were military HF (high frequency) radio links in the late 50s and early 60s [7].

In the conventional multi-carrier systems using frequency division multiplexing (FDM), a block of K serial data symbols, each of duration T_s , is converted into a block of K parallel data symbols, each of duration $T = KT_s$. The K parallel data symbols are modulated by K different carrier signal $\phi_k(t)$ [8, 9].

However the guard band between adjacent sub-channels is a waste of spectrum and leads to an inefficient use of radio spectrum. By developing the orthogonal frequency-division multiplexing, the most popular technique of the MCM scheme, generally known as orthogonal frequency-division multiplexing (OFDM) in brief, in the mid-1960s, spectral efficiency was significantly improved. In OFDM, the sub-carrier frequencies are chosen in a way that the sub-carriers are orthogonal to each other, which means that the cross-talk between the sub-channels is avoided and inter-carrier guard bands are not necessary, as shown in Fig.1.1. This approach significantly simplifies both the transmitter and the receiver design. In comparison to the single-carrier and the conventional FDM transmission technology, OFDM offers many advantages. Some of those advantages are summarised as follows [10,11]:

- In contrast to conventional FDM, a separate filter for every sub-channel is not required.

- In OFDM, each sub-channel experiences relatively flat fading so that the frequency selective fading can be effectively suppressed.

- The inter-symbol interference (ISI) and inter-carrier interference (ICI) can be effectively mitigated by using the concepts cyclic prefix and guard band.
- Compared to other double side-band modulation schemes, higher spectral efficiency can be achieved.
- It can be conveniently implemented by using inverse fast Fourier transform (IFFT) and fast Fourier transform (FFT) for modulation and demodulation respectively.
- More tolerant to time synchronization errors and delay spread.

Despite advantageous features of the OFDM, there are, however, certain disadvantages associated with implementing OFDM to be considered. Some of the disadvantages are as :

- OFDM signal can experience a large peak-to-average power ratio (PAPR), which may result in a signal distortion due to the non-linearity of the high power amplifier (HPA). To reduce the distortion caused by the non-linearity of HPA, usually, HPA requires a larger back-off from the peak power, which generally results in high power consumption in mobile devices.
- OFDM is very sensitive to Doppler shift.
- It is also more sensitive to distortions that may remove the orthogonality between carriers, i.e. carrier-frequency offsets (CFOs), due to Doppler shift and/or local oscillator drift.

1.3.2 Mathematical Description

Generally, a conventional multi-carrier transmitter is made of a set of modulators, each at a different carrier frequency. The transmitter then generates the transmitted signal by combining the individual modulator outputs [12]. Assume that the K data symbols to be transmitted are $X_k, k = 0, 1, ..., K-1$, where X_k is a complex number in an appropriate signal constellation, such as QPSK or quadrature amplitude modulation (QAM). Also assume that the k_{th} sub-carrier frequency for X_k is

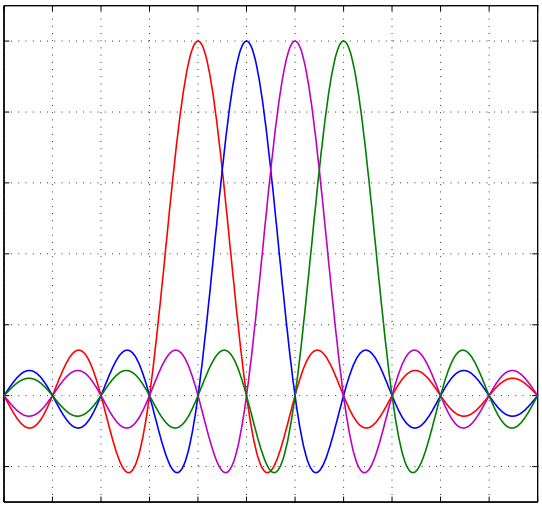

Figure 1.1: Frequency spectrum of OFDM subcarrier signals.

f_k. To study the orthogonality conditions of a set of signals, $\phi_k(t) = e^{j2\pi f_k t}$, where $0 \leq k \leq K$, we examine the time orthogonality of this set through the following stages. Let $\phi_k(t) = e^{j2\pi f_k t}$, and $\phi_k(t) = e^{j2\pi f_l t}$ be two subcarriers. Orthogonality is achieved if $\langle \phi_k(t).\phi_l(t) \rangle = 0$

$$\begin{aligned}
\langle \phi_k(t).\phi_l(t) \rangle &= \int_0^T \phi_k(t)\phi_l^*(t)dt \\
&= \int_0^T e^{j2\pi f_k t} e^{-j2\pi f_l t} \\
&= \frac{e^{j2\pi(f_k - f_l)T} - 1}{j2\pi(f_k - f_l)}, k \neq l \\
&= e^{j2\pi(f_k - f_l)T} \left(\frac{sin\{\pi(f_k - f_l)T\}}{\pi(f_k - f_l)} \right), k \neq l. \qquad (1.1)
\end{aligned}$$

The condition that 1.1 to be zero is $2\pi(f_k - f_l) = v\pi$, where v is an integer value [8]. Thus, to ensure the orthogonality between $\phi_k(t)$ and $\phi_l(t)$, their frequencies must be separated by integer multiplies of $1/2T$. However in the practical scenarios, the frequency separation used in OFDM, is larger than $1/T$. This is to ensure the orthogonality even when the subcarrier modulated signals experience some random phases. Assume the two considered subcarriers has random phases, i.e., θ_k and θ_l

respectively, the orthogonality condition can be written as

$$\begin{aligned}\langle \phi_k(t), \phi_l(t) \rangle &= \int_0^T \phi_k(t)\phi_l^*(t)dt \\ &= \int_0^T e^{-j2\pi f_k t + j\theta_k} e^{j2\pi f_l t - j\theta_l} \\ &= \frac{e^{j2\pi(f_k - f_l)T + (\theta_k - \theta_l)} - e^{\theta_k - \theta_l}}{j2\pi(f_k - f_l)}, k \neq l. \end{aligned} \tag{1.2}$$

To guarantee the orthogonality for any random phases θ_k, and θ_l, the subcarriers must be separated by $1/T$ in frequency. Fig. 1.2 shows four orthogonal subcarriers of an OFDM signal in time domain. Eq. 1.2 shows that the subcarriers are orthogonal in the symbol interval of $[0, T]$. As the orthogonality conditions are not satisfied beyond the interval $t \in [0, T]$, to preserve the orthogonality at any given time $t \in (-\infty, \infty)$, the subcarrier function is required to be windowed by a rectangular pulse function u_T [10]. This can be efficiently implemented by using a rectangular pulse shaping function at the transmitter ($h_a(t) = u_T(t)$). The complex envelope of an OFDM system output signal is given by

$$\tilde{s}(t) = A \sum_n b(t - nT, \mathbf{x}_n), n = 0, 1, ..., K - 1, \tag{1.3}$$

where

$$b(t, \mathbf{x}_n) = h_a \sum_{k=0}^{K-1} x_{n,k} e^{\frac{j2\pi(k - \frac{K-1}{2})t}{T}}, \tag{1.4}$$

where $\mathbf{x}_n$, is the data block, n is the block index, and h_a is the pulse shaping function. $\mathbf{x}_n$ consists of n data symbols and can be defined as

$$\mathbf{x}_n = \{x_{n0}, x_{n1}, ..., x_{nK-1}\}, \tag{1.5}$$

where x_{n0} is the complex data symbol, usually chosen from QAM or phase-shift keying (PSK) constellation. Therefore the OFDM complex envelop, $\tilde{s}(t)$, in (1.3),

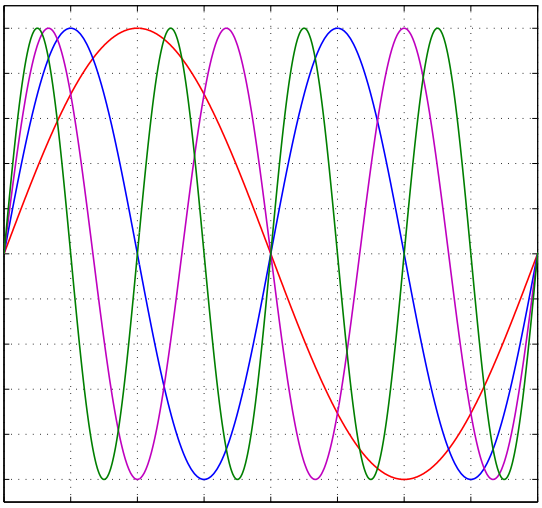

Figure 1.2: Time domain OFDM subcarrier signals.

considering the rectangular pulse shaping function can be written as

$$\tilde{s}(t) = A \sum_{n=-\infty}^{\infty} \sum_{k=0}^{K-1} x_{n,k} e^{\frac{j2\pi(k-\frac{K-1}{2})t}{KT_s}} u_T(t). \tag{1.6}$$

The bandpass signal and the complex baseband-equivalent signal in the interval $[0, T)$, respectively can be noted as [1]

$$s(t) = \Re[\tilde{s}(t)e^{j2\pi f_c t}], \tag{1.7}$$

$$s_b(t) = A \sum_{k=0}^{K-1} x_{n,k} e^{\frac{j2\pi(k-\frac{K-1}{2})t}{KT_s}} u_T(t), \tag{1.8}$$

where f_c is the carrier frequency.

1.3.3 OFDM implementation using IFFT/FFT

The simplicity and efficiency of transmitter and receiver implementation of OFDM system , is one of the key features in the OFDM. By assuming T_s the sampling time,

[1] For the sake of brevity, we henceforth omit the index reference n.

and removing the fixed delay of $\frac{K-1}{2}$, the first term of (1.8) can be given by

$$X_m = A \sum_{k=0}^{K-1} x_k e^{\frac{j2\pi km}{K}}. \tag{1.9}$$

Except for the multiplier A, the base band equivalent signal (1.9) is the formulation of a K-point inverse discrete Fourier transform (IDFT) [10]. If K is a power of two, then there are many fast architectures and algorithms that can implement such an IDFT operation efficiently. However, according to Nyquist-Shannon sampling theorem, infinite number of samples are required to exactly represent the rectangular pulse shaping function, in which means, that by assuming a finite sampling number, the rectangular nature of the shaping function cannot be achieved.

$$\begin{aligned} u_T(t) &= \sum_{k=-\infty}^{\infty} sinc\left(\frac{t}{T_s} - k\right), \\ &= \sum_{k=0}^{K-1} sinc\left(\frac{t}{T_s} - k\right) + \epsilon(t), \\ &= h_a(t) + \epsilon(t), \end{aligned} \tag{1.10}$$

where $\epsilon(t)$ is the error function, and $h_a(t)$ is the distorted shaping function.

1.3.4 OFDM Transceiver Block Diagram

OFDM transceiver can be created in different ways. An example of the typical OFDM transceiver is shown in Fig. 1.3 [13]. In the transmitter side, the input binary data is encoded by a conventional error correction encoder. The rate can be 1/2, 2/3, 3/4, etc. After interleaving, the binary bits are mapped into complex numbers representing BPSK, QPSK, 16-QAM, or 64-QAM constellation points, at the symbol mapping unit.

In order to make coherent detection robust against phase noise and frequency offsets, in every OFDM symbol, four of the subcarriers are dedicated to pilot signals. This step is followed by serial to parallel converter to prepare the data signal to be converted to OFDM symbols. Next, by applying the IFFT, the pilot and data values are modulated onto K subcarriers. After reconverting the parallel OFDM

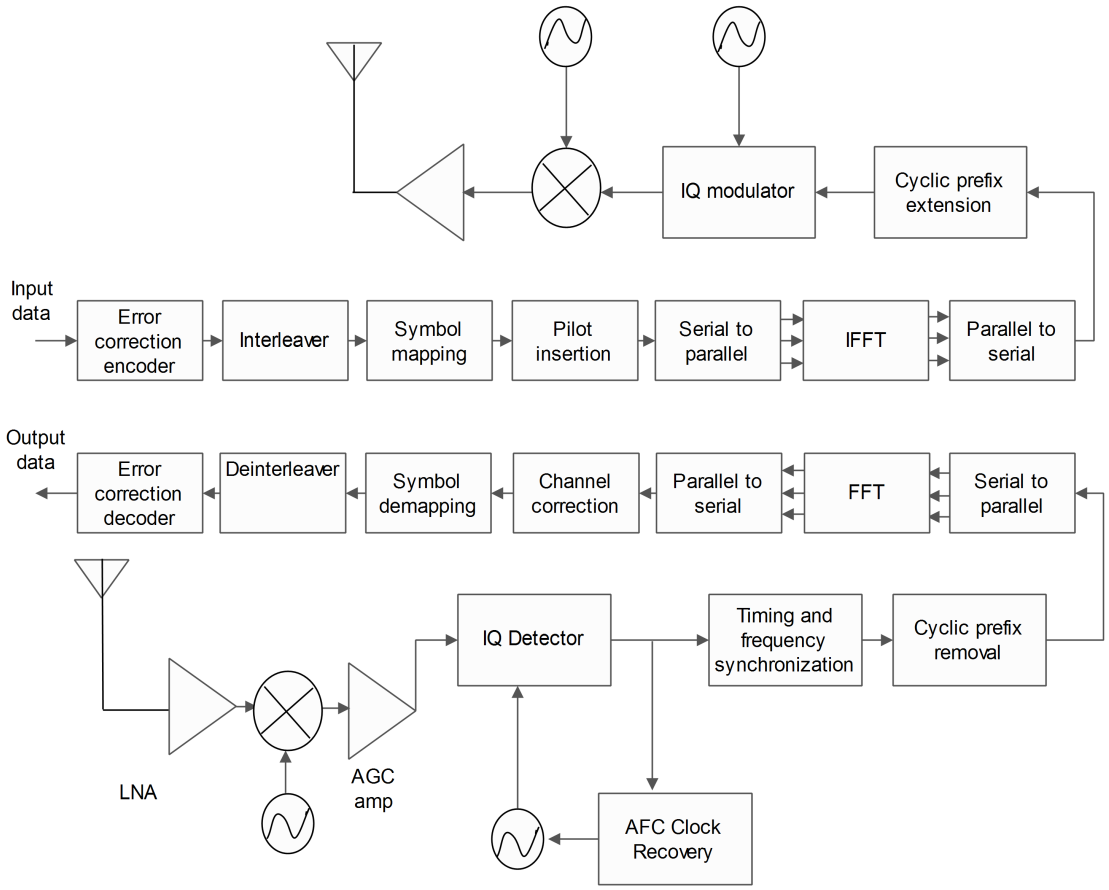

Figure 1.3: Block diagram of an OFDM transceiver.

symbols into serial sequence, to enhance the OFDM system robustness against multipath propagation, a cyclic prefix is added to the OFDM symbol. Following this step, the digital output signals are converted to analog signals, which then can be upconverted, amplified and transmitted through an antenna. Generally, the receiver operates the reverse of the transmitter, with extra training tasks. First, the receiver needs to estimate the frequency offset and the symbol timing, using the special training symbols in the preamble. After removing the cyclic prefix extension, FFT can be applied to the signal to recover the M-QAM values of all subcarriers. The pilot subcarriers and the training symbols are utilized to used for the channel and frequency offset estimation. The M-QAM values are then reconverted into binary values, and finally a the error correction decoder, decodes the information bits. Fig. 1.4 illustrates the structure of the OFDM preamble which precedes OFDM packet [13]. This preamble is important to operate automatic gain control, packet detection, symbol timing, fine frequency offset and channel estimation.

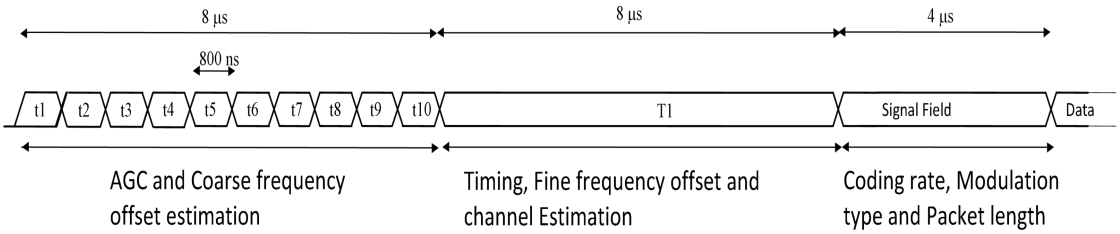

Figure 1.4: OFDM preamble structure.

1.3.5 Wireless Channel Model

The wireless channel presents an essential challenge as a medium toward robust and efficient wireless communication. It is not only susceptible to the deteriorating effects of interference, noise and other channel impairments, but also, these impediments unpredictably change over time as a result of user movement. In this section, we briefly describe the wireless channels and the statistical models used to reflect their effect on the transmitted signals. Detailed information about the channel models can be found in [14]. In a wireless communication system, there may be many paths for a signal from a transmitter to a receiver. Generally, the components of the radio signal are reflected by the landmarks, objects or different atmospheric layers. These reflected signals travel in different paths and combine at the receiver. If we assume that the $a_i(t)$, and $\tau_i(t)$ are, respectively, the overall attenuation, phase shift, and propagation delay from the transmitter to the receiver on path i, time t, and I the total number of arriving multipath components, the received bandpass signal may be expressed as,

$$y(t) = \sum_{i=1}^{I} a_i(t)s(t - \tau_i(t)) + \nu_i(t), \tag{1.11}$$

where $s(t)$ is the transmitted signal, and $\nu_i(t)$ is the additive white Gaussian noise (AWGN). By substituting the results from 1.7 in 1.11, and omitting the noise, we have

$$y(t) = \Re\left[\left(\sum_i a_i(t)e^{-j2\pi f_c\tau_i(t)}\tilde{s}(t - \tau_i(t)\right)\right]e^{j2\pi f_c t}. \tag{1.12}$$

The multipath fading channel is then modelled as a linear time-variant low-pass filter having the complex impulse response as follows:

$$h(t,\tau) = \sum_i a_i(t) e^{-j2\pi f_c \tau_i(t)} \delta(\tau - \tau_i(t)). \tag{1.13}$$

1.3.5.1 Statistical Models for Fading Channels

In order to implement effective receivers and consequently devising robust wireless communication systems, it is critical to tackle the destructive effect of fading. Although deriving an exact mathematical formulation of propagation in wireless channels is too complex, several multipath models have been introduced to explain the experienced statistical nature of a wireless channel. Those statistical models effectively approximate and characterise the behaviour of fading channels based on the nature of the wireless propagation environment and the design of communication scenarios. In this subsection, we briefly describe some of the most widely utilized multipath fading distributions, for modelling the indoor and outdoor propagation channels in cellular communication systems. Detailed information of statistical models, can be found in the literature [15–18].

Rayleigh Fading Channel

When there are a large number of propagation paths, the central limit theorem can be applied to show that the multipath fading channel 1.13 can be modelled as a complex Gaussian random variable. [19, 20]. In the case that there is no direct line-of-sight (LOS) path, the mean of the Gaussian distribution is zero. In this scenario, the envelope $|h(t)|$, at any instant t, is said to be Rayleigh-distributed. [21, 22]. Therefore, the channel gain $|h(t)|^2$, and consequently instantaneous received signal-to-noise ratio (SNR), γ, are Exponentially-distributed with the following probability density function (pdf):

$$f(\gamma) = \frac{1}{\bar{\gamma}} \exp(\frac{-\gamma}{\bar{\gamma}}), \tag{1.14}$$

where $\bar{\gamma}$ denotes the average received SNR. Rayleigh fading is a reasonable model for ionospheric and tropospheric radio signal propagation as well as for macro-cell (i.e. relatively large coverage cells) and heavily built-up urban environments, in general,

where there is no direct LOS path between transmitter and receiver.

Ricean Fading Channel

In the event where there are fixed signal reflectors or scatters beside the randomly moving scatters in the channel, $h(t)$ distribution can no longer be modelled as a complex Gaussian distribution with zero mean. In this case the envelope $|h(t)|$ follows a Rician distribution. The Rician fading model typically assumes a dominant LOS path component and a large number of independent and identically distributed (i.i.d.) reflected signals. The channel gain $|h(t)|^2$, and consequently instantaneous received SNR, γ, are distributed with the following pdf:

$$f(\gamma) = \frac{(1+n^2)e^{-n^2}}{\bar{\gamma}} \exp\left(\frac{-(1+n^2)\gamma}{\bar{\gamma}}\right) I_0\left[2n\sqrt{\frac{(1+n^2)\gamma}{\bar{\gamma}}}\right] \quad , \quad n \geq 0, \tag{1.15}$$

where n is the Nakagami-n fading parameter and $I_0[.]$ is the 0^{th} order modified Bessel function of the first kind. Moreover, Rician parameter ($L = n^2$), is the ratio between the power of the direct path and the average power of the scattered path components and indicates the Rician-distributed channel quality [23,24]. In the case where there is no LOS signal, i.e. $n = 0$, the Rician fading is equivalent to Rayleigh fading, whereas it converges to a non-fading channel in the limit as $n \longrightarrow \infty$. Compared to Rayleigh fading, Rician fading levels are more benign, therefore Rician fading channel models are typically employed for micro-cellular (i.e. relatively small coverage cells) environments, such as urban and sub-urban areas [25–27].

Nakagami-m Fading Channel

The Nakagami-m distribution, where m denotes the Nakagami-m fading parameter, provides a generalized fading model introduced by Nakagami in th 1940s [28]. Particularly, it features the Rayleigh, Rician and many and other fading distributions over the parameter m. The pdf of received SNR, γ, over Nakagami-m fading, is given by

$$f(\gamma) = \frac{1}{\Gamma(m)} \left(\frac{m}{\bar{\gamma}}\right)^m \gamma^{(m-1)} \exp(\frac{-m\gamma}{\bar{\gamma}}) \quad , \quad m \geq \frac{1}{2}, \tag{1.16}$$

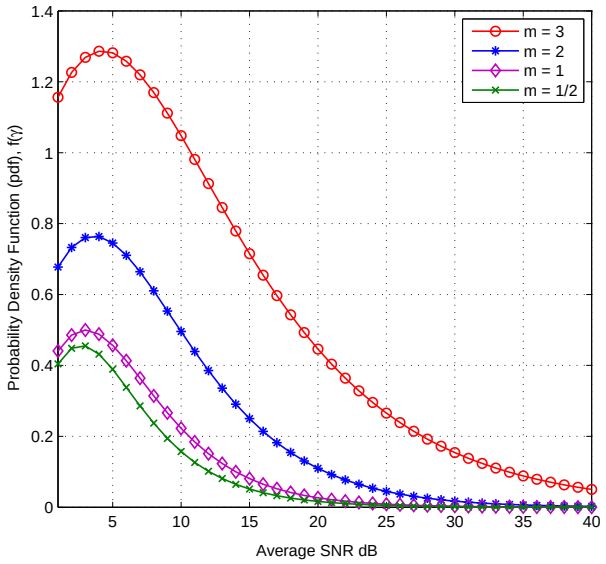

Figure 1.5: Gamma-distributed probability density function for various values of the Nakagami parameter m.

where $\Gamma(m)$ is the Gamma function, denoted by

$$\Gamma(m) = \int_0^\infty t^{m-1} e^{-t} dt. \tag{1.17}$$

When $m = 1$, and $m = 2$ Nakagami distribution is approximately equivalent to Rayleigh distribution and Rayleigh distribution with two-antenna diversity respectively. For m approach infinity the Nakagami distribution becomes an impulse, which means there is no fading. Fig. 1.5 illustrates that in higher values of m the severity of fading decreases. The most severe fading levels are experienced where $m = \frac{1}{2}$, which corresponds to one-sided Gaussian fading distribution. Further, Rician distribution can be approximated by the Nakagami-m distribution for $m \geq 1$, and the following relation between Rician parameter and Nakagami fading factor m [29–31],

$$L = \frac{\sqrt{m^2 - m}}{m - \sqrt{m^2 - m}} \quad , \quad m \geq 1. \tag{1.18}$$

The wireless mediums for indoor and sub-urban, urban and ionospheric environments can usually be better modelled by Nakagami distribution [28, 32, 33].

1.4 Cognitive Radio

Most of the current radio systems are not aware of the surrendering spectrum environment and operate in a pre-assigned specific frequency spectrum using a specific spectrum access technology. Researches on the spectrum utilization show that a large part of the spectrum is under utilized or not used in a specific space (geographic location) or time due to legacy command-and-control regulation. For example, Fig. 1.6 shows the spectrum utilization for different locations in the Untied Kingdom [34]. The limited precious available spectrum and the inefficiency in the spectrum utilization necessitate a new wireless communication concept to exploit the available wireless spectrum in a more efficient approach. Cognitive radio is introduced as a prominent candidate to solve this problem of spectrum crunch. The terms of cognitive radio (CR) and software-defined radio was first proposed by J. Mitola in his paper [35]. The outline "what cognitive radio is" given in [36] describes the cognitive radios as:

Cognitive radio is an intelligent wireless communication system that is aware of its surrounding environment (i.e., outside world), and uses the methodology of understanding-by-building to learn from the environment and adapt its internal states to statistical variations in the incoming RF stimuli by making corresponding changes in certain operating parameters (e.g., transmit-power, carrier-frequency, and modulation strategy) in real-time, with two primary objectives in mind:

- *highly reliable communications whenever and wherever needed;*
- *efficient utilization of the radio spectrum.*

Although the initial term and definition of CR had not been specifically on spectrum use, the concept of CR has become almost exclusively utilized to imply intelligent spectrum radios. Basically, CRs (often defined as secondary users) can effectively use the under-utilized or unused parts of the spectrum of licensed users (primary users) by actively observing the spectrum and dynamically adapting their parameters according to this observation.

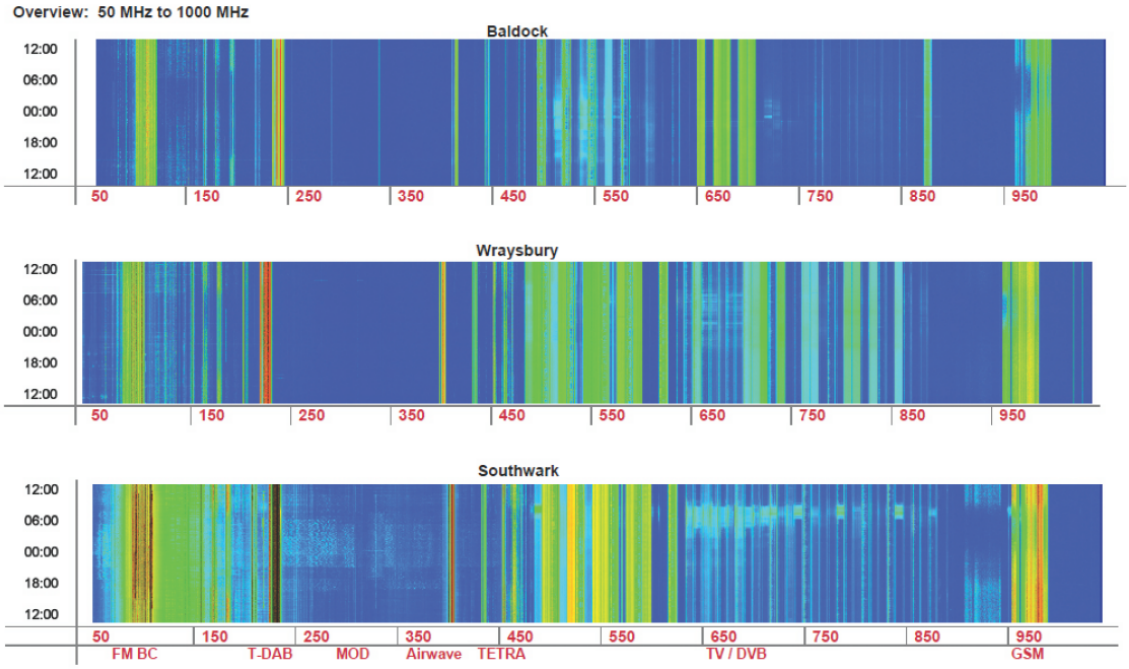

Figure 1.6: Signal strength data obtained over a 24 hour period from midday to midday, the time ascends from the bottom to top of the plot i.e. the earliest time is at the baseline.

1.4.1 Cognitive Radio functions

Realizing this simple theory of the concept incorporates a range of requirements, limitations, and decisions associated with the amount of available information about the primary user (PU) activities and how to acquire this information. In order to clear up from the implementation perspective, the most important functions of cognitive radio are categorized as, spectrum sensing, spectrum management, spectrum mobility, and spectrum sharing. Along with maximizing the overall performance of the secondary user (SU), the main objective of these functions is to ensure an efficient and robust operation of the PUs without destructive intervention from the SUs. These functions can be summarized as follows:

1.4.1.1 Spectrum sensing

Spectrum sensing is one of the main functionalities of CR concept. It can be considered as the task of acquiring information and awareness about the spectrum usage and PUs activities in the surrounding of a CR transceiver, across different dimensions such as space (location), time, frequency, and code. The current spectrum

sensing methods are mostly based on either interference-based detection, transmission detection, and cooperative detection approach. However, there are many challenges related to spectrum sensing which make the process of detecting spectrum conditions difficult for a CR user. Some of those challenges are related to hardware requirements, sensing frequency and duration, hidden PU problems, detecting spread spectrum PUs, and security issues [37,38]. The concept of the dedicated sensing network has been introduced to tackle the hidden PU problems, which separates the sensing systems from the secondary transceiver and the spectrum information is provided by the SUs' service provider [39]. Different methods of spectrum sensing and their benefits and drawbacks have been outlined in [40–43].

1.4.1.2 Spectrum management

Following spectrum deduction functionality, the CR networks evaluate the available spectrum and the limitation of this availability to relatively select the appropriate channels over which they can establish transmission. This process is basically known as spectrum management. Spectrum management functionality consists of two components, namely, spectrum assignment, and spectrum access. Spectrum assignment involves allocating the idle or underutilized spectrum bands to CR users according to a specific policy. In the spectrum access part, the physical (PHY) layer parameters, e.g., transmit power, modulation and coding scheme with certain constraints on power and bit error rate (BER) requirements are adapted based on the spectrum sensing information and the spectrum assignment policy.

1.4.1.3 Spectrum mobility

The spectrum environment that CR network is operating on is dynamic, and may change with time, location and even be reoccupied by the PUs at any instant. Therefore, a CR network also needs to be able to adjust its operating parameters when required. Another option for a CR is to modify its operating bands by using p-persistent carrier sense multiple access (CSMA) rule. CSMA is a probabilistic media access control (MAC) protocol, which a CR user verifies the absence of other traffic before transmitting on a shared transmission channel. If the primary channel

availability probability is known to be p, then the probability of data loss of a CR user employing p-persistent CSMA to switch the operating band will be reduced. The process of SUs changing their operating bands can be defined as frequency handoff, in which a SU needs to terminate its communication on the current band, vacate the channel, and identify a new available channel to continue its communication. Spectrum handoff mechanisms are usually categorized into two types based on the decision timing of selecting target channels, namely reactive-decision spectrum handoff and proactive-decision spectrum handoff.

In the reactive spectrum handoff approach the target channel is searched in an on-demand way, and the spectrum switching and reconfiguration are conducted after detecting a PU, therefore this approach has a non-negligible sensing and switching delay [44]. The concept of proactive method is to exploit the long-term traffic statistics to predict the channel availability condition and conduct spectrum switching and reconfiguration before the reacquisition of the channel by the PU.

1.4.1.4 Spectrum sharing

The shared nature of the spectrum requires to coordinate the transmission attempts between CR users. Spectrum sharing handles this coordination, so that all SUs fairly can have access to the available spectrum. Spectrum sharing strategies can be classified into different categories based on the architecture of the CR system, spectrum assignment behaviour, and spectrum access techniques. The first classification based on the network architecture can be defined as which can be centralized or distributed spectrum sharing. Centralized spectrum sharing applies a centralised entity to control the spectrum assignment and access activities of all active SUs. Whereas distributed spectrum sharing does not need any controlling entity and based on local (or global) policies that are performed by each user distributively allows the CR users to conduct spectrum allocation and access themselves.

Furthermore, the spectrum allocation behaviour classifies the spectrum sharing approaches into two categories: cooperative spectrum sharing, and non-cooperative spectrum sharing. Cooperative spectrum sharing, as the title implies, involves sharing some information by SUs with each other. A typical technique used in these

approaches is forming clusters to share information, which make a balance between a centralized and distributed approaches. In non-cooperative spectrum sharing techniques, individual nodes do not collaborate and spectrum sharing is conducted considering only a single user.

Third classification for spectrum sharing is based on the spectrum access approach, which has three classes: spectrum underlay, and spectrum overlays and spectrum hybrid. The underlay spectrum access technique allows simultaneous access of available spectrum to PUs and SUs, while imposing PU interference threshold [45] on the CR network transmission parameters. The overlay spectrum access approach enables opportunistic access to the idle primary frequency bands by SUs. The third spectrum access approach provides a combination of the two aforementioned approaches. The basic concept is to opportunistically access the idle licensed frequency bands and limit the interference imposed on the PUs for the simultaneous access of the frequency bands. There is a rich literature available, providing good insight on various aspects of spectrum sharing fundamentals such as potential and capacity of spectrum sharing systems, optimal limits of spectrum sharing, etc. [37,45–47]. Implementation of CR functions involves more than one layer of the protocol stack rather than being performed at a single layer. The role of different OSI network layers in performing these CR functionalities, thus the need for cross-layer design and certain cross-layer design ideas for CR systems, will be dealt with more detail in Section 1.5. The following subsections cover the details of potential transmission strategy and spectrum access techniques used in CR systems.

1.4.2 OFDM in cognitive radio systems

CR or software defined network implementation includes exploitation of the local unused spectrum, interaction across several networks, protocols, and devices, moving across the spectrum while being able to stay in abidance with local regulations, adapting the transmission, reception and system parameters without users intervention, and having the capability to learn from the long-term users' reaction statistics. To achieve these objectives, PHY is required to be highly flexible and adaptable. One of the questions that arise as part of considering implementation of CR sys-

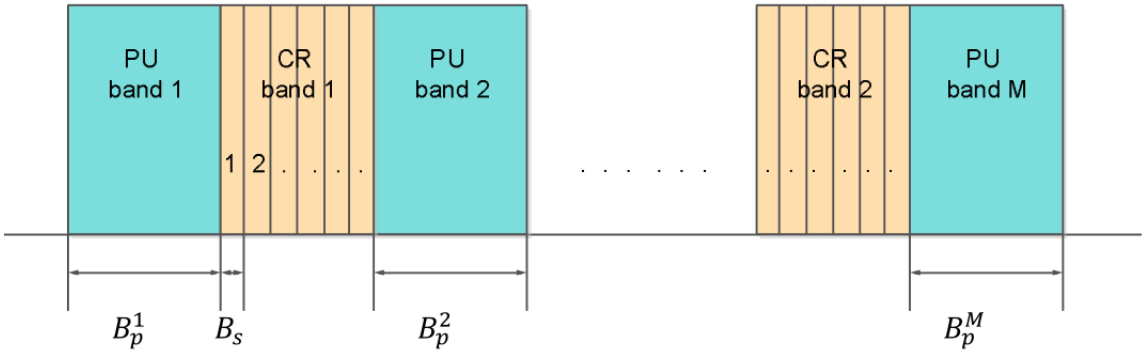

Figure 1.7: PUs and SUs distributed in frequency domain

tems is about which transmission technique to employ in CR systems. OFDM as a PHY transmission strategy in CR system has the potential of fulfilling the aforementioned requirements, particularly the ability to avail the idle or underutilized part of licensed spectrum by choosing those specific sub-bands. Considering a spectrum consisting of m primary bands with bandwidths $B_p^1, B_p^2, \ldots, B_p^M$. In the event some of these bands are not being used by the PUs, then those bands can be utilized by the CR network. Each band is divided into several OFDM subchannels with bandwidth B_s and therefore a vacant band can be utilized by multiple SUs, each SU using a certain number of subchannels based on the scheduling strategy. Furthermore, if any subchannel in the PUs' spectral band is free then there is a possibility of assigning this to a SU. Fig. 1.7 illustrates the opportunistic spectrum access in OFDM-based CR network.

Underlay and hybrid spectrum access strategies, allow the PUs and SUs to coexist at the same band. Since the PUs are the certified users of the spectrum, any type of disruption at the primary receivers (PRx) from the SUs is not desirable. Therefore, in these cases, the SUs need to ensure a predefined interference level limit specified by PUs [48, 49].

1.5 Cross-layer Design

The open systems interconnection (OSI) model organizes a networking framework in waterfall-like certain number of layers, with virtually rigid boundaries between them.

Each layer is responsible for a well-defined function to offer services to the higher layers without revealing the details of how the service was implemented. Although the conventional layered structure offers the benefits of modularity, standardization, and expandability, its firm and strict architecture make the layered structure inefficient to deal with the problems arise due to the random nature of the wireless medium. As a result, the strict boundary between different layers of network in the new designs is blurring and the so-called cross-layer design has received popularity in wireless networks due to its high performance, especially in delivering QoS satisfaction for real-time applications.

The following examples merely illustrate the idea of cross-layer design. Link adaptation, for example, involves adaptation of certain parameters according to the wireless channel characteristics while meeting user-specified QoS demands. However, these parameters are not limited to a specific layer of the protocol structure, e.g., transmission power and data rate are PHY parameters, whereas delay is a performance measure at the data link layer (DLL) and transmission control protocol (TCP), and packet loss may occur due to bad wireless channel condition (PHY), or congestion (TCP), or queueing (DLL). Moreover, user-specified QoS demands lie in the application layer, therefore other layers need to get some details from the application layer to adapt their parameters accordingly. In essence, today's wireless networks and applications demand for flexible interactions among different layers of network. As in any other case, these flexible interactions also come at a cost of design complication [50,51]. Instead of solving the problem in parts at different layers, cross-layer design problems extend to a broader region ranging across multiple layers. This makes the process of obtaining global solutions more difficult.

Over the past few years, a large number of cross-layer designs have been proposed in the literature [52, 53]. Fig. 1.8 demonstrates some of these cross- layer design concepts. Backward and forward information flow cross layer design provides information flow across layers via specialized interfaces. Information received from other layers provides useful knowledge of network status and communication characteristics, that may be exploited in better decision making, parameters modification, etc. In design coupling without new interfaces cross-layer method, multiple

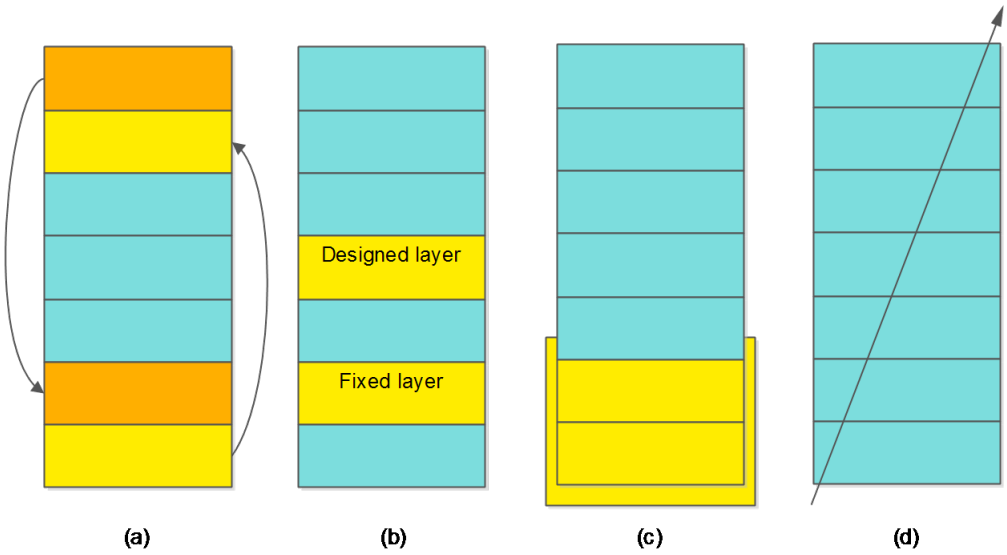

Figure 1.8: Illustrating the different kinds of cross-layer design proposals. (a) backward and forward information flow cross-layer, (b) design coupling without new interfaces, (c) merging of adjacent layers, (d) vertical calibration [52, 53].

layers are developed in a collaborative approach. The design of one is conducted by considering another layer functionality, therefore dependency is created at the time of designing. The referenced layer is called fixed layer and the dependent layer is called designed layer. Since the designed layer is developed based on fixed layer, an explicit interface between them is not required. In merging of adjacent layers method a single super-layer is created by combining the adjacent layers service and functionalities. In this method joint optimization can be applied directly to the super-layer. Obviously, this approach does not involve any additional interfaces. However, this method is uncommon due to the complexity it introduces to the network. The final method is vertical calibration across layers. As the name indicates, this method refers to parameter adjustment that span across layers. Basically, the application layer performance is a function of the parameters at all the stack layers. Hence, it is reasonable that jointly optimizing all parameters of downstream layers can help to achieve better performance than individual layer configuration.

Cross-layer design, in the case of CR networks, becomes even more challenging, due to the inherent characteristics of sensing, managing, reasoning, and adaptation. A CR user is required to consider a variety of input sources at the same time in-

cluding its own observations statistics in order to implement the learning process. In addition, a CR system needs to take into account several parameters simultaneously, such as user perspective application requirements of the SUs, a number of constraints, including the interference limit and sensing functionality, and its own potential to exploit the available spectrum and channel conditions. Achieving a reasonably optimal solution through merging all the specifications, requirements and limitations into a single optimization problem needs an adaptation and engagement covering multiple layers. In this work three particular cross-layer designs are proposed in chapters 2, 3, and 4.

1.6 Wireless Video Communications

Video communication has developed from a simple way of visual communication to an essential empower for different video applications. Various remarkable video applications have been efficiently deployed recently, with the aim of delivering users with more adaptable, flexible, customized, and rich viewing experience. Ubiquitous video applications, accompanied by paradigm shift from wired, passive, and non-interactive video content access to wireless, interactive, and distributed content access, certainly, required a new way for advanced video communications. However, given the resource-limited, distributed as well as the heterogeneous nature of wireless systems, the support of rich wireless video communications is still challenging.

To deal with the limited radio resources and to provide adaptivity for the severe wireless channel conditions, packet scheduling, rate control, along with error control strategies are usually involved in the development of codecs to enable reliable and efficient wireless video communications. At the same time, due to devices energy limitation, as well as transmit power and interference constraints in the context of CR wireless networks, video coding and transmission algorithms need to operate with the minimum possible power consumption. Hence, video coding and transmission over wireless networks is inherently a complex optimization problem with a set of limitations. To sum up, wireless video communications involve an extensive range of challenges and possibilities, offering the grounds for technical innovations. In this

section we briefly discuss the fundamentals of scalable video coding and in Chapter 4 we investigate the challenge of resource allocation for scalable videos over MQAM OFDMA-based CR networks.

1.7 Scalable Video Coding (SVC)

The need for scalable video coding, that enables on-the-fly adaptation to specific application demands such as processing capabilities and display features of the involved devices, and varying wireless channel conditions, arises from the continuous development of receiving devices and the growing usage of wireless transmission systems that are characterized by a widely changing connection quality [54–56]. In these heterogeneous environments, interoperability of the encoder and decoder solutions from various manufacturers as well as flexible adaptation of once-encoded content is desired. Scalability has already been provided in the earlier video coding standards such as, MPEG-2, H.263, and MPEG-4 video coders by means of scalable profiles. However, the availability of quality and spatial scalability in these standards comes with a significant increase in decoder complexity and a considerable decrease in coding efficiency compared to the corresponding non-scalable schemes. These disadvantages, which reduced the scalable schemes potentials, are addressed in SVC modification of the H.264/AVC standard [57, 58].

1.7.1 Types of Video Stream Scalability

A video stream is known as scalable when parts of the bit stream can be dropped in a manner that the resulting stream provides another appropriate substream for some receiver decoder, and the substream delivers the source content with a reasonable reconstructed quality which is less than the associated complete original video bit stream but is high considering the lower amount of valid received data. The substream can be a lower temporal resolution (frame rate), lower spatial resolution (picture size), or a lower quality (signal-to-noise ratio) video stream (each individually or in combination) compared to the original corresponding bitstream.

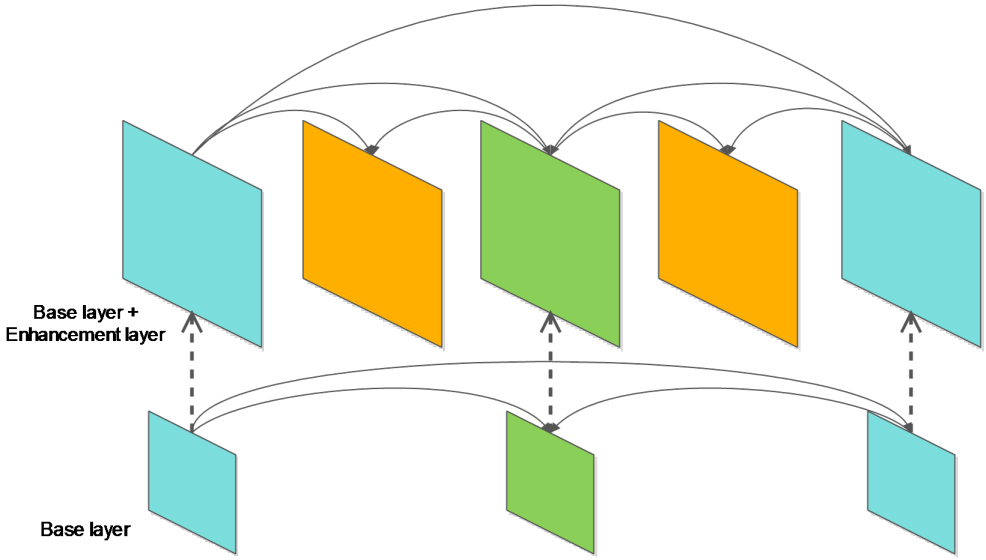

Figure 1.9: Spatial scalability with additional inter-layer prediction (dash arrows).

1.7.1.1 Spatial Scalability

In spatial scalability the encoder generates two or more layers with different spatial resolutions from a single video source in a way that the base layer is encoded independently to deliver the basic spatial resolution and the enhancement layer(s) uses the spatial reconstructed base layer to provide higher or full spatial resolution of the video stream. To support spatial scalability, SVC employs the conventional multi-layer coding approach, which is already included in H.262/MPEG-2, H.263, and MPEG-4. Similar to single-layer coding, SVC employs motion-compensated prediction and intra prediction in each spatial layer. Moreover, SVC offers so-called inter-layer prediction techniques as shown in Fig. 1.9, in which exploit the statistical dependencies between different spatial layers to enhance the coding efficiency of enhancement layers.

1.7.1.2 Temporal Scalability

Temporal scalability allows dividing the video stream frames into several layers, in which, the base layer is coded to provide the basic frame rate and the enhancement layer(s) is coded using temporal prediction corresponding to the base layer or higher enhancement layers. The layers could have either the same or different temporal

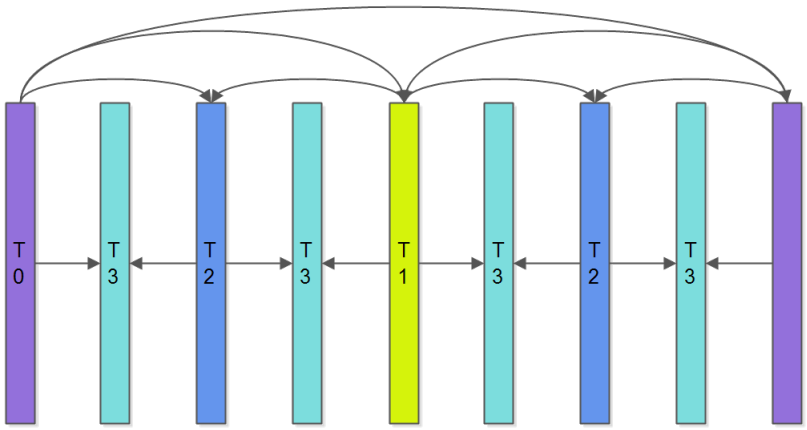

Figure 1.10: Temporal scalability with with hierarchical B or P pictures. Tx define the temporal layers with x addressing the corresponding temporal layer identifier.

resolutions, and when combined, produce full temporal resolution video stream at the decoder. Furthermore, the concept of hierarchical B or P pictures can enable the dyadic temporal enhancement layers in temporal scalability as shown in Fig. 1.10.

1.7.1.3 Quality Scalability

Quality scalability provides generating two or more SNR layers of the same spatial-temporal resolution but different fidelity from a single video source such that the base layer is coded to produce the basic video quality and the enhancement layer(s), in which, when combined with the base layer reconstructs a higher quality reproduction of the original video stream. As the enhancement layer is considered to enhance the SNR of the base layer, this form of scalability is also called SNR scalability. The H.264/SVC extension supports two SNR scalability modes, namely coarse grain scalability (CGS) and medium grain scalability (MGS). [1]For CGS, a refinement of quality is obtained by requantizing the video stream with a smaller quantization step size. Therefore, interlayer texture, motion and residual prediction may be used to improve efficiency of CGS. However, CGS quality layers number is limited to the number of quantization steps. MGS is introduced to enhance the flexibility of the rate adaptation and potentially better coding efficiency. MGS provides finer

[1]An outdated mode of SNR scalability called fine grain scalability (FGS) has been removed from the h.264/ SVC extension, due to the mode's high computational complexity.

granularity level of quality scalability by distributing the CGS enhancement layer transform coefficients into more layers and therefore, a CGS layer can be divided into several MGS layers [58].

1.8 Aim, Contributions, and Outline of Thesis

The main purpose of this thesis is to strike a balance between the conflicting goals of minimizing the interference introduced to the primary users and maximizing the performance of the SUs. To address this issue we introduce an efficient framework to integrate adaptive resource allocation techniques into the shared-spectrum problem. The main focus is particularly on the PHY layer design, while integrating this layer and higher layers' parameters, specifically, the application and MAC layers. The resources considered consist of subcarriers, transmission power, and transmission rate, while the constraints include instantiates total interference, average and peak total power, BER, and minimum required quality based on the defined scenario. The proposed algorithms differ from the literature works mainly in three aspects. Firstly, probabilistic interference management has been combined with the imperfect secondary-primary channel estimation, adaptive modulation and coding (AMC), and the proposed resource allocation scheme. Secondly, we proposed a stochastic radio resource allocation algorithm in both hybrid- (i.e., mixed underlay and overlay) and opportunistic (i.e., overlay) OFDMA-Based CR systems. Finally, the proposed strategy is deployed to optimize the user's perspective video quality quality based on a the probabilistic interference management to provide the secondary users with high robustness, scalability, extendibility. In summary, the contribution of the work can be listed as:

1. A closed-form expression for the cdf of the OFDMA CR's received SINR is derived.

2. A new low-complexity formulation for the probabilistic imperfect STx to PRx cross-link CSI is proposed.

3. The issue of violating interference limits associated with imperfect cross-link

CSI for the average case, worst case, and probabilistic case, scenarios of channel estimation error is examined.

4. The aggregate transmission rate of the OFDMA CR network through incorporating the stochastic information on the different number of subcarriers experiencing different scenarios is derived.

5. The comprehensive problem of power, rate, and subcarrier allocation for enhancing the average spectral efficiency of downlink multi-user OFDMA CR systems subject to satisfying total average transmission power and peak aggregate interference constraint is proposed.

6. Stochastic total transmit and interference power constraints under imperfect sensing information is formulated.

7. We devise the stochastic radio resource allocation algorithms based on the spectrum sensing probabilistic information on channel availability.

8. A new closed-form expression for the deterministic approximation of the probabilistic PRx interference constraint, in order to solve the probabilistic constrained mixed discrete-continuous non-linear programing (MDCNLP) problem is proposed.

9. A new cross-layer design is proposed to maximize overall SRx quality of multi-user scalable video applications subject to prescribed total transmission power, maximum interference limit on the PRx and minimum acceptable video quality.

The thesis is outlined as follows: In Chapter 2, the comprehensive problem of joint power, rate, and subcarrier allocation have been investigated for enhancing the spectral efficiency of multi-user orthogonal frequency-division multiple access (OFDMA) CR networks subject to satisfying total average transmission power and aggregate interference constraints. We propose novel optimal radio resource allocation (RRA) algorithms under different scenarios with deterministic and probabilistic interference violation limits based on perfect and imperfect availability of cross-link

channel state information (CSI). In particular, in contrast to the 'average case' and 'worst case' estimation error scenarios in the literature, we propose a probabilistic approach to mitigate the total imposed interference on the primary service under imperfect cross-link CSI. An expression for the cumulative density function (cdf) of the received signal-to-interference-plus-noise ratio (SINR) is developed to evaluate the average spectral efficiency. Dual decomposition is utilized to obtain sub-optimal solutions for the non-convex optimization problems. Through simulation results, we investigate the achievable performance and the impact of parameters uncertainty on the overall system performance. Furthermore, we show that the proposed RRA algorithms can significantly improve the cognitive performance whilst obeying the imposed power constraints. In particular, the performance under imperfect cross-link CSI knowledge for the proposed 'probabilistic case' is compared over the conventional scenarios to show the potential gain in employing this scheme.

In Chapter 3, a stochastic RRA algorithm is designed to maximize the total transmission rate of OFDMA-based CRs in both hybrid (i.e., joint underlay and overlay) and opportunistic- (i.e., overlay) spectrum access strategies. Our novel solution incorporates the probabilities of channel availability obtained through spectrum sensing for allocating power and subcarrier in a multi-user multi-band environment. In order to protect the licensed users from harmful intervention under imperfect sensing information, stochastic transmit and interference power constraints are imposed on the CRs. The performance of the proposed RRA algorithm and advantages over the conventional hard-decision-based approaches are demonstrated using numerical results.

In Chapter 4 we investigate an optimal RRA scheme for multiple users scalable H.264/SVC video transmission OFDMA-based CR networks. The framework exploits a new probabilistic approach to mitigate the total imposed interference by cognitive users on the licensed networks. We contemplate two fundamental network's service objectives, number of satisfied users, and the aggregate transmitted video quality. We first write the 3-dimensional scalable video quality of the H.264/SVC video transmission over an OFDMA-based CR networks. The total quality is expressed following four physical layer parameters: subcarrier allocation,

modulation spectral efficiency, power allocation, and stochastic interference limitation. An efficient suboptimal algorithm is proposed in two steps to solve the probabilistic constrained mixed discrete-continuous non-linear programing (MDCNLP) problem. Adaptive MQAM/OFDMA systems under imperfect channel information at the transmitter are shown to have substantial gain in average PSNR compared to conventional quality blind OFDMA-based CR RRA algorithms.

Finally, a conclusion of this thesis is provided in Chapter 5, and ample suggestions for future research are included at the end of this chapter.

Chapter 2

Spectral Efficiency of Adaptive MQAM/OFDMA Cognitive Radio Networks

2.1 Introduction

In recent years, significant effort has been made towards improving the spectral efficiency of cellular networks in order to meet the growing demand and sophistication of wireless applications. Several spectral-efficient technologies, such as machine-to-machine (M2M) communications, small-cell (SC) solution, massive multiple-input multiple-output (MIMO), and cognitive radio (CR) - each with respective advantages and challenges - are promising candidates in this direction [59].

In this chapter, we consider underlay spectrum-sharing, where robust interference management is critical for tackling any harmful cross-service interference. Orthogonal frequency-division multiplexing (OFDM) has emerged as a prominent radio access technology for new generation of wireless communication systems including LTE and LTE-advanced [60]. For OFDM-based multi-user applications, multiple-access can be accommodated through orthogonal frequency-division multiple-access (OFDMA) technique [61]. In OFDMA systems, different subcarriers may be assigned to different users in order to exploit the channel quality random variations of users across each subcarrier. OFDMA technology is considered as a de facto

standard for CR networks due to its inherent advantages in terms of flexibility and adaptability in allocating spectrum resources in shared-spectrum environments [62].

Radio resource allocation (RRA) plays a significant role in optimizing the overall spectral efficiency of conventional OFDMA systems [63]. In addition, adaptive RRA is an active area of research in the context of OFDMA-based CR networks with the aim of achieving a balance between maximizing the cognitive network performance and minimizing the inflicted interference on the licensed users. Suboptimal and optimal power allocation policies are studied in [64], where the aggregate capacity of the CR system is maximized under a primary receiver (PRx) interference limit. In [65], a queue-aware RRA algorithm is proposed to maximize the fairness in OFDMA-based CR networks subject to a total power constraint at the base station. A Lagrangian relaxation algorithm is adopted in [62] to probabilistically allocate resources based on the availability of the primary frequency band via spectrum sensing.

Most of the RRA algorithms on CR networks in the literature assume perfect channel state information (CSI) between the secondary transmitter (STx) and PRx, and few have considered imperfect cross-link CSI. However, due to technical reasons such as estimation errors and wireless channel delay, obtaining perfect cross-link CSI is difficult in practical scenarios. In [66] and [67], the ergodic capacity is derived over fading channels with imperfect cross-link knowledge, however, the analysis is carried out for a single cognitive user (CU). Furthermore, due to noisy cross-link information, it is unrealistic to assume that the secondary network strictly satisfies a deterministic interference constraint. The authors in [68] propose a RRA algorithm for maximizing the instantaneous rate in downlink OFDMA CR systems subject to satisfying a collision probability constraint. However, [68] only considers the individual impact of probabilistic interference constraint per subcarrier. Motivated by the above, we thoroughly investigate different scenarios by analysing the impact of deterministic and probabilistic interference constraints depending on perfect and noisy cross-link knowledge. In particular, we develop novel RRA algorithms under 'average case', 'worst case', and 'probabilistic case' scenarios of channel estimation uncertainty for *multi-user* OFDMA CR networks.

On the other hand, to the best of the author's knowledge, enhancing the average

spectral efficiency of multi-user OFDMA-based CR systems has not been addressed in the literature. In this work, by exploiting the advantages of channel adaptation techniques, we propose novel joint power, subcarrier, and rate allocation algorithms for enhancing the average spectral efficiency of downlink multi-user adaptive M-ary quadrature amplitude modulation (MQAM)/OFDMA CR systems. Given the received power restrictions on the STx in order to satisfy the primary network interference limit and the cognitive network power constraint, the STx transmit power is a function of the cognitive-cognitive direct-link and cognitive-primary cross-link fading states. We derive the cumulative distribution function (cdf) of the CR's received signal-to-interference-plus-noise ratio (SINR) to evaluate the average spectral efficiency of the adaptive MQAM/OFDMA CR system.

The main novelties and contributions of this work are summarized as follows:

1. The comprehensive problem of power, rate, and subcarrier allocation for enhancing the average spectral efficiency of downlink multi-user OFDMA CR systems subject to satisfying total average transmission power and peak aggregate interference constraint has been studied.

2. A closed-form expression for the cdf of the OFDMA CR's received SINR is derived under limitations imposed on the STx through the power and interference constraints. Consequently, an upper-bound expression for the average spectral efficiency of the adaptive multi-user MQAM/OFDMA CR system is formulated.

3. The critical issue of violating interference limits associated with imperfect cross-link CSI availability is examined by carrying out the analysis for the 'average case', 'worst case', and 'probabilistic case' scenarios of channel estimation error.

4. The impact of deterministic and probabilistic interference constraints on the system performance is considered with perfect and imperfect cross-link CSI. In particular, we propose a new low-complexity deterministic formulation for the probabilistic cross-link interference.

The organization of this chapter is as follows: Section II presents the network model and operation assumptions. In Section III, the resource allocation problem for enhancing average spectral efficiency of the adaptive multi-user MQAM/OFDMA under perfect cross-link CSI subject to power and deterministic interference constraints is developed. In Section IV, under noisy cross-link knowledge, the impact of 'average case' and 'worst case' of channel estimation error based on a posterior distribution of the perfect channel conditioned on its estimate is examined. Section V investigates the performance under a collision probability constraint with imperfect cross-link CSI and proposes a deterministic formulation of the probabilistic aggregate cross-link interference. In all of the RRAs derived in the chapter, optimal power, rate, and subcarrier assignments are obtained. Illustrative numerical results for various scenarios under consideration are provided in Section VI. Finally, concluding remarks are presented in Section VII.

2.2 System Model and Preliminaries

In this section, the multi-user OFDMA CR network model, wireless channel, and operational assumptions are introduced. Further, interference management schemes and spectral efficiency of the adaptive MQAM/OFDMA system under consideration are studied.

2.2.1 Network Architecture and Wireless Channel

We consider an underlay shared-spectrum environment, as shown in Fig. 2.1, where a cognitive network with a single STx and $n = 1, ..., N$ secondary receivers (SRx)s coexist with a primary network with a primary transmitter (PTx) and $m = 1, ..., M$ PRxs. The cognitive network can access a spectrum licensed to the primary network with a total bandwidth of B which is divided into K non-overlapping subchannels subject to not violating the imposed interference constraint set by a regulatory authority. The sub-channel bandwidth is assumed to be much smaller than the coherence bandwidth of the wireless channel, thus, each subcarrier experiences frequency-flat fading. Let $H^{ss}_{n,k}(t)$, $H^{ps}_{n,k}(t)$, and $H^{sp}_{m,k}(t)$, at time t, denote the chan-

nel gains over subchannel k from the STx to n^{th} SRx, PTx to n^{th} SRx, and STx to m^{th} PRx. The channel power gains $|H^{ss}_{n,k}(t)|^2$, $|H^{ps}_{n,k}(t)|^2$, and $|H^{sp}_{m,k}(t)|^2$ are assumed to be ergodic and stationary with continuous probability density functions (pdf)s $f_{|H^{ss}_{n,k}(t)|^2}(.)$, $f_{|H^{ps}_{n,k}(t)|^2}(.)$, and $f_{|H^{sp}_{m,k}(t)|^2}(.)$, respectively. In addition, the instantaneous values and distribution information of secondary-secondary channel power gains is assumed to be available at the STx [67]. In this work, we consider different cases with perfect and noisy cross-link knowledge between STx and PRxs.

Each sub-channel is assigned exclusively to at most one SRx at any given time, hence, there is no mutual interference between different cognitive users [69]. It should also be noted that by utilizing an appropriate cyclic prefix, the inter-symbol-interference (ISI) can be ignored [70]. The received SINR of cognitive user n over sub-channel k at time interval t is

$$\gamma_{n,k}(t) = \frac{P_{n,k}|H^{ss}_{n,k}(t)|^2}{\sigma_n^2 + \sigma_{ps}^2} \tag{2.1}$$

where $P_{n,k}$ is a fixed transmit power allocated to cognitive user n over sub-channel k, σ_n^2 is the noise power, and σ_{ps}^2 is the received power from the primary network. Without loss of generality, σ_n^2 and σ_{ps}^2 are assumed to be the same across all users and sub-channels [71,72]. For the sake of brevity, we henceforth omit the time reference t. Due to the impact of several factors, such as channel estimation error, feedback delay, and mobility, perfect cross-link information is not available. With noisy cross-link STx to PRxs knowledge, we model the inherent uncertainty in channel estimation in the following form

$$H^{sp}_{m,k} = \hat{H}^{sp}_{m,k} + \Delta H^{sp}_{m,k} \tag{2.2}$$

where over subcarrier k, $H^{sp}_{m,k}$ is the actual cross-link gain, $\hat{H}^{sp}_{m,k}$ is the channel estimation considered to be known, and $\Delta H^{sp}_{m,k}$ denotes the estimation error. $H^{sp}_{m,k}$, $\hat{H}^{sp}_{m,k}$, and $\Delta H^{sp}_{m,k}$ are assumed to be zero-mean complex Gaussian random variables with respective variances $\delta^2_{H^{sp}_{m,k}}$, $\delta^2_{\hat{H}^{sp}_{m,k}}$, and $\delta^2_{\Delta H^{sp}_{m,k}}$ [66, 73]. For robust receiver design, we consider the estimation $\hat{H}^{sp}_{m,k}$ and error $\Delta H^{sp}_{m,k}$ to be statistically correlated

random variables with a correlation factor $\rho = \sqrt{\delta^2_{\Delta H^{sp}_{m,k}} / (\delta^2_{\Delta H^{sp}_{m,k}} + \delta^2_{H^{sp}_{m,k}})}$, where $0 \leq \rho \leq 1$.

2.2.2 Interference Management

In a shared-spectrum environment, and particularly for delay-sensitive services, the licensed users' quality of service (QoS) is highly dependent on the instantaneous received SINRs of cognitive users. In order to protect the licensed spectrum from harmful interference we pose a deterministic peak total interference constraint between STx and primary users

$$\sum_{n=1}^{N} \sum_{k=1}^{K} \varphi_{n,k}(\gamma_{n,k}) P_{n,k}(\gamma_{n,k}) |H^{sp}_{m,k}|^2 \leq I^m_{th}, \forall m \in \{1, ..., M\} \tag{2.3}$$

where $\varphi_{n,k}(\gamma_{n,k})$ is the time-sharing factor (subcarrier allocation policy), $P_{n,k}(\gamma_{n,k})$ is the allocated transmit power, and I^m_{th} denotes the maximum tolerable interference threshold.

However, as a consequence of uncertainties about the shared-spectrum environment and primary service operation, it is unrealistic to assume that the STx always satisfies the deterministic peak total interference constraint. In practical scenarios, probability of violating the interference constraint is confined to a certain value that satisfies the minimum QoS requirements of primary users. The probabilistic interference constraint is particularly critical for robust interference management given noisy cross-link knowledge. To improve overall system performance and to mitigate the impact of channel estimation errors, the following allowable probabilistic interference limit violation is considered

$$\mathscr{P}\left(\sum_{n=1}^{N} \sum_{k=1}^{K} \varphi_{n,k}(\gamma_{n,k}) P_{n,k}(\gamma_{n,k}) |H^{sp}_{m,k}|^2 > I^m_{th}\right) \leq \epsilon^m$$
$$, \forall m \in \{1, ..., M\} \tag{2.4}$$

where $\mathscr{P}(.)$ denotes probability, and ϵ^m is the collision probability constraint of m^{th} PRx.

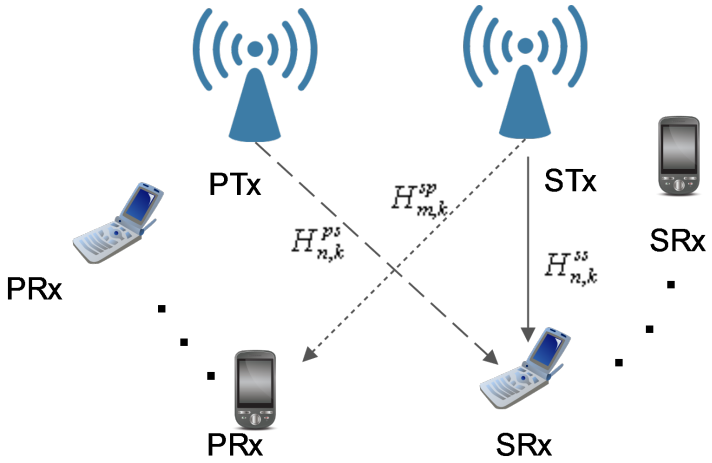

Figure 2.1: Schematic diagram of the shared-spectrum OFDMA system. For simplicity purposes, channels of a single cognitive user are drawn.

On the other hand, mitigating the interference between neighbouring cells is a vital issue due to the increasing frequency reuse aggressiveness in modern wireless communication systems [74]. As a remedy to inter-cell interference, and to maintain effective and efficient power consumption, we impose a total average transmit power constraint on the cognitive network as follows

$$\sum_{n=1}^{N}\sum_{k=1}^{K} E_{\gamma_{n,k}}\Big\{\varphi_{n,k}(\gamma_{n,k})P_{n,k}(\gamma_{n,k})\Big\} \leq P_t. \tag{2.5}$$

where $E_x(.)$ denotes the expectation with respect to x, and P_t denotes the total average transmit power limit.

2.2.3 Spectral Efficiency

The focus of this work is mainly on optimal power, rate, and subcarrier allocation for enhancing the average spectral efficiency of the adaptive MQAM/OFDMA CR network. In a multi-user scenario, various subcarriers may be allocated to different users. In other words, users may experience different channel fading conditions over each sub-channel. Therefore, any efficient resource allocation scheme in OFDMA must be based on the sub-channel quality of each user. Furthermore, in a shared-spectrum environment, satisfying the interference constraints is an important factor in allocating resources.

Employing square MQAM with Gray-coded bit mapping, the approximate instantaneous bit-error-rate (BER) expression for user n over subcarrier k is given by [70]

$$\xi^{b}_{n,k}(\gamma_{n,k}) = \frac{4}{\log_2(M_{n,k}(\gamma_{n,k}))}\left(1 - \frac{1}{\sqrt{M_{n,k}(\gamma_{n,k})}}\right) \times Q\left(\sqrt{\frac{3\gamma_{n,k}}{M_{n,k}(\gamma_{n,k}) - 1}}\right) \tag{2.6}$$

where $M_{n,k}(\gamma_{n,k})$ denotes the constellation size vector of MQAM which each element is a function of the instantaneous received SINR of the cognitive user n over subcarrier k, and $Q(.)$ represents the Gaussian Q-function. The aggregate average spectral efficiency (AASE) of the adaptive multi-user MQAM/OFDMA system per subcarrier per user over the fading channel is defined as

$$AASE = \sum_{n=1}^{N}\sum_{k=1}^{K} E_{\gamma_{n,k}}\Big\{ \log_2\left(M_{n,k}(\gamma_{n,k})\varphi_{n,k}(\gamma_{n,k})\right)\Big\}. \tag{2.7}$$

In order to evaluate the $AASE$, the distribution of the received SINR, a function of secondary-secondary and secondary-primary channels, must be developed.

2.3 Deterministic Interference Constraint with Perfect Cross-Link CSI

The objective of this work is to maximize the aggregate average spectral efficiency of cognitive users while satisfying total transmission power and peak maximum tolerable interference constraints. In this section, we solve the resource allocation problem with the perfect cross-link knowledge and deterministic interference constraint.

2.3.1 Problem Formulation

Mathematically, the optimization problem can be stated as follows.

Problem $\mathscr{O}_1$:

$$\max_{\varphi_{n,k}(\gamma_{n,k}),P_{n,k}(\gamma_{n,k})} \sum_{n=1}^{N}\sum_{k=1}^{K} E_{\gamma_{n,k}}\Big\{ \log_2(M_{n,k}(\gamma_{n,k}))\varphi_{n,k}(\gamma_{n,k})\Big\} \tag{2.8a}$$

$$\text{s. t.:} \quad \sum_{n=1}^{N}\sum_{k=1}^{K} E_{\gamma_{n,k}}\Big\{\varphi_{n,k}(\gamma_{n,k})P_{n,k}(\gamma_{n,k})\Big\} \leq P_t \tag{2.8b}$$

$$\sum_{n=1}^{N}\sum_{k=1}^{K} \varphi_{n,k}(\gamma_{n,k})P_{n,k}(\gamma_{n,k})|H_{m,k}^{sp}|^2 \leq I_{th}^{m}, \forall m \in \{1,...,M\} \tag{2.8c}$$

$$\sum_{n=1}^{N} \varphi_{n,k}(\gamma_{n,k}) = 1, \forall k \in \{1,...,K\} \tag{2.8d}$$

$$\varphi_{n,k}(\gamma_{n,k}) \in \{0,1\}, \forall n \in \{1,...,N\}, \forall k \in \{1,...,K\} \tag{2.8e}$$

$$\xi_{n,k}^{b}(\gamma_{n,k}) \leq \xi, \forall n \in \{1,...,N\}, \forall k \in \{1,...,K\} \tag{2.8f}$$

where ξ denotes the common BER-target.

In the adaptive multi-user MQAM/OFDMA CR system under consideration, different transmit power and constellation sizes are allocated to different users and subcarriers. Using the upper-bound expression for the Gaussian Q-function, i.e., $Q(x) \leq (1/2)\exp(-x^2/2)$, the instantaneous BER for user n over subcarrier k, subject to an instantaneous constraint $\xi_{n,k}^{b}(\gamma_{n,k}) = \xi$ can be expressed as

$$\xi_{n,k}^{b}(\gamma_{n,k}) \leq 0.3\exp\left(\frac{-1.5\gamma_{n,k}}{M_{n,k}(\gamma_{n,k})-1}\frac{P_{n,k}(\gamma_{n,k})}{\min\left(\frac{P_t}{K},\frac{I_{th}^{m}}{N_m^{sp}}\right)}\right). \tag{2.9}$$

where $N_m^{sp} = \sum_{k=1}^{K}|H_{m,k}^{sp}|^2$. With further manipulation, for a BER-target ξ, the maximum constellation size for user n over subcarrier k is obtained as

$$M_{n,k}^{*}(\gamma_{n,k}) = 1 + \frac{\zeta\gamma_{n,k}P_{n,k}(\gamma_{n,k})}{\min\left(\frac{P_t}{K},\frac{I_{th}^{m}}{N_m^{sp}}\right)} \tag{2.10}$$

where

$$\zeta = \frac{-1.5}{\ln(\xi/0.3)}. \tag{2.11}$$

According the constraints (2.8b) and (2.8c) in the optimization problem $\mathscr{O}_1$, the

cumulative density function (cdf) of $\gamma_{n,k}$ can be written

$$F_{\gamma_{n,k}}(\Gamma) = \mathscr{P}\left(\frac{P_t|H^{ss}_{n,k}|^2}{K(\sigma_n^2+\sigma_{ps}^2)} \leq \Gamma, \frac{I^m_{th}|H^{ss}_{n,k}|^2}{N^{sp}_m(\sigma_n^2+\sigma_{ps}^2)} \leq \Gamma\right). \tag{2.12}$$

The probability expression in (2.12) can be further simplified by considering the cases $\frac{P_t|H^{ss}_{n,k}|^2}{K(\sigma_n^2+\sigma_{ps}^2)} \underset{>}{\leq} \frac{I^m_{th}|H^{ss}_{n,k}|^2}{N^{sp}_m(\sigma_n^2+\sigma_{ps}^2)}$ and conditioning on N^{sp}_m

$$\begin{aligned} &1-\mathscr{P}\left(\frac{P_t|H^{ss}_{n,k}|^2}{K(\sigma_n^2+\sigma_{ps}^2)} > \Gamma, \frac{I^m_{th}|H^{ss}_{n,k}|^2}{N^{sp}_m(\sigma_n^2+\sigma_{ps}^2)} > \Gamma\right) = \\ &1-\begin{cases} \mathscr{P}\left(|H^{ss}_{n,k}|^2 > \dfrac{K\Gamma(\sigma_n^2+\sigma_{ps}^2)}{P_t}\right) & N^{sp}_m \leq \dfrac{I^m_{th}K}{P_t} \\ \mathscr{P}\left(|H^{ss}_{n,k}|^2 > \dfrac{N^{sp}_m\Gamma(\sigma_n^2+\sigma_{ps}^2)}{I^m_{th}}\right) & N^{sp}_m > \dfrac{I^m_{th}K}{P_t}. \end{cases} \end{aligned} \tag{2.13}$$

Lemma 1: For large values of K, given complex Gaussian random variables $H^{sp}_{m,k}$ with means $\mu_{H^{sp}_{m,k}}$ and equal variance $\delta^2_{H^{sp}_{m,k}}$ for all $k \in \{1,...,K\}$, the non-central Chi-square random variable $N^{sp}_m = \sum_{k=1}^K |H^{sp}_{m,k}|^2$ can be approximated as a Gaussian random variable with respective mean and variance $\mu_{N^{sp}_m} = \delta^2_{H^{sp}_{m,k}}\left[2K+\mu'\right]$ and $\delta^2_{N^{sp}_m} = \delta^4_{H^{sp}_{m,k}}\left[4K+4\mu'\right]$, where $\mu' = \sum_{k=1}^K (\frac{\mu_{H^{sp}_{m,k}}}{\delta_{H^{sp}_{m,k}}})^2$.

Proof 1: We can write $H^{sp}_{m,k} = \delta_{H^{sp}_{m,k}} G^{sp}_{m,k}$, where $G^{sp}_{m,k} \sim CN(\frac{\mu_{H^{sp}_{m,k}}}{\delta_{H^{sp}_{m,k}}}, 1)$. Assuming equal variance for random variables $H^{sp}_{m,k}$, $\sum_{k=1}^K |G^{sp}_{m,k}|^2$ is a non-central Chi-Square random variable with degree of freedom $2K$ and non-centrality parameter $\mu' = \sum_{k=1}^K (\frac{\mu_{H^{sp}_{m,k}}}{\delta_{H^{sp}_{m,k}}})^2$. For large values of K, central limit theorem (CLT) can be invoked to show that the non-central Chi-Square random variable $\sum_{k=1}^K |G^{sp}_{m,k}|^2$, can be approximated as a Gaussian random variable as follows

$$\sum_{k=1}^K |G^{sp}_{m,k}|^2 \sim N\left(2K+\mu', 4K+4\mu'\right). \tag{2.14}$$

Hence, $N_m^{sp} = \sum_{k=1}^{K} |H_{m,k}^{sp}|^2$ can be approximated by

$$N_m^{sp} = \sum_{k=1}^{K} |H_{m,k}^{sp}|^2 \sim N\left(\mu_{N_m^{sp}}, \delta_{N_m^{sp}}^2\right) \tag{2.15}$$

where $\mu_{N_m^{sp}} = \delta_{H_{m,k}^{sp}}^2 \left[2K + \mu^{'}\right]$ and $\delta_{N_m^{sp}}^2 = \delta_{H_{m,k}^{sp}}^4 \left[4K + 4\mu^{'}\right]$. Denoting the pdf of N_m^{sp} with $f_{N_m^{sp}}(.)$, and the cdfs of $|H_{n,k}^{ss}|^2$ and N_m^{sp} with $F_{|H_{n,k}^{ss}|^2}(.)$ and $F_{N_m^{sp}}(.)$, respectively, we write the cdf of $\gamma_{n,k}$ as

$$F_{\gamma_{n,k}}(\Gamma) = 1 - A - B, \tag{2.16}$$

$$\begin{aligned}
A =& \int_0^{\frac{I_{th}^m K}{P_t}} \mathscr{P}\left(|H_{n,k}^{ss}|^2 > \frac{K\Gamma(\sigma_n^2 + \sigma_{ps}^2)}{P_t}\right) f_{N_m^{sp}}(N_m^{sp}) dN_m^{sp} \\
=& \mathscr{P}\left(|H_{n,k}^{ss}|^2 > \frac{K\Gamma(\sigma_n^2 + \sigma_{ps}^2)}{P_t}\right) \int_0^{\frac{I_{th}^m K}{P_t}} f_{N_m^{sp}}(N_m^{sp})\, dN_m^{sp} \\
=& \mathscr{P}\left(|H_{n,k}^{ss}|^2 > \frac{K\Gamma(\sigma_n^2 + \sigma_{ps}^2)}{P_t}\right) \mathscr{P}\left(N_m^{sp} \leq \frac{I_{th}^m K}{P_t}\right) \\
=& \left(1 - F_{|H_{ss}|^2}\left(\frac{K\Gamma(\sigma_n^2 + \sigma_{ps}^2)}{P_t}\right)\right) F_{N_m^{sp}}\left(\frac{I_{th}^m K}{P_t}\right)
\end{aligned} \tag{2.17}$$

and

$$B = \int_{\frac{I_{th}^m K}{P_t}}^{\infty} \mathscr{P}\left(|H_{n,k}^{ss}|^2 > \frac{N_m^{sp}\Gamma(\sigma_n^2 + \sigma_{ps}^2)}{I_{th}^m}\right) f_{N_m^{sp}}(N_m^{sp})\, dN_m^{sp}. \tag{2.18}$$

Recall that the cdf of a Normally-distributed random variable X with mean μ and standard deviation σ is given by $F_X(x) = \frac{1}{2}\left[1 + erf\left(\frac{x-\mu}{2\sigma^2}\right)\right]$, and the cdf of an Exponentially-distributed random variable Y is computed by $F_Y(y) = 1 - e^{-y/\mu}$, where μ is the mean. Suppose that $|H_{n,k}^{ss}|^2$ follows an exponential distribution with mean $\mu_{|H_{n,k}^{ss}|^2}$, hence, the integrals in (2.17) and (2.18) can be simplified to (2.19) and (2.21), respectively. Finally, a closed-form expression for cdf of $\gamma_{n,k}$ is developed in (2.22). Trivially, through respective differentiation of (2.22), the pdf of $\gamma_{n,k}$ is obtained in (2.23).

$$A = \frac{1}{2}\exp\left(\frac{-K\Gamma(\sigma_n^2+\sigma_{ps}^2)}{P_t\mu_{|H_{n,k}^{ss}|^2}}\right)\left[1+erf\left(\frac{\frac{I_{th}^m K}{P_t}-\mu_{N_m^{sp}}}{\sqrt{2\delta_{N_m^{sp}}^2}}\right)\right] \tag{2.19}$$

$$B = \int_{\frac{I_{th}^m K}{P_t}}^{\infty} \frac{\exp\left(\frac{-N_m^{sp}\Gamma(\sigma_n^2+\sigma_{ps}^2)}{\mu_{|H_{n,k}^{ss}|^2 I_{th}^m}}\right)\exp\left(\frac{-(N_m^{sp}-\mu_{N_m^{sp}})^2}{2\delta_{N_m^{sp}}^2}\right)}{\sqrt{2\pi\delta_{N_m^{sp}}^2}} dN_m^{sp} \approx \tag{2.20}$$

$$\frac{1}{2}\exp\left(\frac{\Gamma(\sigma_n^2+\sigma_{ps}^2)(-2\mu_{N_m^{sp}}\mu_{|H_{n,k}^{ss}|^2}I_{th}^m+\delta_{N_m^{sp}}^2\Gamma(\sigma_n^2+\sigma_{ps}^2))}{2\mu_{H_{n,k}^{ss}}^2 I_{th}^{m2}}\right)$$

$$\left[1-erf\left(\frac{\mu_{|H_{n,k}^{ss}|^2}I_{th}^m\left(-\mu_{N_m^{sp}}+\frac{I_{th}^m K}{P_t}\right)+\delta_{N_m^{sp}}^2\Gamma(\sigma_n^2+\sigma_{ps}^2)}{\sqrt{2}\mu_{|H_{n,k}^{ss}|^2}I_{th}^m\delta_{N_m^{sp}}}\right)\right]. \tag{2.21}$$

$$F_{\gamma_{n,k}}(\Gamma) \approx 1-\frac{1}{2}\exp\left(\frac{-K\Gamma(\sigma_n^2+\sigma_{ps}^2)}{P_t\mu_{|H_{n,k}^{ss}|^2}}\right)\left[1+erf\left(\frac{\frac{I_{th}^m K}{P_t}-\mu_{N_m^{sp}}}{\sqrt{2\delta_{N_m^{sp}}^2}}\right)\right]$$

$$-\frac{1}{2}\exp\left(\frac{\Gamma(\sigma_n^2+\sigma_{ps}^2)(-2\mu_{N_m^{sp}}\mu_{|H_{n,k}^{ss}|^2}I_{th}^m+\delta_{N_m^{sp}}^2\Gamma(\sigma_n^2+\sigma_{ps}^2))}{2\mu_{H_{n,k}^{ss}}^2 I_{th}^{m2}}\right)$$

$$\left[1-erf\left(\frac{\mu_{|H_{n,k}^{ss}|^2}I_{th}^m\left(-\mu_{N_m^{sp}}+\frac{I_{th}^m K}{P_t}\right)+\delta_{N_m^{sp}}^2\Gamma(\sigma_n^2+\sigma_{ps}^2)}{\sqrt{2}\mu_{|H_{n,k}^{ss}|^2}I_{th}^m\delta_{N_m^{sp}}}\right)\right]. \tag{2.22}$$

$$f_{\gamma_{n,k}}(\Gamma) \approx \frac{K(\sigma_n^2+\sigma_{ps}^2)\exp\left(-\frac{K\Gamma(\sigma_n^2+\sigma_{ps}^2)}{P_t\mu_{|H_{n,k}^{ss}|^2}}\right)\left(erf\left(\frac{\frac{I_{th}^m K}{P_t}-\mu_{N_m^{sp}}}{\sqrt{2\delta_{N_m^{sp}}^2}}\right)+1\right)}{2P_t\mu_{|H_{n,k}^{ss}|^2}}$$

$$+\frac{(\sigma_n^2+\sigma_{ps}^2)\delta_{N_m^{sp}}\exp\left(-\frac{I_{th}^{m2}K^2\mu_{|H_{n,k}^{ss}|^2}-2I_{th}^m K\mu_{N_m^{sp}}\mu_{|H_{n,k}^{ss}|^2}P_t+2K(\sigma_n^2+\sigma_{ps}^2)P_t\delta_{N_m^{sp}}\Gamma+\mu_{N_m^{sp}}^2\mu_{|H_{n,k}^{ss}|^2}P_t^2}{2\mu_{|H_{n,k}^{ss}|^2}P_t^2\delta_{N_m^{sp}}}\right)}{\sqrt{2\pi}I_{th}^m\mu_{|H_{n,k}^{ss}|^2}}$$

$$-\frac{0.5(\sigma_n^2+\sigma_{ps}^2)(I_{th}^m\mu_{N_m^{sp}}\mu_{|H_{n,k}^{ss}|^2}-(\sigma_n^2+\sigma_{ps}^2)\delta_{N_m^{sp}}\Gamma)}{I_{th}^{m2}\mu_{|H_{n,k}^{ss}|^2}^2}$$

$$\times\exp\left(\frac{(\sigma_n^2+\sigma_{ps}^2)\Gamma((\sigma_n^2+\sigma_{ps}^2)\delta_{N_m^{sp}}\Gamma-2I_{th}^m\mu_{N_m^{sp}}\mu_{|H_{n,k}^{ss}|^2})}{2I_{th}^{m2}\mu_{|H_{n,k}^{ss}|^2}{}^2}\right)$$

$$\times\left(erf\left(\frac{\left(I_{th}^m\mu_{|H_{n,k}^{ss}|^2}\left(\frac{I_{th}^m K}{P_t}-\mu_{N_m^{sp}}\right)+(\sigma_n^2+\sigma_{ps}^2)\delta_{N_m^{sp}}\Gamma\right)}{\sqrt{2\delta_{N_m^{sp}}^2}I_{th}^m\mu_{|H_{n,k}^{ss}|^2}}\right)-1\right) \tag{2.23}$$

2.3.2 Obtaining Solutions

It can be observed that the optimization problem, $\mathscr{O}_1$, is convex with respect to the transmit power $P_{n,k}(\gamma_{n,k})$, however, it is non-convex with respect to $\varphi_{n,k}(\gamma_{n,k})$ as the time-sharing factor only takes binary values. To obtain a sub-optimal solution for problem $\mathscr{O}_1$, we employ the Lagrangian dual decomposition algorithm. By applying dual decomposition, the non-convex optimization problem, $\mathscr{O}_1$, is decomposed into independent sub-problems each corresponding to a given cognitive user.

The Lagrangian function of problem $\mathscr{O}_1$ is expressed as[1]

$$
\begin{aligned}
&L\Bigg(\varphi_{n,k}(\gamma_{n,k}), P_{n,k}(\gamma_{n,k}), \lambda(\gamma_{n,k}), \mu, \eta(\gamma_{n,k})\Bigg) = \\
&\sum_{k=1}^{K}\sum_{n=1}^{N} E_{\gamma_{n,k}}\left\{\log_2\left(1+\frac{\zeta\gamma_{n,k}P_{n,k}(\gamma_{n,k})}{\min\left(\frac{P_t}{K},\frac{I_{th}^m}{N_m^{sp}}\right)}\right)\varphi_{n,k}(\gamma_{n,k})\right\} \\
&-\sum_{k=1}^{K}\sum_{\gamma_{n,k}}\lambda_k(\gamma_{n,k})\left(\sum_{n=1}^{N}\varphi_{n,k}(\gamma_{n,k})-1\right) \\
&-\mu\left(\sum_{k=1}^{K}\sum_{n=1}^{N}E_{\gamma_{n,k}}\Big\{\varphi_{n,k}(\gamma_{n,k})P_{n,k}(\gamma_{n,k})\Big\}-P_t\right) \\
&-\sum_{\gamma_{n,k}}\eta(\gamma_{n,k})\left(\sum_{k=1}^{K}\sum_{n=1}^{N}\varphi_{n,k}(\gamma_{n,k})P_{n,k}(\gamma_{n,k})|H_{m,k}^{sp}|^2-I_{th}^m\right)
\end{aligned}
\tag{2.24}
$$

where μ, $\eta(\gamma_{n,k})$, and $\lambda_k(\gamma_{n,k})$ are the non-negative Lagrangian multipliers. Define

$$
\begin{aligned}
&l\Bigg(\varphi_{n,k}(\gamma_{n,k}), P_{n,k}(\gamma_{n,k}), \lambda(\gamma_{n,k}), \mu, \eta(\gamma_{n,k})\Bigg) = \\
&\sum_{k=1}^{K}\sum_{n=1}^{N}\log_2\left(1+\frac{\zeta\gamma_{n,k}P_{n,k}(\gamma_{n,k})}{\min\left(\frac{P_t}{K},\frac{I_{th}^m}{N_m^{sp}}\right)}\right)\varphi_{n,k}(\gamma_{n,k})f_{\gamma_{n,k}}(\gamma_{n,k}) \\
&-\sum_{k=1}^{K}\lambda_k(\gamma_{n,k})\left(\sum_{n=1}^{N}\varphi_{n,k}(\gamma_{n,k})-1\right) \\
&-\mu\left(\sum_{k=1}^{K}\sum_{n=1}^{N}\varphi_{n,k}(\gamma_{n,k})P_{n,k}(\gamma_{n,k})f_{\gamma_{n,k}}(\gamma_{n,k})\right)
\end{aligned}
$$

[1]For simplicity, the analysis is carried out for a single primary receiver.

$$- \eta(\gamma_{n,k}) \left(\sum_{k=1}^{K} \sum_{n=1}^{N} \varphi_{n,k}(\gamma_{n,k}) P_{n,k}(\gamma_{n,k}) |H_{m,k}^{sp}|^2 \right). \tag{2.25}$$

Note that the variation of the Lagrangian function, (2.24) with respect to the optimization parameters, $\varphi_{n,k}(\gamma_{n,k})$ and $P_{n,k}(\gamma_{n,k})$, is equal to zero if and only if the derivative of $l\left(\varphi_{n,k}(\gamma_{n,k}), P_{n,k}(\gamma_{n,k}), \lambda(\gamma_{n,k}), \mu, \eta(\gamma_{n,k})\right)$ with respect to $\varphi_{n,k}(\gamma_{n,k})$ and $P_{n,k}(\gamma_{n,k})$ is equal to zero [75].

Based on the Karush-Kuhn-Tucker (KKT) necessary conditions theorem [76], the optimum solutions $\left(P_{n,k}^{*}(\gamma_{n,k}), \varphi_{n,k}^{*}(\gamma_{n,k})\right)$ must satisfy the following conditions:

$$\frac{\partial l(\varphi_{n,k}(\gamma_{n,k}), P_{n,k}(\gamma_{n,k}), \lambda(\gamma_{n,k}), \mu, \eta(\gamma_{n,k}))}{\partial P_{n,k}(\gamma_{n,k})} \begin{cases} = 0, \ P_{n,k}(\gamma_{n,k}) > 0 \\ < 0, \ P_{n,k}(\gamma_{n,k}) = 0 \end{cases} \tag{2.26}$$

$$\frac{\partial l(\varphi_{n,k}(\gamma_{n,k}), P_{n,k}(\gamma_{n,k}), \lambda(\gamma_{n,k}), \mu, \eta(\gamma_{n,k}))}{\partial \varphi_{n,k}(\gamma_{n,k})} \begin{cases} < 0, \ \varphi_{n,k}(\gamma_{n,k}) = 0 \\ = 0, \ \varphi_{n,k}(\gamma_{n,k}) \in (0,1) \\ > 0, \ \varphi_{n,k}(\gamma_{n,k}) = 1 \end{cases} \tag{2.27}$$

$$\lambda_k(\gamma_{n,k}) \left(\sum_{n=1}^{N} \varphi_{n,k}(\gamma_{n,k}) - 1 \right) = 0 \tag{2.28}$$

$$\mu \left(\sum_{k=1}^{K} \sum_{n=1}^{N} E_{\gamma_{n,k}} \left\{ \varphi_{n,k}(\gamma_{n,k}) P_{n,k}(\gamma_{n,k}) \right\} - P_t \right) = 0 \tag{2.29}$$

$$\eta(\gamma_{n,k}) \left(\sum_{k=1}^{K} \sum_{n=1}^{N} \varphi_{n,k}(\gamma_{n,k}) P_{n,k}(\gamma_{n,k}) |H_{m,k}^{sp}|^2 - I_{th}^{m} \right) = 0 \tag{2.30}$$

The Lagrangian dual optimization problem associated with (2.24) is given by

$$\min_{\lambda(\gamma_{n,k}), \mu, \eta(\gamma_{n,k})} \left(F\left(\lambda(\gamma_{n,k}), \mu, \eta(\gamma_{n,k})\right) \ , \text{s.t.:} \, \lambda(\gamma_{n,k}), \mu, \eta(\gamma_{n,k}) \geq 0 \right. \tag{2.31}$$

where $F(\lambda(\gamma_{n,k}), \mu, \eta(\gamma_{n,k}))$ denotes the Lagrangian dual function formulated below

$$\begin{aligned} F(\lambda(\gamma_{n,k}), \mu, \eta(\gamma_{n,k})) = & \sum_{n=1}^{N} f_n(\varphi_{n,k}(\gamma_{n,k}), P_{n,k}(\gamma_{n,k})) + \sum_{k=1}^{K} \sum_{\gamma_{n,k}} \lambda_k(\gamma_{n,k}) \\ & + \mu P_t + \sum_{\gamma_{n,k}} \eta(\gamma_{n,k}) I_{th}^{m} \end{aligned} \tag{2.32}$$

where

$$f_n(\varphi_{n,k}(\gamma_{n,k}), P_{n,k}(\gamma_{n,k})) =$$
$$\max_{\varphi_{n,k}(\gamma_{n,k}), P_{n,k}(\gamma_{n,k})} \Bigg(\sum_{k=1}^{K} E_{\gamma_{n,k}} \Bigg\{ \log_2 \Bigg(1 + \frac{\zeta \gamma_{n,k} P_{n,k}(\gamma_{n,k})}{\min\left(\frac{P_t}{K}, \frac{I_{th}^m}{N_m^{sp}}\right)} \Bigg) \varphi_{n,k}(\gamma_{n,k}) \Bigg\}$$
$$- \sum_{k=1}^{K} \sum_{\gamma_{n,k}} \lambda_k(\gamma_{n,k}) \varphi_{n,k}(\gamma_{n,k}) - \mu \sum_{k=1}^{K} E_{\gamma_{n,k}} \Big\{ \varphi_{n,k}(\gamma_{n,k}) P_{n,k}(\gamma_{n,k}) \Big\}$$
$$- \sum_{\gamma_{n,k}} \eta(\gamma_{n,k}) \sum_{k=1}^{K} \varphi_{n,k}(\gamma_{n,k}) P_{n,k}(\gamma_{n,k}) |H_{m,k}^{sp}|^2 \Bigg). \tag{2.33}$$

To find the optimum solution of problem (2.33), we differentiate $l\Bigg(\varphi_{n,k}(\gamma_{n,k}), P_{n,k}(\gamma_{n,k}), \lambda(\gamma_{n,k}), \mu, \eta(\gamma_{n,k}) \Bigg)$ with respect to $\varphi_{n,k}(\gamma_{n,k}) P_{n,k}(\gamma_{n,k})$

$$\frac{\partial l\Bigg(\varphi_{n,k}(\gamma_{n,k}), P_{n,k}(\gamma_{n,k}), \lambda(\gamma_{n,k}), \mu, \eta(\gamma_{n,k}) \Bigg)}{\partial (\varphi_{n,k}(\gamma_{n,k}) P_{n,k}(\gamma_{n,k}))} = \frac{\frac{\zeta \gamma_{n,k}}{\min\left(\frac{P_t}{K}, \frac{I_{th}^m}{N_m^{sp}}\right)} f_{\gamma_{n,k}}(\gamma_{n,k})}{\ln(2) \left(1 + \frac{\zeta \gamma_{n,k} P_{n,k}(\gamma_{n,k})}{\min\left(\frac{P_t}{K}, \frac{I_{th}^m}{N_m^{sp}}\right)} \right)}$$
$$- \mu f_{\gamma_{n,k}}(\gamma_{n,k}) - \eta(\gamma_{n,k}) |H_{m,k}^{sp}|^2. \tag{2.34}$$

Applying the KKT conditions yields the optimal potential power allocation policy for Lagrangian multipliers μ and $\eta(\gamma_{n,k})$

$$P_{n,k}^*(\gamma_{n,k}) = \left[\frac{f_{\gamma_{n,k}}(\gamma_{n,k})}{\ln(2)(\mu f_{\gamma_{n,k}}(\gamma_{n,k}) + \eta(\gamma_{n,k}) |H_{m,k}^{sp}|^2)} - \frac{\min\left(\frac{P_t}{K}, \frac{I_{th}^m}{N_m^{sp}}\right)}{\zeta \gamma_{n,k}} \right]^+ \tag{2.35}$$

where $[x]^+ \triangleq \max\{x, 0\}$. The solution in (2.35) can be considered as a multi-level water-filling algorithm where each subcarrier has a distinct water-level for a given user. Note that the water levels determine the potential optimum amount of power that may be allocated to n^{th} SRx over subcarrier k. The result in (2.35) can be used to find the optimal subcarrier allocation strategy. By differentiating

$l\left(\varphi_{n,k}(\gamma_{n,k}), P_{n,k}(\gamma_{n,k}), \lambda(\gamma_{n,k}), \mu, \eta(\gamma_{n,k})\right)$ with respect to $\varphi_{n,k}(\gamma_{n,k})$ we have

$$\frac{\partial l\left(\varphi_{n,k}(\gamma_{n,k}), P_{n,k}(\gamma_{n,k}), \lambda(\gamma_{n,k}), \mu, \eta(\gamma_{n,k})\right)}{\partial \varphi_{n,k}(\gamma_{n,k})} = \frac{\frac{\zeta \gamma_{n,k} P^*_{n,k}(\gamma_{n,k})}{\min\left(\frac{P_t}{K}, \frac{I^m_{th}}{N^{sp}_m}\right)} f_{\gamma_{n,k}}(\gamma_{n,k})}{\ln(2)\left(1 + \frac{\zeta \gamma_{n,k} P^*_{n,k}(\gamma_{n,k})}{\min\left(\frac{P_t}{K}, \frac{I^m_{th}}{N^{sp}_m}\right)}\right)}$$

$$+ \frac{\ln\left(1 + \frac{\zeta \gamma_{n,k} P^*_{n,k}(\gamma_{n,k})}{\min\left(\frac{P_t}{K}, \frac{I^m_{th}}{N^{sp}_m}\right)}\right) f_{\gamma_{n,k}}(\gamma_{n,k})}{\ln(2)} - \lambda_k(\gamma_{n,k}). \tag{2.36}$$

By substituting the optimal power policy (2.35) in (2.36) and by applying the KKT conditions, the optimal subcarrier allocation problem is formulated as:

$$n^* = argmax(\Lambda(\gamma_{n,k}))\ ,\ \forall n \in \{1, ..., N\}\ ,\ \forall k \in \{1, ..., K\} \tag{2.37}$$

where n^* is the optimal SRx index, and

$$\Lambda(\gamma_{n,k}) =$$

$$\frac{\frac{\zeta \gamma_{n,k} n,k P^*_{n,k}(\gamma_{n,k})}{\min\left(\frac{P_t}{K}, \frac{I^m_{th}}{N^{sp}_m}\right)} f_{\gamma_{n,k}}(\gamma_{n,k})}{\ln(2)\left(1 + \frac{\zeta \gamma_{n,k} n,k P^*_{n,k}(\gamma_{n,k})}{\min\left(\frac{P_t}{K}, \frac{I^m_{th}}{N^{sp}_m}\right)}\right)} + \frac{\ln\left(1 + \frac{\zeta \gamma_{n,k} n,k P^*_{n,k}(\gamma_{n,k})}{\min\left(\frac{P_t}{K}, \frac{I^m_{th}}{N^{sp}_m}\right)}\right) f_{\gamma_{n,k}}(\gamma_{n,k})}{\ln(2)}. \tag{2.38}$$

The optimal subcarrier allocation policy is therefore achieved by assigning the k^{th} subcarrier to the user with the highest value of $\Lambda(\gamma_{n,k})$ for all corresponding $\gamma_{n,k}$. To ensure optimality, $\lambda_k(\gamma_{n,k})$ should be between first and second maxima of $\Lambda(\gamma_{n,k})$. If there are multiple equal maxima, the time-slot can be identically shared among the respective users. Substituting (2.35) and (2.38) in (2.33), derives $f_n(\varphi_{n,k}(\gamma_{n,k}), P_{n,k}(\gamma_{n,k}))$, therefore, the solution for (2.32) can be obtained. To compute the solution for the non-differentiable dual problem in (2.31), different optimization algorithms can be applied, including subgradient, ellipsoid, and cutting-plane.

Algorithm 1: Subgradient-based method; $AASE^*$, $M^*_{n,k}(\gamma_{n,k})$, $\varphi^*_{n,k}(\gamma_{n,k})$, and $P^*_{n,k}(\gamma_{n,k})$, are the optimal values of $AASE$, $M_{n,k}(\gamma_{n,k})$, $\varphi_{n,k}(\gamma_{n,k})$, and $P_{n,k}(\gamma_{n,k})$, respectively.

1. Assign initial values to $\lambda_k(\gamma_{n,k})$, μ, $\eta(\gamma_{n,k})$, τ_1^i, and τ_2^i, $\forall n \in \{1, ..., N\}$, and $\forall k \in \{1, ..., K\}$, respectively.
2. Calculate $P_{n,k}(\gamma_{n,k})$ and $\varphi_{n,k}(\gamma_{n,k})$, $\forall n \in \{1, ..., N\}$, and $\forall k \in \{1, ..., K\}$, using (2.35) and (2.37), respectively.
3. Update $\lambda_k(\gamma_{n,k})$, μ, $\eta(\gamma_{n,k})$, τ_1^i, and τ_2^i, for any $n \in \{1, ..., N\}$, and $k \in \{1, ..., K\}$, according to (2.39) and (2.40).
4. Repeat steps 2 and 3 until convergence.
5. Determine $P^*_{n,k}(\gamma_{n,k})$ and $\varphi^*_{n,k}(\gamma_{n,k})$, using (2.35) and (2.37), respectively.
6. Based on the obtained results from step 5, calculate $M^*_{n,k}(\gamma_{n,k})$ using (2.10), hence, compute $AASE^*$ according to (2.7).

In this work, we use the subgradient-based method to update the values of the coefficients $\lambda_k(\gamma_{n,k})$, μ, and $\eta(\gamma_{n,k})$, in order to determine the optimal solution to (2.31).

The subgradient method has been widely used for solving Lagrangian relaxation problems. The master problem sets the user resource allocation prices, and in order to update the dual variables, in every iteration of the subgradient method, the algorithm repeatedly finds the maximizing assignment for the sub-problems individually. For any optimal pair of $(\varphi^*_{n,k}(\gamma_{n,k}), P^*_{n,k}(\gamma_{n,k}))$, the dual variables of the problem (2.32) are updated using the following iterations

$$\mu^{i+1} = \mu^i - \tau_1^i \left(P_t - \sum_{n=1}^{N} \sum_{k=1}^{K} E_{\gamma_{n,k}} \left\{ \varphi^*_{n,k}(\gamma_{n,k}) P^*_{n,k}(\gamma_{n,k}) \right\} \right) \tag{2.39}$$

$$\eta^{i+1}(\gamma_{n,k}) = \eta^i(\gamma_{n,k}) - \tau_2^i \times \left(I^m_{th} - \sum_{n=1}^{N} \sum_{k=1}^{K} \varphi^*_{n,k}(\gamma_{n,k}) P^*_{n,k}(\gamma_{n,k}) |H^{sp}_{m,k}|^2 \right) \tag{2.40}$$

where for the iteration number i, τ_1^i and τ_2^i are the step sizes. The initial values of dual multipliers and step size selection are important towards obtaining the optimal solution, and can greatly affect the optimization problem convergence.

The potential optimum continuous-rate adaptive constellation size vector for user n over subcarrier k is written as

$$M^*_{n,k}(\gamma_{n,k}) = \max\left(1, \frac{\zeta\gamma_{n,k} f_{\gamma_{n,k}}(\gamma_{n,k})}{\ln(2)\min\left(\frac{P_t}{K}, \frac{I^m_{th}}{N^{sp}_m}\right)\left(\mu f_{\gamma_{n,k}}(\gamma_{n,k}) + \eta(\gamma_{n,k})|H^{sp}_{m,k}|^2\right)}\right). \tag{2.41}$$

Note that the aforementioned expression serves as an upper-bound for practical scenarios where only discrete-valued constellation sizes are applicable. Nevertheless, the real-valued $M^*_{n,k}(\gamma_{n,k})$ in (2.41) may be truncated to the nearest integer. The corresponding maximum aggregate average spectral efficiency of the adaptive MQAM/OFDMA system is thus derived below

$$AASE^* = \sum_{n=1}^{N}\sum_{k=1}^{K} E_{\gamma_{n,k}}\left\{\log_2\left[\max\left(1, \frac{\zeta\gamma_{n,k} f_{\gamma_{n,k}}(\gamma_{n,k})}{\ln(2)\min\left(\frac{P_t}{K}, \frac{I^m_{th}}{N^{sp}_m}\right)\left(\mu f_{\gamma_{n,k}}(\gamma_{n,k}) + \eta(\gamma_{n,k})|H^{sp}_{m,k}|^2\right)}\right)\right]\varphi^*_{n,k}(\gamma_{n,k})\right\}. \tag{2.42}$$

According to (2.41), no transmission takes place, i.e., $M^*_{n,k}(\gamma_{n,k}) = 1$, when $P^*_{n,k}(\gamma_{n,k}) = 0$. Consequently, the optimized cut-off threshold, dictated by the channel quality, power constraint, and interference constraint, is given by: $\gamma_{th} = \frac{\ln(2)(\mu+\eta(\gamma_{n,k})|H^m_{sp}|^2)}{\zeta}$.

2.4 Interference Constraint with Average Case/ Worst Case Imperfect Cross-Link CSI

Due to technical reasons such as estimation errors and wireless channel delay, perfect channel information is not available. In shared-spectrum environments, controlling the interference on the primary receivers is highly dependent on the accuracy of the cross-service channel estimation. Here, we assume that imperfect cross-link knowledge between STx and PRxs is available at the secondary transmitter. The interference management at the cognitive base station is based on the noisy estimation of STx and PRx channel-to-noise-plus-interference ratio (CINR) by $\hat{H}^{sp}_{m,k}$

in (2.2). As previously mentioned, by considering the 'correlated case' of the estimation $\hat{H}^{sp}_{m,k}$ and error $\Delta H^{sp}_{m,k}$ random variables, we derive a *posterior* distribution of the actual channel conditioned on its estimate, to facilitate robust and reliable interference management.

The maximum achievable aggregate spectral efficiency in bits per second per Hertz (bps/Hz), for the cognitive radio system operating under peak aggregate interference constraint and total average transmit power constraint, for a given BER-target quality, with noisy cross-link CSI, is the solution to the following optimization problem.

Problem $\mathscr{O}_2$:

$$\max_{\varphi_{n,k}(\gamma_{n,k}),P_{n,k}(\gamma_{n,k})} \sum_{n=1}^{N}\sum_{k=1}^{K} E_{\gamma_{n,k}|\hat{h}^{sp}}\Big\{ \log_2(M_{n,k}(\gamma_{n,k}))\varphi_{n,k}(\gamma_{n,k})\Big\} \tag{2.43a}$$

$$\text{s. t.:} \quad \text{constraints in (2.8b), (2.8d), (2.8e), and (2.8f),}$$

$$\sum_{n=1}^{N}\sum_{k=1}^{K} \varphi_{n,k}(\gamma_{n,k})P_{n,k}(\gamma_{n,k})|H^{sp}_{m,k}|\hat{H}^{sp}_{m,k}|^2 \leq I^m_{th}, \forall m \in \{1,...,M\} \tag{2.43b}$$

where $\hat{h}^{sp}$ is defined as a vector containing $\hat{H}^{sp}_{m,k}$ of all time intervals. The objective of this section is to devise an estimation framework by employing a posteriori pdf of the channel estimation error given the channel estimation. This general framework enables us to formulate the 'average case' and 'worst case' scenarios of the channel estimation error.

2.4.1 Analysis for the Average Case of Estimation Error

Proposition 1: Given $\hat{H}^{sp}_{m,k}$ and $\Delta H^{sp}_{m,k}$ are statistically correlated random variables with a correlation factor $\rho = \sqrt{\delta^2_{\Delta H^{sp}_{m,k}}/(\delta^2_{\Delta H^{sp}_{m,k}} + \delta^2_{H^{sp}_{m,k}})}$, where $0 \leq \rho \leq 1$, hence, $cov(\hat{H}^{sp}_{m,k}, \Delta H^{sp}_{m,k}) = \delta^2_{\Delta H^{sp}_{m,k}}$ [1]. The posterior distribution of $\Delta H^{sp}_{m,k}$ given $\hat{H}^{sp}_{m,k}$ is a complex Gaussian random variable with respective mean and variance of

$$\mu_{\Delta H^{sp}_{m,k}|\hat{H}^{sp}_{m,k}} = E_{\Delta H^{sp}_{m,k}|\hat{H}^{sp}_{m,k}}(\Delta H^{sp}_{m,k}|\hat{H}^{sp}_{m,k})$$

[1] $var(x)$ denotes the variance of x and $cov(y,z)$ is defined as the covariance of y and z.

$$= E_{\Delta H^{sp}_{m,k}}(\Delta H^{sp}_{m,k}) + \frac{cov(\Delta H^{sp}_{m,k}, \hat{H}^{sp}_{m,k})}{\delta^2_{\Delta H^{sp}_{m,k}} + \delta^2_{H^{sp}_{m,k}}}$$
$$\times \left(\hat{H}^{sp}_{m,k} - E_{\hat{H}^{sp}_{m,k}}(\hat{H}^{sp}_{m,k}) \right) = \rho^2 \hat{H}^{sp}_{m,k} \tag{2.44}$$

and

$$\begin{aligned} \delta^2_{\Delta H^{sp}_{m,k}|\hat{H}^{sp}_{m,k}} &= var(\Delta H^{sp}_{m,k}|\hat{H}^{sp}_{m,k}) \\ &= \delta^2_{\Delta H^{sp}_{m,k}} \left[1 - \frac{cov^2(\Delta H^{sp}_{m,k}, \hat{H}^{sp}_{m,k})}{\delta^2_{\Delta H^{sp}_{m,k}} \delta^2_{\hat{H}^{sp}_{m,k}}} \right] \\ &= (1-\rho^2)\delta^2_{\Delta H^{sp}_{m,k}}. \end{aligned} \tag{2.45}$$

Using (2.2), the interference constraint in (2.43b) for the 'average case' of estimation error can be written as

$$\sum_{n=1}^{N} \sum_{k=1}^{K} \varphi_{n,k}(\gamma_{n,k}) P_{n,k}(\gamma_{n,k})$$
$$\times \left(|\hat{H}^{sp}_{m,k} + \Delta H^{sp}_{m,k}|\hat{H}^{sp}_{m,k}| \right)^2 \leq I^m_{th}. \tag{2.46}$$

With further analysis, the above is reduced to

$$\sum_{n=1}^{N} \sum_{k=1}^{K} \varphi_{n,k}(\gamma_{n,k}) P_{n,k}(\gamma_{n,k})$$
$$\left(|\hat{H}^{sp}_{m,k}|\hat{H}^{sp}_{m,k} + \Delta H^{sp}_{m,k}|\hat{H}^{sp}_{m,k}| \right)^2 \leq I^m_{th} \tag{2.47}$$

where $\hat{H}^{sp}_{m,k}|\hat{H}^{sp}_{m,k}$ is a constant. Thus, by substituting the expectation in (2.44), we have

$$\sum_{n=1}^{N} \sum_{k=1}^{K} \varphi_{n,k}(\gamma_{n,k}) P_{n,k}(\gamma_{n,k}) \left(|\hat{H}^{sp}_{m,k} + \rho^2 \hat{H}^{sp}_{m,k}| \right)^2 \leq I^m_{th}. \tag{2.48}$$

By adopting a similar approach to that in the previous section, we employ the Lagrangian dual optimization method to obtain $AASE^*$ for the 'average case' scenario. The potential optimum power allocation policy for user n and subcarrier k is

given by

$$P^*_{n,k}(\gamma_{n,k}) = \left[\frac{f_{\gamma_{n,k}}(\gamma_{n,k})}{\ln(2)(\mu f_{\gamma_{n,k}}(\gamma_{n,k}) + \eta(\gamma_{n,k})|\hat{H}^{sp}_{m,k}(1+\rho^2)|^2)} - \frac{\min\left(\frac{P_t}{K}, \frac{I^m_{th}}{N^{sp}_m}\right)}{\zeta\gamma_{n,k}}\right]^+ \tag{2.49}$$

where in the 'average case', $N^{sp}_m = \sum_{k=1}^{K}(|\hat{H}^{sp}_{m,k}(1+\rho^2|)^2$. The optimal subcarrier allocation policy is the solution to the following problem

$$n^* = argmax(\Lambda(\gamma_{n,k}))\ ,\ \forall n \in \{1,...,N\}\ ,\ \forall k \in \{1,...,K\} \tag{2.50}$$

where n^* is the optimal SRx index, and

$$\Lambda(\gamma_{n,k}) = \frac{\frac{\zeta\gamma_{n,k}P^*_{n,k}(\gamma_{n,k})}{\min\left(\frac{P_t}{K}, \frac{I^m_{th}}{N^{sp}_m}\right)} f_{\gamma_{n,k}}(\gamma_{n,k})}{\ln(2)\left(1 + \frac{\zeta\gamma_{n,k}P^*_{n,k}(\gamma_{n,k})}{\min\left(\frac{P_t}{K}, \frac{I^m_{th}}{N^{sp}_m}\right)}\right)} + \frac{\ln\left(1 + \frac{\zeta\gamma_{n,k}P^*_{n,k}(\gamma_{n,k})}{\min\left(\frac{P_t}{K}, \frac{I^m_{th}}{N^{sp}_m}\right)}\right) f_{\gamma_{n,k}}(\gamma_{n,k})}{\ln(2)}. \tag{2.51}$$

Subsequently, the optimal continuous-rate solution for the constellation size of user n over subcarrier k is derived

$$M^*_{n,k}(\gamma_{n,k}) = \max\left(1, \frac{\zeta\gamma_{n,k}f_{\gamma_{n,k}}(\gamma_{n,k})}{\ln(2)(\min\left(\frac{P_t}{K}, \frac{I^m_{th}}{N^{sp}_m}\right))(\mu f_{\gamma_{n,k}}(\gamma_{n,k}) + \eta(\gamma_{n,k})|\hat{H}^{sp}_{m,k}(1+\rho^2)|^2)}\right). \tag{2.52}$$

Hence, the following maximum aggregate average spectral efficiency for the spectrum-sharing system under imperfect cross-link CSI knowledge for the 'average case' of estimation error can be achieved based on the optimal power, rate, and subcarrier allocation policies

$$AASE^* = \sum_{n=1}^{N}\sum_{k=1}^{K} E_{\gamma_{n,k}|\hat{h}^{n,k}}\left\{\log_2\left[\max\left(1,\right.\right.\right.$$

$$\frac{\zeta\gamma_{n,k}f_{\gamma_{n,k}}(\gamma_{n,k})}{\ln(2)\min\left(\frac{P_t}{K},\frac{I_{th}^m}{N_m^{sp}}\right)\left(\mu f_{\gamma_{n,k}}(\gamma_{n,k})+\eta(\gamma_{n,k})|\hat{H}_{m,k}^{sp}(1+\rho^2)|^2\right)}\Bigg)\Bigg]\varphi_{n,k}^*(\gamma_{n,k})\Bigg\}. \quad (2.53)$$

2.4.2 Analysis for the Worst Case of Estimation Error

To derive the interference constraint for the worst case scenario, we must obtain a formulation for the upper-bound of $\Delta H_{m,k}^{sp}$. Recall that $\Delta H_{m,k}^{sp}$ is a Gaussian random variable. Therefore, we proceed by bounding the channel estimation error with a certain probability. By employing the Chebyshev's inequality, for any $Y > 0$, we have

$$\underbrace{\mathscr{P}\left(|\Delta H_{m,k}^{sp}|\hat{H}_{m,k}^{sp}| \leq \Omega\right)}_{pr} \geq 1 - \frac{1}{Y^2} \quad (2.54)$$

where

$$\begin{aligned}\Omega = & E_{\Delta H_{m,k}^{sp}|\hat{H}_{m,k}^{sp}}(\Delta H_{m,k}^{sp}|\hat{H}_{m,k}^{sp}) \\ & + Y\sqrt{var(\Delta H_{m,k}^{sp}|\hat{H}_{m,k}^{sp})}. \end{aligned} \quad (2.55)$$

With further manipulation, for a given probability of error, pr, the following holds

$$\Omega = \sqrt{\frac{var(\Delta H_{m,k}^{sp}|\hat{H}_{m,k}^{sp})}{1-pr}} + E_{\Delta H_{m,k}^{sp}|\hat{H}_{m,k}^{sp}}(\Delta H_{m,k}^{sp}|\hat{H}_{m,k}^{sp}). \quad (2.56)$$

The interference constraint for the 'worst case' scenario of estimation error is expressed as

$$\sum_{n=1}^{N}\sum_{k=1}^{K}\varphi_{n,k}(\gamma_{n,k})P_{n,k}(\gamma_{n,k})|\hat{H}_{m,k}^{sp} + \Omega|^2 \leq I_{th}^m. \quad (2.57)$$

Utilizing one-level dual decomposition method, and by applying KKT conditions, the optimum adaptive power allocation scheme for user n over subcarrier k is derived as

$$P_{n,k}^*(\gamma_{n,k}) =$$

$$\left[\frac{f_{\gamma_{n,k}}(\gamma_{n,k})}{\ln(2)(\mu f_{\gamma_{n,k}}(\gamma_{n,k})+\eta(\gamma_{n,k})|\hat{H}^{sp}_{m,k}+\Omega|^2)}-\frac{\min\left(\frac{P_t}{K},\frac{I^m_{th}}{N^{sp}_m}\right)}{\zeta\gamma_{n,k}}\right]^+ \tag{2.58}$$

where in the 'worst case', $N^{sp}_m=\sum_{k=1}^{K}|\hat{H}^{sp}_{m,k}+\Omega|^2$. To derive the optimal subcarrier allocation policy, the following maximization problem is formulated

$$n^*=argmax(\Lambda(\gamma_{n,k}))\ ,\ \forall n\in\{1,...,N\}\ ,\ \forall k\in\{1,...,K\} \tag{2.59}$$

where the optimal cognitive user index, n^*, can be obtained by substituting (2.58) in (2.51) and thus solving the optimization problem in (2.59). The optimal continuous-rate solution for the constellation size of user n over subcarrier k is derived

$$M^*_{n,k}(\gamma_{n,k})= \max\left(1,\frac{\zeta\gamma_{n,k}f_{\gamma_{n,k}}(\gamma_{n,k})}{\ln(2)\min\left(\frac{P_t}{K},\frac{I^m_{th}}{N^{sp}_m}\right)(\mu f_{\gamma_{n,k}}(\gamma_{n,k})+\eta(\gamma_{n,k})|\hat{H}^{sp}_{m,k}+\Omega|^2)}\right). \tag{2.60}$$

The maximum aggregate average spectral efficiency for the adaptive MQAM/OFDMA system under imperfect cross-link CSI availability for the 'worst case' of estimation error with a given probability of error, pr, is expressed as

$$AASE^*=\sum_{n=1}^{N}\sum_{k=1}^{K}E_{\gamma_{n,k}|\hat{h}^{n,k}}\left\{\log_2\left[\max\left(1,\right.\right.\right. \frac{\zeta\gamma_{n,k}f_{\gamma_{n,k}}(\gamma_{n,k})}{\ln(2)\min\left(\frac{P_t}{K},\frac{I^m_{th}}{N^{sp}_m}\right)(\mu f_{\gamma_{n,k}}(\gamma_{n,k})+\eta(\gamma_{n,k})|\hat{H}^{sp}_{m,k}+\Omega|^2)}\left.\left.\left.\right)\right]\varphi^*_{n,k}(\gamma_{n,k})\right\}. \tag{2.61}$$

2.5 Probabilistic Interference Constraint

In a practical spectrum-sharing system, the collision tolerable level is confined by a maximum collision probability allowed by the licensed network. The collision tolerable level is highly dependent on the primary service type. For example, in case of real-time video streaming, a high collision probability is not desirable, however, delay-insensitive services can tolerate higher packet loss rates. In this section, we consider an underlay spectrum-sharing scenario where the primary users can toler-

ate a maximum collision probability ε^m, $\forall m \in \{1, ..., M\}$. We derive optimal power, rate, and subcarrier allocation algorithms for the multi-user OFDMA CR system under noisy cross-link CSI availability subject to satisfying the imposed peak aggregate power and collision probability constraints. The maximization problem can be formulated as follows.

Problem $\mathscr{O}_3$:

$$\max_{\varphi_{n,k}(\gamma_{n,k}), P_{n,k}(\gamma_{n,k})} \sum_{n=1}^{N} \sum_{k=1}^{K} E_{\gamma_{n,k}|\hat{h}^{sp}} \Big\{ \log_2(M_{n,k}(\gamma_{n,k})) \varphi_{n,k}(\gamma_{n,k}) \Big\} \tag{2.62a}$$

$$\text{s. t.:} \quad \text{constraints in (2.8b), (2.8d), (2.8e), and (2.8f),}$$

$$\mathscr{P}\left(\sum_{n=1}^{N} \sum_{k=1}^{K} \varphi_{n,k}(\gamma_{n,k}) P_{n,k}(\gamma_{n,k}) |H^{sp}_{m,k}| \hat{H}^{sp}_{m,k}|^2 > I^m_{th} \right) \leq \epsilon^m$$

$$, \forall m \in \{1, ..., M\} \tag{2.62b}$$

We proceed by deriving a posterior distribution of the actual cross-link given the estimated channel gains.

Proposition 2: The posterior distribution of the actual channel $H^{sp}_{m,k}$ given the estimation $\hat{H}^{sp}_{m,k}$ is a complex Gaussian random variable with respective mean and variance of

$$\begin{aligned} \mu_{H^{sp}_{m,k}|\hat{H}^{sp}_{m,k}} &= E_{H^{sp}_{m,k}|\hat{H}^{sp}_{m,k}} (\hat{H}^{sp}_{m,k} + \Delta H^{sp}_{m,k} | \hat{H}^{sp}_{m,k}) \\ &= E_{\hat{H}^{sp}_{m,k}|\hat{H}^{sp}_{m,k}} (\hat{H}^{sp}_{m,k} | \hat{H}^{sp}_{m,k}) \\ &+ E_{\Delta H^{sp}_{m,k}|\hat{H}^{sp}_{m,k}} (\Delta H^{sp}_{m,k} | \hat{H}^{sp}_{m,k}) = (1+\rho^2) \hat{H}^{sp}_{m,k} \end{aligned} \tag{2.63}$$

and

$$\begin{aligned} \delta^2_{H^{sp}_{m,k}|\hat{H}^{sp}_{m,k}} &= var(\hat{H}^{sp}_{m,k} + \Delta H^{sp}_{m,k} | \hat{H}^{sp}_{m,k}) \\ &= var(\hat{H}^{sp}_{m,k} | \hat{H}^{sp}_{m,k}) + var(\Delta H^{sp}_{m,k} | \hat{H}^{sp}_{m,k}) \\ &+ 2cov(\Delta H^{sp}_{m,k} | \hat{H}^{sp}_{m,k}, \hat{H}^{sp}_{m,k} | \hat{H}^{sp}_{m,k}) \\ &= (1-\rho^2) \delta^2_{\Delta H^{sp}_{m,k}}. \end{aligned} \tag{2.64}$$

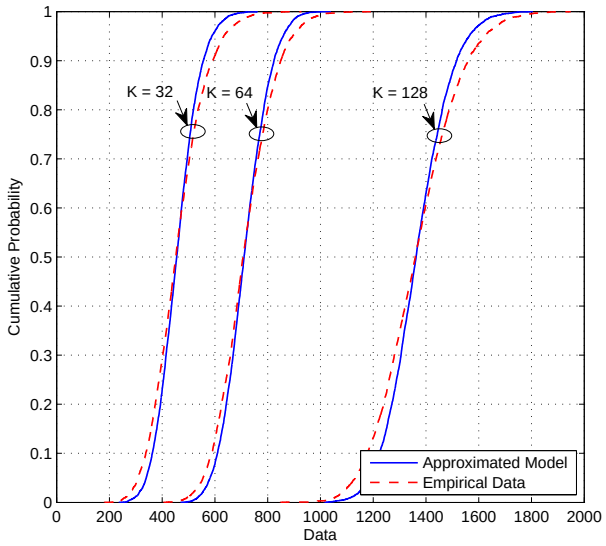

Figure 2.2: PApproximated Model and Empirical Data cdfs, obtained from Monte-Carlo simulations. System parameters are: $\beta_k^m \sim$ Chi-Square$(2,2)$, $\delta^2_{H^{sp}_{m,k}|\hat{H}^{sp}_{m,k}} = 1$.

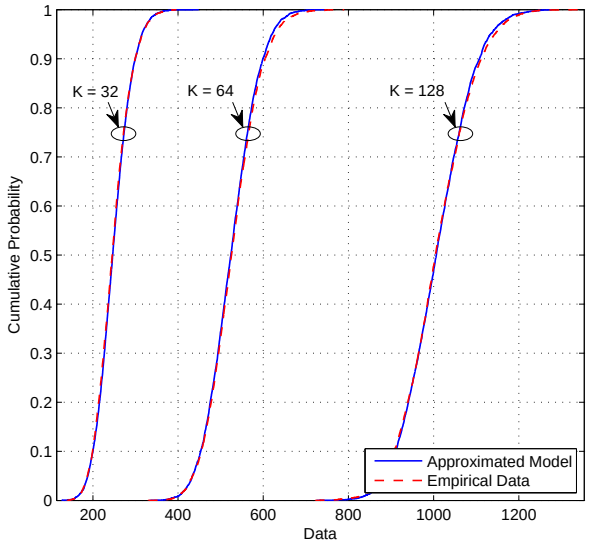

Figure 2.3: Approximated Model and Empirical Data cdfs, obtained from Monte-Carlo simulations. System parameters are: $\beta_k^m \sim$ Gamma$(2, 0.5, 4)$, $\delta^2_{H^{sp}_{m,k}|\hat{H}^{sp}_{m,k}} = 0.5$.

Assuming equal variance $\delta^2_{H^{sp}_{m,k}|\hat{H}^{sp}_{m,k}}$ across all users and subcarriers, the collision probability constraint in (2.62b) can be expressed as

$$\mathscr{P}\left(\delta^2_{H^{sp}_{m,k}|\hat{H}^{sp}_{m,k}} \sum_{n=1}^{N}\sum_{k=1}^{K} \varphi_{n,k}(\gamma_{n,k}) P_{n,k}(\gamma_{n,k}) |\Xi^m[k]|^2 > I^m_{th}\right) \leq \varepsilon^m \qquad (2.65)$$

where $\Xi^m[k]$ is a complex Gaussian random variable with variance of one and mean of

$$\mu_{\Xi^m[k]} = \left| \frac{\mu_{H^{sp}_{m,k}|\hat{H}^{sp}_{m,k}}}{\delta_{H^{sp}_{m,k}|\hat{H}^{sp}_{m,k}}} \right|^2. \tag{2.66}$$

It should be noted that in contrast to the sum of equal-weighted Chi-Square random variables in Lemma 1, (2.65) includes a sum of non-equal-weighted Chi-Square random variables. In general, obtaining the exact distribution of the linear combination of weighted Chi-Square random variables is rather complex. Although several approximations have been proposed in the literature, e.g., [77–79], most are not easy to implement. In this work, we propose a simple approximation based on the moments of $\delta^2_{H^{sp}_{m,k}|\hat{H}^{sp}_{m,k}} \sum_{n=1}^{N}\sum_{k=1}^{K}\varphi_{n,k}(\gamma_{n,k})P_{n,k}(\gamma_{n,k})|\Xi^m[k]|^2$. Consider the following equality

$$\delta^2_{H^{sp}_{m,k}|\hat{H}^{sp}_{m,k}} \sum_{n=1}^{N}\sum_{k=1}^{K}\varphi_{n,k}(\gamma_{n,k})P_{n,k}(\gamma_{n,k})|\Xi^m[k]|^2 = \sum_{k=1}^{K}\beta^m_k|\Xi^m[k]|^2 \tag{2.67}$$

where $\beta^m_k = \sum_{n=1}^{N} \delta^2_{H^{sp}_{m,k}|\hat{H}^{sp}_{m,k}} \varphi_{n,k}(\gamma_{n,k})P_{n,k}(\gamma_{n,k})$.

Proposition 3: The distribution of the sum of non-equal-weighted non-central Chi-Square random variables, i.e., $\sum_{k=1}^{K}\beta^m_k|\Xi^m[k]|^2$, is similar to that of a weighted non-central Chi-Square-distributed random variable $\xi\chi^2_D(\delta')$, where δ', D, and ξ are respectively the non-centrality parameter, degree of freedom, and weight of the new random variable:

$$\delta' = \sum_{k=1}^{K}\mu_{\Xi^m[k]} \tag{2.68}$$

$$D = 2K \tag{2.69}$$

$$\xi = \frac{\sum_{k=1}^{K}\beta^m_k(2+\mu_{\Xi^m[k]})}{2K+\sum_{k=1}^{K}\mu_{\Xi^m[k]}}. \tag{2.70}$$

To investigate the above similarity, or the accuracy of the proposed approximation, we compare the cdf of the proposed Chi-Square distribution with that of (2.67), using Monte-Carlo simulations. The results in Fig. 2.2 and Fig. 2.3 illustrate that the approximation is accurate over a wide range of practical values for K over

randomly-distributed - e.g., Chi-Square or Gamma - weights β_k^m. Now (2.65) can be simplified to:

$$\mathscr{P}\left(\delta^2_{H^{sp}_{m,k}|\hat{H}^{sp}_{m,k}} \sum_{n=1}^{N}\sum_{k=1}^{K} \varphi_{n,k}(\gamma_{n,k}) P_{n,k}(\gamma_{n,k}) |\Xi^m[k]|^2 > I^m_{th}\right)$$
$$\approx Pr(\xi \chi^2_D(\delta^{'}) > I^m_{th}). \tag{2.71}$$

According to [79], since the non-centrality parameter is small relative to the degree of freedom, we can approximate the non-central Chi-Square distribution with a central one using the following

$$\mathscr{P}(\xi \chi^2_D(\delta^{'}) > I^m_{th}) \approx \mathscr{P}(\chi^2_D(0) > \frac{I^m_{th}/\xi}{1+\delta^{'}/D}). \tag{2.72}$$

The right hand side (RHS) of (2.72) can be formulated using the upper Gamma function [80] as

$$\mathscr{P}(\chi^2_D(0) > \frac{I^m_{th}/\xi}{1+\delta^{'}/D}) = \frac{\Gamma(K, \frac{I^m_{th}/\xi}{2(1+\delta^{'}/D)})}{\Gamma(K)} \tag{2.73}$$

where $\Gamma(.,.)$ is the upper incomplete Gamma function, and $\Gamma(.)$ is the complete Gamma function.

Proposition 4: For all integer values $K \neq 1$, and all positive $\frac{I^m_{th}/\xi}{1+\delta^{'}/D}$ - this condition is always true because, I^m_{th}, $\delta^{'}$ β^m_k, and K are positive; consequently, ξ, $\delta^{'}$, and D are also positive - the deterministic inequality

$$\delta^2_{H^{sp}_{m,k}|\hat{H}^{sp}_{m,k}} \sum_{k=1}^{K}(2+\mu_{\Xi^m[k]}) \sum_{n=1}^{N} \varphi_{n,k}(\gamma_{n,k}) P_{n,k}(\gamma_{n,k})$$
$$\leq \frac{K\, I^m_{th}}{(K!)^{1/K} \ln\left(1-(1-\varepsilon^m)^{1/K}\right)} \tag{2.74}$$

satisfies the probabilistic inequality (2.65). Therefore, the constraint (2.65) can be replaced by (2.74).

Proof: The proof is given in the Appendix A.

To obtain $AASE^*$ for the probabilistic interference constraint and 'probabilis-

tic case' of estimation error scenario, we employ the Lagrangian dual optimization method as in the previous sections, where

$$\alpha_k = \delta^2_{H^{sp}_{m,k}|\hat{H}^{sp}_{m,k}}(2 + \mu_{\Xi^m[k]}) \tag{2.75}$$

and

$$\overline{I^m_{th}} = \frac{K\, I^m_{th}}{(K!)^{1/K} \ln\left(1 - (1-\varepsilon^m)^{1/K}\right)}. \tag{2.76}$$

Therefore, by solving the Lagrangian optimization problem the following potential optimal power allocation solution can be obtained for user n over subcarrier k

$$P^*_{n,k}(\gamma_{n,k}) = \left[\frac{f_{\gamma_{n,k}}(\gamma_{n,k})}{\ln(2)(\mu f_{\gamma_{n,k}}(\gamma_{n,k}) + \eta(\gamma_{n,k})\alpha_k)} - \frac{\min\left(\frac{P_t}{K}, \frac{\overline{I^m_{th}}}{\hat{N}^{sp}_m}\right)}{\zeta\gamma_{n,k}}\right]^+ \tag{2.77}$$

where $\hat{N}^{sp}_m$ in the 'probabilistic case' is derived in Appendix A, Section C. The optimal subcarrier allocation policy is the solution to the following problem

$$n^* = argmax(\Lambda(\gamma_{n,k}))\ ,\ \forall n \in \{1, ..., N\}\ ,\ \forall k \in \{1, ..., K\} \tag{2.78}$$

where n^* is the optimal SRx index, and

$$\Lambda(\gamma_{n,k}) = \frac{\frac{\zeta\gamma_{n,k}P^*_{n,k}(\gamma_{n,k})}{\min\left(\frac{P_t}{K}, \frac{\overline{I^m_{th}}}{\hat{N}^{sp}_m}\right)} f_{\gamma_{n,k}}(\gamma_{n,k})}{\ln(2)\left(1 + \frac{\zeta\gamma_{n,k}P^*_{n,k}(\gamma_{n,k})}{\min\left(\frac{P_t}{K}, \frac{\overline{I^m_{th}}}{\hat{N}^{sp}_m}\right)}\right)} + \frac{\ln\left(1 + \frac{\zeta\gamma_{n,k}P^*_{n,k}(\gamma_{n,k})}{\min\left(\frac{P_t}{K}, \frac{\overline{I^m_{th}}}{\hat{N}^{sp}_m}\right)}\right) f_{\gamma_{n,k}}(\gamma_{n,k})}{\ln(2)}. \tag{2.79}$$

By employing the sub-gradient method in Algorithm 1, the Lagrangian multipliers μ and $\eta(\gamma_{n,k})$ can be updated by

$$\mu^{i+1} = \mu^i - \tau^i_1\left(P_t - \sum_{n=1}^{N}\sum_{k=1}^{K} \varphi^*_{n,k}(\gamma_{n,k})P^*_{n,k}(\gamma_{n,k})\right) \tag{2.80}$$

$$\eta^{i+1}(\gamma_{n,k}) = \eta^{i}(\gamma_{n,k}) - \tau_2^i$$
$$\times \left(\overline{I_{th}^m} - \delta^2_{H^{sp}_{m,k}|\hat{H}^{sp}_{m,k}} \sum_{k=1}^{K} (2+\mu_{\Xi[k]}) \sum_{n=1}^{N} \varphi^*(\gamma_{n,k}) P^*_{n,k}(\gamma_{n,k}) \right). \quad (2.81)$$

Subsequently, optimal expressions are derived for the constellation size and hence aggregate spectral efficiency under collision probability constraint and imperfect cross-link CSI:

$$M^*_{n,k}(\gamma_{n,k}) = \max\left(1, \frac{\zeta \gamma_{n,k} f_{\gamma_{n,k}}(\gamma_{n,k})}{\ln(2)\min\left(\frac{P_t}{K}, \frac{\overline{I_{th}^m}}{\hat{N}_m^{sp}}\right)(\mu f_{\gamma_{n,k}}(\gamma_{n,k}) + \eta(\gamma_{n,k})\alpha_k)}\right), \quad (2.82)$$

$$AASE^* = \sum_{n=1}^{N}\sum_{k=1}^{K}\sum_{\gamma_{n,k}|\hat{h}^{n,k}} \left\{ \log_2 \left[\max\left(1, \right.\right.\right.$$
$$\left.\left.\left. \frac{\zeta \gamma_{n,k} f_{\gamma_{n,k}}(\gamma_{n,k})}{\ln(2)\min\left(\frac{P_t}{K}, \frac{\overline{I_{th}^m}}{\hat{N}_m^{sp}}\right)(\mu f_{\gamma_{n,k}}(\gamma_{n,k}) + \eta(\gamma_{n,k})\alpha_k)} \right) \right] \varphi^*_{n,k}(\gamma_{n,k}) \right\}. \quad (2.83)$$

The methodologies for deriving the expressions of the cdf of the received SINR given the estimation, for different 'average case', 'worst case', and 'probabilistic case' scenarios of estimation error, are elucidated in Appendix B.

2.6 Discussion of Results

In this section, we examine the performance of the OFDMA CR network operating under total average transmit power and deterministic/probabilistic peak aggregate interference constraints with perfect/imperfect cross-channel estimation using the respective optimal resource allocation solutions. In the following results, perfect CSI knowledge of the cognitive user link is assumed to be available at the STx through an error-free feedback channel. Thus, $|H^{ss}_{n,k}|$, $\forall\{n,k\}$, are drawn through a Rayleigh distribution. Further, the secondary-secondary power gain mean values, $\mu_{|H^{ss}_{n,k}|^2}$, $\forall\{n,k\}$, are taken as Uniformly-distributed random variables within 0 to 2. It should be noted that the sub-channels are assumed to be narrow-enough so that they experience frequency-flat fading. Interfering cross-channel values, $H^{sp}_{m,k}$,

$\forall\{m,k\}$, are distributed according to a complex Gaussian distribution with mean 0.05 and variance 0.1. For the inaccurate cross-link CSI case, the channel estimation and error for all sub-channels are taken as independent and identically distributed (i.i.d.) zero-mean Normally-distributed random variables. In addition, the AWGN power spectral density is set to -174 dBm. The total average power constraint is imposed on the system in all cases. Discrete-rate cases with real-valued MQAM signal constellations, i.e., $\log_2(M) \in \{2,4,6,8,10\}$ bits/symbol, are also considered for practical scenarios. All results correspond to the scenario with three secondary receivers and a single primary receiver, hence, the subscript m is hereafter omitted.

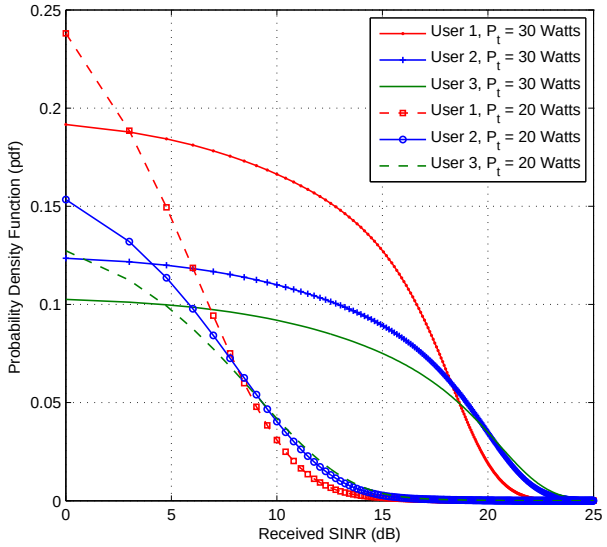

Figure 2.4: Probability density functions of the received SINR for OFDMA users in a given subcarrier k under different average power constraint values. System parameters are: $K = 64$, $k = 16$, $I_{th} = 5$ Watts.

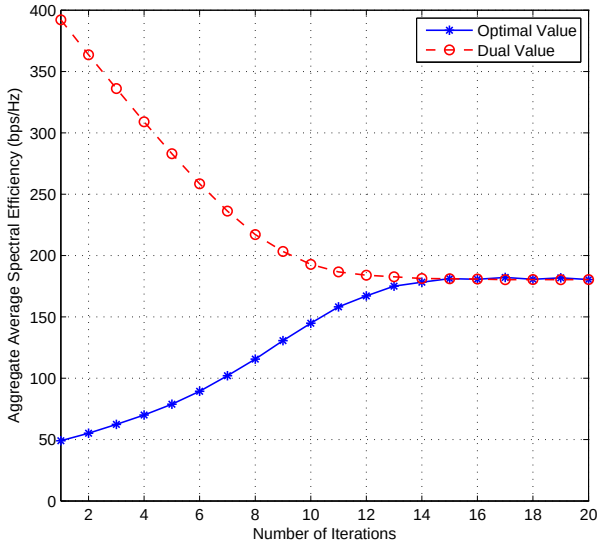

Figure 2.5: Optimal and dual values versus the number of iterations using the sub-gradient method. Results for the case with deterministic interference constraint and perfect cross-link CSI knowledge. System parameters are: $K = 64$, $P_t = 30$ Watts, $I_{th} = 10$ Watts, $\xi = 10^{-2}$.

The approximated probability distributions of the received SINRs for cognitive users in a randomly taken subcarrier, i.e., here $k = 16$, under different total average power constraint limits P_t is plotted in Fig. 2.4. For a fixed interference constraint of $I_{th} = 5$ Watts, it can be observed that the probability of higher received SINR improves as the value of P_t increases. For example, for user 3, the probability of receiving $\gamma_{3,16} = 10$ dB is 54.5% higher as the value of P_t is increased from 20 to 30 Watts.

Fig. 2.5 illustrates the evolution of the optimal and dual values using the sub-gradient method over time. The results correspond to the maximum deliverable AASE for the case with deterministic interference constraint and perfect cross-link CSI knowledge. The iterative sub-gradient algorithm converges quickly and typically achieves a lower-bound at 96.5% of the optimal value within 12 iterations. It can easily be shown that the proposed dual decomposition algorithm converges fast for different parameters of system settings.

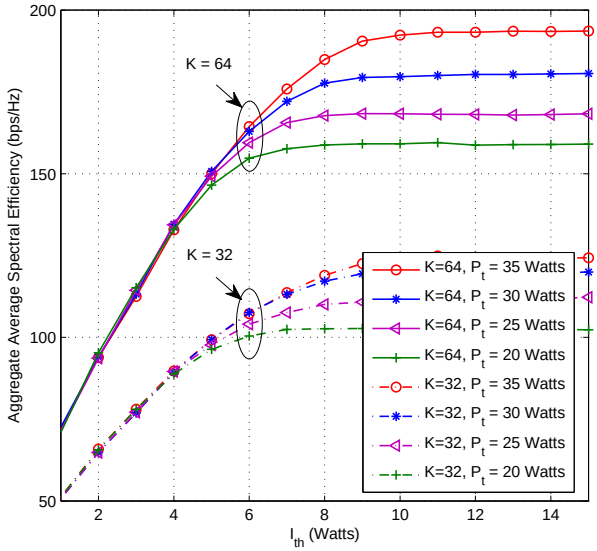

Figure 2.6: AASE performance versus the tolerable interference power threshold level with different values of P_t and K. Results for the case with deterministic interference constraint and perfect cross-link CSI knowledge. System parameters are: $I_{th} = 10$ Watts, $\xi = 10^{-2}$.

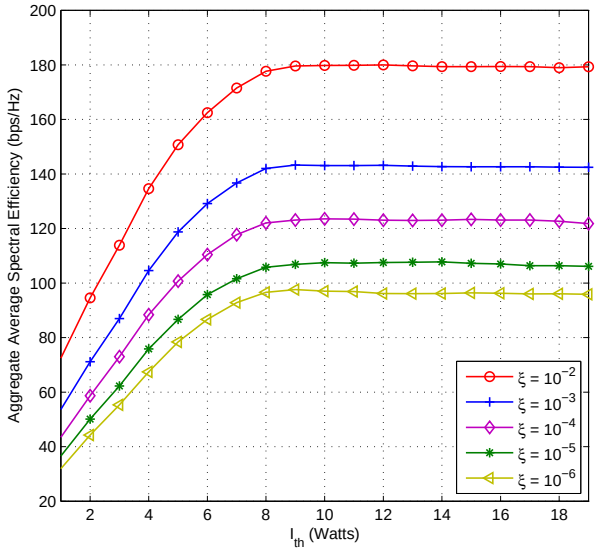

Figure 2.7: AASE performance using the proposed RRA algorithm versus I_{th} constraint for different BER-target values. Results correspond to the case with deterministic interference constraint and perfect cross-link CSI. System parameters are: $K = 64$, $P_t = 30$ Watts.

Fig. 2.6 shows the achievable AASE of the adaptive MQAM/OFDMA CR system versus STx-PRx interference power threshold levels under total average power and deterministic interference constraints with perfect cross-link CSI knowledge. As

expected, greater AASE values are achieved for higher maximum tolerable interference since I_{th} limits the cognitive users' transmit power. The improved performance however approaches a plateau in the high I_{th} region as the P_t threshold becomes the dominant power constraint. Note that the improved performance by increasing I_{th} comes at the cost of increased probability for violating the primary users' QoS. Further, imposing a higher maximum peak average power setting enhances the achievable AASE in high I_{th} region - P_t, for the particular values taken in this example, achieve the same AASE over small I_{th} settings. Moreover, increasing the number of subcarriers results in higher attainable performance.

Achievable AASE performance under different maximum tolerable interference thresholds for respective values of BER-target with perfect cross-link CSI availability is shown in Fig. 2.7. It can be seen that the system performance is improved under less stringent QoS constraints. For example, a 26.9% gain in AASE performance is achieved by imposing $\xi = 10^{-2}$ in comparison to $\xi = 10^{-3}$. However, the gap in performance becomes less significant for lower BER-target regimes.

System performance with noisy cross-link CSI and 'average case' of estimation error versus the correlation factor between estimation and error variables ρ is depicted in Fig. 2.8. It can be seen that a higher correlation factor increases the maximum likelihood between true and estimated interfering channels, hence, the probability of violating the interference constraint on average is improved and in turn a lower AASE for the cognitive system is realized. Further, the achievable AASE with imperfect cross-link CSI knowledge and 'worst case' of estimation error against ρ for different probabilities of channel estimation error bound pr is studied in Fig. 2.9. Apart from the effect of ρ on the performance, higher values of pr increase the robustness of the interference management scheme but come at the cost of lower achievable spectral efficiencies. The results indicate that the improved AASE performance by decreasing pr in the lower half region (i.e., $pr \leq 0.5$) is not significant yet it may cause critical interference to the primary service operation. For example, given $\rho = 0.5$, varying the value of pr from 0.5 to 0.1 results in a 40% increase in the probability of error bound violation but only provides an effective gain of 2.3% in the cognitive system performance.

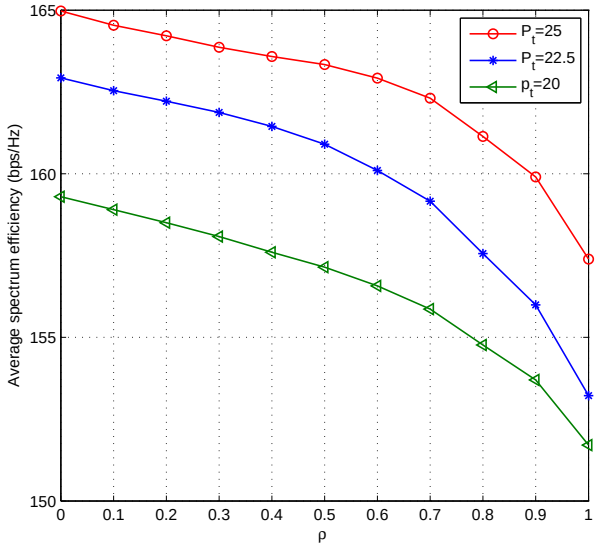

Figure 2.8: Achievable AASE with imperfect cross-link CSI and 'average case' of estimation error against ρ for different values of P_t. System parameters are: $K = 64$, $I_{th} = 25$ Watts, $\xi = 10^{-2}$, $\delta^2_{\hat{H}_k^{sp}} = 1$.

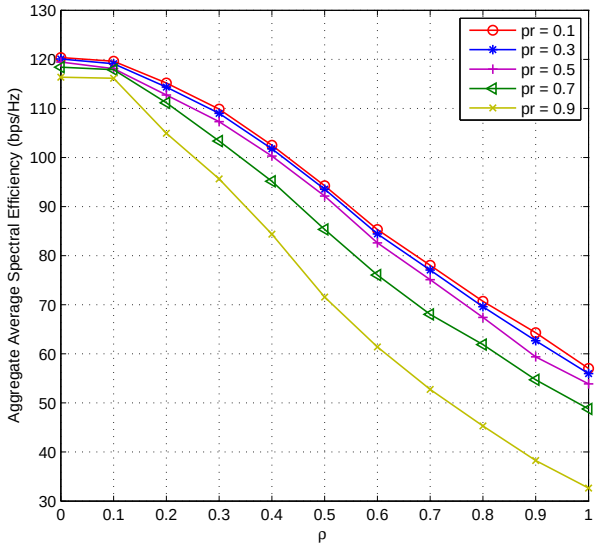

Figure 2.9: Achievable AASE with imperfect cross-link CSI and 'worst case' of estimation error against ρ with pr. System parameters are: $K = 64$, $P_t = 20$ Watts, $I_{th} = 5$ Watts, $\xi = 10^{-3}$, $\delta^2_{\hat{H}_k^{sp}} = 1$.

The achievable performance with imperfect cross-channel information and 'probabilistic case' of estimation error versus the collision probability ϵ with respective I_{th} values is illustrated in Fig. 2.10. Increasing the maximum probability of vi-

olating the interference constraint set by the a regulatory authority significantly improves the spectral efficiency of the cognitive network. The trade-off is, however, the degradation of the primary service operation which is deemed highly undesirable in practical scenarios.

System performance with noisy cross-link CSI for different 'average case', 'worst case', and 'probabilistic case' of estimation error is demonstrated in Fig. 2.11. The results show that the 'probabilistic case' with 5% collision probability outperforms the achievable AASE under the 'worst case' scenario with an error bound of $pr = 0.95$. For example, given $I_{th} = 6$ Watts, the 'probabilistic case' achieves a 26.7% gain in AASE over the 'worst case'. Further, employing the 'average case' provides higher spectral efficiencies. For instance, a 7.0% increase in performance in achieved utilizing the 'average case' over the 'probabilistic case'. For high values of I_{th}, the total average power constraint becomes the dominant limit and therefore the performance under different cases of estimation error eventually converge. Note that the 'average case' controls the interference based on the average error estimation, therefore, it cannot mitigate the potential instantaneous interference violations. On the other hand, implementing the 'worst case' can guarantee that the interference constraints are obeyed at any given time, thus, preserving the primary users' QoS. The proposed 'probabilistic case' of estimation error provides an optimal trade-off between the achievable performance of cognitive system and managing the QoS of primary users. In particular, the 'probabilistic case' is advantageous in terms of performance and flexibility over the conventional 'average case' and 'worst case' scenarios.

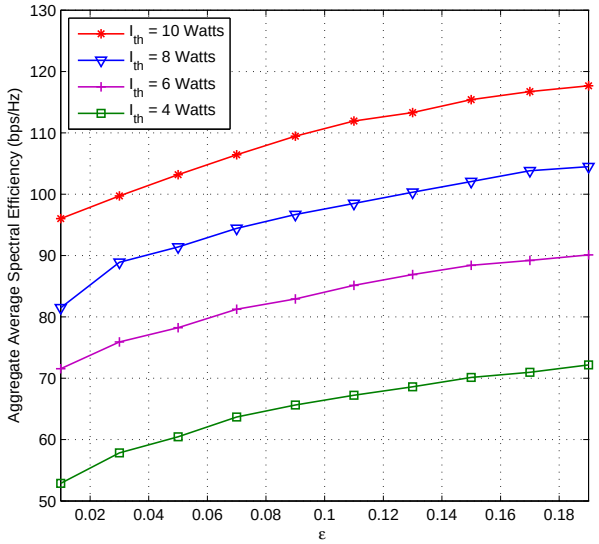

Figure 2.10: Achievable AASE with imperfect cross-link CSI and 'probabilistic case' of estimation error against ϵ with I_{th}. System parameters are: $K = 64$, $P_t = 40$ Watts, $\xi = 10^{-3}$, $\rho = 0.5$, $\delta^2_{\hat{H}_k^{sp}} = 1$.

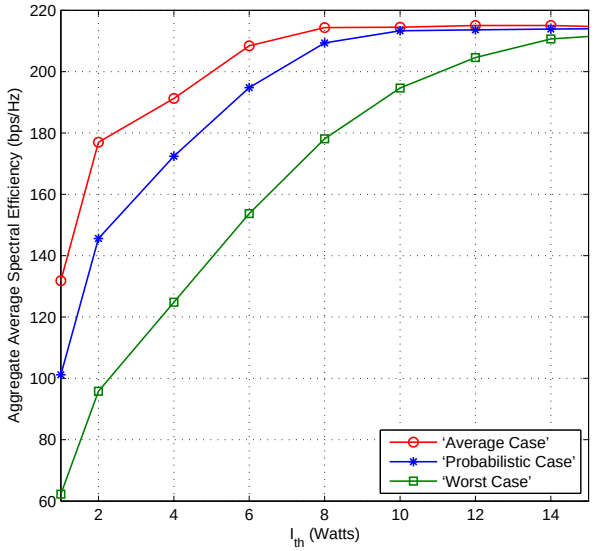

Figure 2.11: Performance under imperfect cross-link CSI for different cases of estimation error against I_{th}. System parameters are: $K = 64$, $P_t = 45$ Watts, $\xi = 10^{-2}$, $pr = 0.95$, $\rho = 0.2$, $\epsilon = 5\%$, $\delta^2_{\hat{H}_k^{sp}} = 0.1$.

2.7 Conclusions

In this chapter, we have studied the spectral efficiency performance of adaptive MQAM/OFDMA underlay CR networks with certain/uncertain interfering channel information. We derived novel RRA algorithms to enhance the overall cognitive system performance subject to satisfying total average power and peak aggregate interference constraints. The proposed framework considers both cases of perfect and imperfect cross-link CSI knowledge at the secondary transmitter. In the latter, different 'average case', 'worst case', and 'probabilistic case' scenarios of channel estimation error were modelled and analysed. To compute the aggregate average spectral efficiency, we developed unique approximated distributions of the received SINR for given users over different sub-channels in the respective cases under consideration. Through numerical results we studied the achievable performance of the cognitive system using our proposed RRA algorithms. By adapting the power, rate, and subcarrier allocation policies to the time-varying secondary-secondary fading channels and secondary-primary interfering channels, a significant gain in the spectral efficiency performance of the cognitive system can be realized, whilst controlling the interference on the primary service receivers. Furthermore, the impact of parameters uncertainty on overall system performance was investigated. In particular, simulation results were provided for different cases of error estimation. It was understood that the 'average case' results in higher cognitive system performance, however, comes at the cost of potential instantaneous interference violations. Subsequently, the 'worst case' can guarantee that the power constraints are obeyed at all times, yet it does not result in desirable cognitive performance. In contrast, the proposed 'probabilistic case' in this chapter, which was derived as a low complexity deterministic constraint, provided an optimal trade-off between the achievable performance of the cognitive network and preserving the QoS of the primary users. In summary, the 'probabilistic case' can replace the conventional 'average case' and 'worst case' scenarios in practical situations as a result of enhanced performance and flexibility.

Chapter 3

Stochastic Resource Allocation for Hybrid and Opportunistic-Access OFDMA Cognitive Radios

3.1 Introduction

Based on the concept of CR, Ofcom and other spectrum regulators have recently enabled white space devices (WSDs) to operate in the spatially unused TV broadcasting spectrum [81]. The use cases include rural broadband, WiFi coverage, and machine-to-machine (M2M) communication, where WSDs avoid interfering with licensed TV services using geolocation databases in conjunction with cognitive and sensing technologies [82].

Three main paradigms have been proposed for CR in regards to the unlicensed users access to the primary frequency band: (i) underlay spectrum access (USA) where secondary users (SUs) silently coexist with primary users (PUs), provided they satisfy an interference limit set by a regulatory authority, (ii) overlay spectrum access (OSA) in which SUs are only allowed to access the vacant parts of the primary spectrum, and (iii) hybrid spectrum access (HSA), a combination of the two former strategies in which SUs can dynamically select between the USA and OSA modes depending on the traffic characteristics and interference constraints [83]. In this chapter, we focus on both OSA and HSA paradigms, where the overall shared-

spectrum system performance is closely related to accurate determination of licensed spectrum availability.

Various solutions for detecting and monitoring the PU' activity have been proposed in the literature, e.g., geolocation database, beacon signalling through a dedicated channel, and spectrum sensing [84], [85]. In practice, there are inevitable uncertainties associated with the spectrum monitoring information due to the erroneous decisions caused by the adverse characteristics of wireless environment [86]. In this contribution, we invoke spectrum sensing capabilities at CRs via energy detectors which are commonly used due to their relatively low infrastructure price and favourable compatibility with legacy systems [87]. Nevertheless, the framework presented in this work can be extended and analyzed for other sensing schemes.

Orthogonal frequency-division multiplexing (OFDM) has emerged as a prominent modulation scheme for a new generation of wireless communication systems, including, long term evolution (LTE) and LTE-advanced [60]. For OFDM-based multiuser applications, multiple-access can be accommodated via orthogonal frequency-division multiple-access (OFDMA) technology [61]. In OFDMA systems, different subcarriers may be assigned to different users in order to exploit the random variations in channel quality. In addition, OFDMA is considered as a tangible standard for CR due to its inherent advantages in terms of flexibility and adaptability in allocating spectrum resources in shared-spectrum environments [62].

Radio resource allocation (RRA) plays a significant role in optimizing the overall performance of conventional OFDMA systems [63]. In addition, adaptive RRA is an active area of research in the context of OFDMA-based CR systems to facilitate a balance between maximizing the cognitive network performance and minimizing the inflicted interference on the licensed users. Many of the RRA algorithms on CR in the literature incorporate a hard-decision-based strategy in which resources are allocated according to the conventional binary hypothesis test outcome [88]. Due to the imperfectness of the spectrum sensing mechanism, such RRA algorithms may inflict critical interference to PUs' quality of service (QoS).

The goal of this chapter is to devise stochastic RRA algorithms based on the spectrum sensing probabilistic information on channel availability for both OSA and

HSA paradigms. We study the downlink transmission of a multi-user OFDMA-based CR system operating under QoS constraints and uncertain sensing information.

Suboptimal and optimal power allocation policies are studied in [64], where the aggregate capacity of the CR system is maximized under a primary receiver (PRx) interference limit. In [65], a queue-aware RRA algorithm is proposed to maximize the fairness in OFDMA-based CR networks subject to a total power constraint at the base station. A Lagrangian relaxation algorithm is adopted in [62] to probabilistically allocate resources based on the availability of the primary frequency band via spectrum sensing.

One of the central challenges associated in cognitive wireless communications is controlling the interference levels. In the OSA, the CRs sense the primary frequency band (active/idle) and adjust their transmission power based on the decision made by the spectrum sensing mechanism. Hence, given the spectrum sensing scheme is perfectly accurate, the inactive parts of the licensed spectrum are used by the CRs without imposing any impact on the primary service operation. On the other hand, in the HSA, CRs can exploit both unused and underutilized parts of the spectrum through (1) silent coexistence with PUs in spectral bands at low transmit powers as far as the maximum tolerable cross-service interference constraint is satisfied (2) opportunistically utilizing the white spaces of the spectrum at high transmit powers.

3.2 Preliminaries

3.2.1 System Model

Consider a downlink scenario where a secondary transmitter (STx) communicates with N secondary receivers (SRxs) (indexed by n) over K subcarriers (indexed by k), by dynamically accessing a primary spectrum under certain constraints. Each subcarrier is assumed to experience frequency-flat fading. Let $H^{ss}_{n,k}(t)$, $H^{ps}_{n,k}(t)$, and $g^{sp}_{k}(t)$, at time t, denote the complex channel gains over subcarrier k from the STx to n^{th} SRx, primary transmitter (PTx) to n^{th} SRx, and STx to primary receiver (PRx), respectively. The channel power gains $|H^{ss}_{n,k}(t)|^2$, $|H^{ps}_{n,k}(t)|^2$, and $|g^{sp}_{k}(t)|^2$, are

assumed to be ergodic and stationary [89]. The values and statistics of channel gains are assumed to be available at the STx via error-free feedback channels [62], [90]. Let σ_n^2 and σ_{ps}^2 respectively denote the Gaussian noise and received primary-secondary interference powers [71].

3.2.2 Spectrum Sensing

In the hybrid spectrum access strategy, i.e., mixed opportunistic and non-opportunistic scheme, the secondary user transmits simultaneously on K frequency bands (regardless of the actual status of each frequency band) and adapts its transmit power on each band based on the decision made during the sensing slot at the beginning of each frame. In this section, we study the comprehensive problem of power and rate allocation, in order to maximize the aggregate instantaneous rate in OFDMA CR systems.

At the beginning of each time slot in any frame, the STx performs spectrum sensing on the K subcarriers and decides based on the collected information how to allocate power and frequency resources to SRxs. Due to the limitations of the spectrum sensing mechanism and the inherent characteristics of wireless communications (shadowing and fading), the primary spectrum may be falsely detected. If a primary frequency band is detected idle although the spectrum is actually busy, i.e., mis-detection, cognitive communications causes unwanted interference to primary service operation. On the other hand, detecting a subcarrier as busy whilst it is actually idle, i.e., false-alarm, results in underutilization of the spectrum resource. Based on the sensing information and actual spectrum status, the different scenarios and probabilities of user n over subcarrier k in the OFDMA CR network are

$$\begin{aligned}
S_{n,k}^{ii} : \text{idle} \quad , \quad \mathscr{P}(S_{n,k}^{ii}) &= \{1 - \mathscr{P}_{n,k}^{f}\}\mathscr{P}(\mathscr{H}_{n,k}^{i}) \\
S_{n,k}^{bi} : \text{false-alarm} \quad , \quad \mathscr{P}(S_{n,k}^{bi}) &= \mathscr{P}_{n,k}^{f}\mathscr{P}(\mathscr{H}_{n,k}^{i}) \\
S_{n,k}^{ib} : \text{mis-detection} \quad , \quad \mathscr{P}(S_{n,k}^{ib}) &= \{1 - \mathscr{P}_{n,k}^{d}\}\mathscr{P}(\mathscr{H}_{n,k}^{b}) \\
S_{n,k}^{bb} : \text{busy} \quad , \quad \mathscr{P}(S_{n,k}^{bb}) &= \mathscr{P}_{n,k}^{d}\mathscr{P}(\mathscr{H}_{n,k}^{b})
\end{aligned} \tag{3.1}$$

where $\mathscr{P}^f_{n,k}$ and $\mathscr{P}^d_{n,k}$ are the sensing probabilities of false-alarm and detection, and $\mathscr{P}(\mathscr{H}^i_{n,k})$ and $\mathscr{P}(\mathscr{H}^b_{n,k})$ denote the probabilities that the band is idle and busy, respectively. Using the energy detection technique, the false-alarm and detection probabilities for user n over subcarrier k are [91], [92]

$$\mathscr{P}^f_{n,k} = Q\left(\left(\frac{\epsilon_{n,k}}{\sigma_n^2} - 1\right)\sqrt{\tau f_s}\right) \tag{3.2}$$

$$\mathscr{P}^d_{n,k} = Q\left(\left(\frac{\epsilon_{n,k}}{\sigma_n^2} - \psi_k^{ps} - 1\right)\sqrt{\frac{\tau f_s}{2\psi_k^{ps}+1}}\right) \tag{3.3}$$

where $Q(x)$ is the complementary cumulative distribution function given by $Q(x) = \frac{1}{\sqrt{2\pi}}\int_z^\infty \exp(\frac{-t^2}{2})\,dt$, ψ_k^{ps} is the received signal-to-interference-plus-noise ratio (SINR) of the primary transmitter at the cognitive detector, f_s is the sampling frequency, τ is the sensing time (here assumed to be fixed), and $\epsilon_{n,k}$ is the decision threshold of the cognitive detector.

3.3 Hybrid Spectrum Access

3.4 Stochastic RRA Algorithm

In this section, we study the comprehensive problem of power and rate allocation towards maximizing the transmission rate of multi-user multi-band OFDMA CRs. In the proposed CR network with hybrid spectrum access strategy, the STx transmits simultaneously on K frequency bands (regardless of the actual status of each frequency band) and adapts its transmit power on each band based on the decision made during the sensing slot at the beginning of each frame and the received SINR $\gamma^{ss}_{n,k}$. Let m, b, f, and i denote the number of bands experiencing scenarios $S^{ib}_{n,k}$, $S^{bb}_{n,k}$, $S^{bi}_{n,k}$, and $S^{ii}_{n,k}$, respectively. The STx transmits to user n over subcarrier k using higher power $P^I_{n,k}(\gamma^{ss}_{n,k}, m, b, f, i)$ with subcarrier allocation policy $\varphi^I_{n,k}(\gamma^{ss}_{n,k}, m, b, f, i)$ when the band is detected as idle and lower power $P^B_{n,k}(\gamma^{ss}_{n,k}, m, b, f, i)$ with subcarrier assignment policy $\varphi^B_{n,k}(\gamma^{ss}_{n,k}, m, b, f, i)$ when the channel is detected to be active. At the same time, the band k for user n may be actually idle ($\mathscr{H}^i_{n,k}$) or in use ($\mathscr{H}^b_{n,k}$).

The instantaneous transmission rates of the OFDMA CR network for user n and

subcarrier k based on the sensing information and actual channel status in scenarios $S^{ii}_{n,k}$, $S^{bi}_{n,k}$, $S^{ib}_{n,k}$ and $S^{bb}_{n,k}$ can be respectively expressed as

$$\begin{aligned}
\mathscr{R}^{ii}_{n,k}(\gamma^{ss}_{n,k}, m, b, f, i) &= \log_2\left(1+\frac{P^I_{n,k}(\gamma^{ss}_{n,k}, m, b, f, i)|H^{ss}_{n,k}|^2}{\sigma^2_n}\right)\\
\mathscr{R}^{bi}_{n,k}(\gamma^{ss}_{n,k}, m, b, f, i) &= \log_2\left(1+\frac{P^B_{n,k}(\gamma^{ss}_{n,k}, m, b, f, i)|H^{ss}_{n,k}|^2}{\sigma^2_n}\right)\\
\mathscr{R}^{ib}_{n,k}(\gamma^{ss}_{n,k}, m, b, f, i) &= \log_2\left(1+\frac{P^I_{n,k}(\gamma^{ss}_{n,k}, m, b, f, i)|H^{ss}_{n,k}|^2}{\sigma^2_n+\sigma^2_{ps}}\right)\\
\mathscr{R}^{bb}_{n,k}(\gamma^{ss}_{n,k}, m, b, f, i) &= \log_2\left(1+\frac{P^B_{n,k}(\gamma^{ss}_{n,k}, m, b, f, i)|H^{ss}_{n,k}|^2}{\sigma^2_n+\sigma^2_{ps}}\right).
\end{aligned} \tag{3.4}$$

For the sake of notational brevity, we henceforth omit the reference - $\gamma^{ss}_{n,k}, m, b, f, i$ - where the context is clear.

The aggregate transmission rate of the OFDMA CR network with hybrid spectrum access (R_H) through incorporating the stochastic information on the different number of subcarriers experiencing different scenarios is expressed as

$$\begin{aligned}
R_H = \sum_{m=0}^{K}\sum_{b=0}^{K-m}\sum_{f=0}^{K-(m+b)}\sum_{i=K-(m+b+f)}^{K-(m+b+f)} \mathscr{P}(m,b,f,i)\times\\
\Bigg(\frac{\binom{K-1}{m-1}\binom{K-m}{b}\binom{K-m-b}{f}\binom{K-m-b-f}{i}}{\binom{K}{m}\binom{K-m}{b}\binom{K-m-b}{f}\binom{K-m-b-f}{i}}\sum_{n=1}^{N}\sum_{k=1}^{K}\varphi^I_{n,k}\mathscr{R}^{ib}_{n,k}+\\
\frac{\binom{K-b}{m}\binom{K-1}{b-1}\binom{K-m-b}{f}\binom{K-m-b-f}{i}}{\binom{K}{m}\binom{K-m}{b}\binom{K-m-b}{f}\binom{K-m-b-f}{i}}\sum_{n=1}^{N}\sum_{k=1}^{K}\varphi^B_{n,k}\mathscr{R}^{bb}_{n,k}+\\
\frac{\binom{K-f}{m}\binom{K-f-m}{b}\binom{K-1}{f-1}\binom{K-m-b-f}{i}}{\binom{K}{m}\binom{K-m}{b}\binom{K-m-b}{f}\binom{K-m-b-f}{i}}\sum_{n=1}^{N}\sum_{k=1}^{K}\varphi^B_{n,k}\mathscr{R}^{bi}_{n,k}+\\
\frac{\binom{K-i}{m}\binom{K-i-m}{b}\binom{K-i-m-b}{f}\binom{K-1}{i-1}}{\binom{K}{m}\binom{K-m}{b}\binom{K-m-b}{f}\binom{K-m-b-f}{i}}\sum_{n=1}^{N}\sum_{k=1}^{K}\varphi^I_{n,k}\mathscr{R}^{ii}_{n,k}\Bigg)
\end{aligned} \tag{3.5}$$

where $\mathscr{P}(m,b,f,i)$ is the probability of having m, b, f, and i bands experiencing scenarios $S^{ib}_{n,k}$, $S^{bb}_{n,k}$, $S^{bi}_{n,k}$, and $S^{ii}_{n,k}$, respectively. Using (3.1), and assuming equal receiver operating characteristics (ROC), $\mathscr{P}(m,b,f,i)$ can be computed by

$$\mathscr{P}(m,b,f,i) =$$

$$\left(\mathscr{P}(S_{n,k}^{bi})\right)^{m}\left(\mathscr{P}(S_{n,k}^{bb})\right)^{b}\left(\mathscr{P}(S_{n,k}^{ib})\right)^{f}\left(\mathscr{P}(S_{n,k}^{ii})\right)^{i}. \tag{3.6}$$

We denote the different number of combinations that user n over band k experiences different scenarios $S_{n,k}^{ib}$, $S_{n,k}^{bb}$, $S_{n,k}^{bi}$, $S_{n,k}^{ii}$, and the total number of combinations respectively as

$$\begin{aligned}
\mathscr{M} &= \binom{K-1}{m-1}\binom{K-m}{b}\binom{K-m-b}{f}\binom{K-m-b-f}{i} \\
\mathscr{B} &= \binom{K-b}{m}\binom{K-1}{b-1}\binom{K-m-b}{f}\binom{K-m-b-f}{i} \\
\mathscr{F} &= \binom{K-f}{m}\binom{K-f-m}{b}\binom{K-1}{f-1}\binom{K-m-b-f}{i} \\
\mathscr{I} &= \binom{K-i}{m}\binom{K-i-m}{b}\binom{K-i-m-b}{f}\binom{K-1}{i-1} \\
\mathscr{T} &= \binom{K}{m}\binom{K-m}{b}\binom{K-m-b}{f}\binom{K-m-b-f}{i}.
\end{aligned} \tag{3.7}$$

To protect the primary users QoS from undesirable interference imposed by the CRs under imperfect sensing information, we consider stochastic total transmit and interference power constraints, in which the number of subcarriers in each scenario is Binomially-distributed. Note that, since in scenarios $S_{n,k}^{ii}$ and $S_{n,k}^{bi}$ the band is truly idle, interference arises only in scenarios $S_{n,k}^{ib}$ and $S_{n,k}^{bb}$. In the events of $S_{n,k}^{ib}$ and $S_{n,k}^{bb}$, the STx transmission power is accordingly set to $P_{n,k}^{I}$ and $P_{n,k}^{B}$, respectively. The corresponding stochastic constraints on the aggregate transmission power (C_{H1}) and aggregate received interference power on the primary receiver (C_{H2}) can be respectively expressed as

$$\begin{aligned}
C_{H1}: &\sum_{m=0}^{K}\sum_{b=0}^{K-m}\sum_{f=0}^{K-(m+b)}\sum_{i=K-(m+b+f)}^{K-(m+b+f)}\mathscr{P}(m,b,f,i)\times \\
&\left(\frac{\mathscr{M}}{\mathscr{T}}\sum_{n=1}^{N}\sum_{k=1}^{K}\varphi_{n,k}^{I}P_{n,k}^{I}+\frac{\mathscr{B}}{\mathscr{T}}\sum_{n=1}^{N}\sum_{k=1}^{K}\varphi_{n,k}^{B}P_{n,k}^{B}+\right. \\
&\left.\frac{\mathscr{F}}{\mathscr{T}}\sum_{n=1}^{N}\sum_{k=1}^{K}\varphi_{n,k}^{B}P_{n,k}^{B}+\frac{\mathscr{I}}{\mathscr{T}}\sum_{n=1}^{N}\sum_{k=1}^{K}\varphi_{n,k}^{I}P_{n,k}^{I}\right)
\end{aligned} \tag{3.8}$$

$$C_{H2}: \sum_{m=0}^{K} \sum_{b=0}^{K-m} \sum_{f=0}^{K-(m+b)} \sum_{i=K-(m+b+f)}^{K-(m+b+f)} \mathscr{P}(m,b,f,i) \times$$
$$\left(\frac{\mathscr{M}}{\mathscr{T}} \sum_{n=1}^{N} \sum_{k=1}^{K} \varphi_{n,k}^{I} P_{n,k}^{I} |H_{n,k}^{sp}|^2 + \right.$$
$$\left. \frac{\mathscr{B}}{\mathscr{T}} \sum_{n=1}^{N} \sum_{k=1}^{K} \varphi_{n,k}^{B} P_{n,k}^{B} |H_{n,k}^{sp}|^2 \right) \tag{3.9}$$

where P_t and I_{th} are the total transmit and interference power limits. To maximize the aggregate transmission rate of the proposed OFDMA CR network with joint underlay and overlay spectrum access mechanism, we formulate the following optimization problem.

Problem $\mathscr{O}_1$:

$$\max_{P_{n,k}^{I}, P_{n,k}^{B}, \varphi_{n,k}^{I}, \varphi_{n,k}^{B}} R_H \tag{3.10a}$$

$$\text{s. t.:} \quad C_{H1} \leq P_t \tag{3.10b}$$

$$C_{H2} \leq I_{th} \tag{3.10c}$$

$$\sum_{n=1}^{N} \varphi_{n,k}^{I} = 1 \ , \ k \in \{1,2,...,K\} \tag{3.10d}$$

$$\sum_{n=1}^{N} \varphi_{n,k}^{B} = 1 \ , \ k \in \{1,2,...,K\} \tag{3.10e}$$

$$\varphi_{n,k}^{I} \in \{0,1\} \ , \ n \in \{1,2,...,N\} \ , \ k \in \{1,2,...,K\} \tag{3.10f}$$

$$\varphi_{n,k}^{B} \in \{0,1\} \ , \ n \in \{1,2,...,N\} \ , \ k \in \{1,2,...,K\}. \tag{3.10g}$$

We apply one-level Lagrangian dual decomposition to solve the constrained mixed discrete-continuous non-linear programing (MDCNLOP) optimization problem under consideration.

3.4.1 Lagrangian Function

The Lagrangian function for solving Problem $\mathscr{O}_2$ can be expressed as

$$L(\lambda^I, \lambda^B, \eta, \mu) = R_H - \sum_{k=1}^{K} \lambda_k^I \left(\sum_{n=1}^{N} \varphi_{n,k}^{I} (\gamma_{n,k}^{ss}) - 1 \right) -$$

$$\sum_{k=1}^{K}\lambda_k^B\left(\sum_{n=1}^{N}\varphi_{n,k}^B(\gamma_{n,k}^{ss})-1\right)-\eta\Big(C_{H2}-I_{th}\Big)-$$
$$\mu\Big(C_{H1}-P_t\Big). \tag{3.11}$$

3.4.2 Lagrangian Dual Problem

The Lagrangian dual function under consideration is therefore

$$\min_{\lambda^I,\lambda^B,\eta,\mu}\Big(F(\lambda^I,\lambda^B,\eta,\mu)\Big)\ ,\ s.t.:\ \lambda^I,\lambda^B,\eta,\mu\geq 0 \tag{3.12}$$

where

$$F(\lambda^I,\lambda^B,\eta,\mu)=\sum_{n=1}^{N}f_n(\lambda^I,\lambda^B,\eta,\mu)+\sum_{k=1}^{K}\lambda_k^I+\sum_{k=1}^{K}\lambda_k^B$$
$$+\eta I_{th}+\mu P_t \tag{3.13}$$

and

$$f_n(\lambda^I,\lambda^B,\eta,\mu)=\max_{P_{n,k}^I(\gamma_{n,k}^{ss}),P_{n,k}^B(\gamma_{n,k}^{ss}),\varphi_{n,k}^I(\gamma_{n,k}^{ss}),\varphi_{n,k}^B(\gamma_{n,k}^{ss})}$$
$$\Bigg(R_H^n-\sum_{k=1}^{K}\lambda_k^I\varphi_{n,k}^I(\gamma_{n,k}^{ss})-\sum_{k=1}^{K}\lambda_k^B\varphi_{n,k}^B(\gamma_{n,k}^{ss})-\mu C_{H1}^n$$
$$-\eta C_{H2}^n\Bigg) \tag{3.14}$$

where $\forall n\in\mathcal{N}$, R_H^n is the rate per user, C_{H1}^n denotes the average power per user, and C_{H2}^n is the interference per user, given by,

$$R_H^n=\sum_{m=0}^{K}\sum_{b=0}^{K-m}\sum_{f=0}^{K-(m+f)}\sum_{i=K-(m+b+f)}^{K-(m+b+f)}\mathscr{P}(m,b,f,i)$$
$$\Bigg(\frac{\mathscr{M}}{\mathscr{T}}\sum_{k=1}^{K}\varphi_{n,k}^I(\gamma_{n,k}^{ss})r_{n,k}^{01}+\frac{\mathscr{B}}{\mathscr{T}}\sum_{k=1}^{K}\varphi_{n,k}^B(\gamma_{n,k}^{ss})r_{n,k}^{11}$$
$$+\frac{\mathscr{F}}{\mathscr{T}}\sum_{k=1}^{K}\varphi_{n,k}^B(\gamma_{n,k}^{ss})r_{n,k}^{10}+\frac{\mathscr{I}}{\mathscr{T}}\sum_{k=1}^{K}\varphi_{n,k}^I(\gamma_{n,k}^{ss})r_{n,k}^{00}\Bigg), \tag{3.15}$$

$$C^n_{H1}: \sum_{m=0}^{K} \sum_{b=0}^{K-m} \sum_{f=0}^{K-(m+f)} \sum_{i=K-(m+b+f)}^{K-(m+b+f)} \mathscr{P}(m,b,f,i)$$
$$\left(\frac{\mathscr{M}}{\mathscr{T}} \sum_{k=1}^{K} \varphi^I_{n,k}(\gamma^{ss}_{n,k}) P^I_{n,k}(\gamma^{ss}_{n,k}) + \frac{\mathscr{B}}{\mathscr{T}} \sum_{k=1}^{K} \varphi^B_{n,k}(\gamma^{ss}_{n,k}) P^B_{n,k}(\gamma^{ss}_{n,k}) + \right.$$
$$\left. \frac{\mathscr{F}}{\mathscr{T}} \sum_{k=1}^{K} \varphi^B_{n,k}(\gamma^{ss}_{n,k}) P^B_{n,k}(\gamma^{ss}_{n,k}) + \frac{\mathscr{I}}{\mathscr{T}} \sum_{k=1}^{K} \varphi^I_{n,k}(\gamma^{ss}_{n,k}) P^I_{n,k}(\gamma^{ss}_{n,k}) \right). \tag{3.16}$$

and

$$C^n_{H2}: \sum_{m=0}^{K} \sum_{b=0}^{K-m} \sum_{f=0}^{K-(m+f)} \sum_{i=K-(m+b+f)}^{K-(m+b+f)} \mathscr{P}(m,b,f,i)$$
$$\left(\frac{\mathscr{M}}{\mathscr{T}} \sum_{k=1}^{K} \varphi^I_{n,k}(\gamma^{ss}_{n,k}) P^I_{n,k}(\gamma^{ss}_{n,k}) |H^{sp}_{n,k}|^2 + \right.$$
$$\left. \frac{\mathscr{B}}{\mathscr{T}} \sum_{k=1}^{K} \varphi^B_{n,k}(\gamma^{ss}_{n,k}) P^B_{n,k}(\gamma^{ss}_{n,k}) |H^{sp}_{n,k}|^2 \right) \tag{3.17}$$

In order to solve the Lagrangian dual function, we have formulate it as two independent sub-problems where

$$f_n(\lambda^I, \lambda^B, \eta, \mu) = \max_{P^I_{n,k}(\gamma^{ss}_{n,k}), \varphi^I_{n,k}(\gamma^{ss}_{n,k}))} f^I_n(\lambda^I, \eta, \mu)$$
$$+ \max_{P^B_{n,k}(\gamma^{ss}_{n,k}), \varphi^B_{n,k}(\gamma^{ss}_{n,k})} f^B_n(\lambda^B, \eta, \mu) \tag{3.18}$$

where

$$f^I_n(\lambda^I, \eta, \mu) = \sum_{m=0}^{K} \sum_{b=0}^{K-m} \sum_{f=0}^{K-(m+f)} \sum_{i=K-(m+b+f)}^{K-(m+b+f)} \mathscr{P}(m,b,f,i)$$
$$\left(\frac{\mathscr{M}}{\mathscr{T}} \sum_{k=1}^{K} \varphi^I_{n,k}(\gamma^{ss}_{n,k}) r^{01}_{n,k} + \frac{\mathscr{I}}{\mathscr{T}} \sum_{k=1}^{K} \varphi^B_{n,k}(\gamma^{ss}_{n,k}) r^{00}_{n,k} - \eta \frac{\mathscr{M}}{\mathscr{T}} \sum_{k=1}^{K} \varphi^I_{n,k}(\gamma^{ss}_{n,k}) \right.$$
$$\times P^I_{n,k}(\gamma^{ss}_{n,k}) |H^{sp}_{n,k}|^2 - \mu \sum_{k=1}^{K} \varphi^I_{n,k}(\gamma^{ss}_{n,k}) P^I_{n,k}(\gamma^{ss}_{n,k})$$
$$\left. \times \left\{ \frac{\mathscr{M}}{\mathscr{T}} + \frac{\mathscr{I}}{\mathscr{T}} \right\} \right) - \sum_{k=1}^{K} \lambda^I_k \varphi^I_{n,k}(\gamma^{ss}_{n,k}) \tag{3.19}$$

and

$$f_n^B(\lambda^B,\eta,\mu)=\sum_{m=0}^{K}\sum_{b=0}^{K-m}\sum_{f=0}^{K-(m+f)}\sum_{i=K-(m+b+f)}^{K-(m+b+f)}\mathscr{P}(m,b,f,i)$$
$$\left(\frac{\mathscr{B}}{\mathscr{T}}\sum_{k=1}^{K}\varphi_{n,k}^B(\gamma_{n,k}^{ss})r_{n,k}^{11}+\frac{\mathscr{F}}{\mathscr{T}}\sum_{k=1}^{K}\varphi_{n,k}^B(\gamma_{n,k}^{ss})r_{n,k}^{10}-\eta\frac{\mathscr{B}}{\mathscr{T}}\sum_{k=1}^{K}\varphi_{n,k}^B(\gamma_{n,k}^{ss})\right.$$
$$\times P_{n,k}^B(\gamma_{n,k}^{ss})|H_{n,k}^{sp}|^2-\mu\sum_{k=1}^{K}\varphi_{n,k}^B(\gamma_{n,k}^{ss})P_{n,k}^B(\gamma_{n,k}^{ss})$$
$$\left.\times\left\{\frac{\mathscr{B}}{\mathscr{T}}+\frac{\mathscr{F}}{\mathscr{T}}\right\}\right)-\sum_{k=1}^{K}\lambda_k^B\varphi_{n,k}^B(\gamma_{n,k}^{ss}). \tag{3.20}$$

To find the optimum power solution we compute $\frac{\partial f_n^I(\lambda^I,\eta,\mu)}{\partial\left(\varphi_{n,k}^I(\gamma_{n,k}^{ss})P_{n,k}^I(\gamma_{n,k}^{ss})\right)}$ and $\frac{\partial f_n^B(\lambda^B,\eta,\mu)}{\partial\left(\varphi_{n,k}^B(\gamma_{n,k}^{ss})P_{n,k}^B(\gamma_{n,k}^{ss})\right)}$

$$\sum_{m=0}^{K}\sum_{b=0}^{K-m}\sum_{f=0}^{K-(m+f)}\sum_{i=K-(m+b+f)}^{K-(m+b+f)}\mathscr{P}(m,b,f,i)\left[\left\{\left(\right.\right.\right.$$
$$\left.\frac{\mathscr{M}}{\mathscr{T}}\frac{\frac{|H_{n,k}^{ss}|^2}{\sigma_n^2+\sigma_{ps}^2}}{1+\frac{|H_{n,k}^{ss}|^2P_{n,k}^I(\gamma_{n,k}^{ss})}{\sigma_n^2+\sigma_{ps}^2}}\right)+\left(\frac{\mathscr{I}}{\mathscr{T}}\frac{\frac{|H_{n,k}^{ss}|^2}{\sigma_n^2}}{1+\frac{|H_{n,k}^{ss}|^2P_{n,k}^I(\gamma_{n,k}^{ss})}{\sigma_n^2}}\right)\right\}$$
$$\left.-\left\{\eta\frac{\mathscr{M}}{\mathscr{T}}|H_{n,k}^{sp}|^2\right\}-\left\{\mu\left(\frac{\mathscr{M}}{\mathscr{T}}+\frac{\mathscr{I}}{\mathscr{T}}\right)\right\}\right] \tag{3.21}$$

and

$$\sum_{m=0}^{K}\sum_{b=0}^{K-m}\sum_{f=0}^{K-(m+f)}\sum_{i=K-(m+b+f)}^{K-(m+b+f)}\mathscr{P}(m,b,f,i)\left[\left\{\left(\right.\right.\right.$$
$$\left.\frac{\mathscr{B}}{\mathscr{T}}\frac{\frac{|H_{n,k}^{ss}|^2}{\sigma_n^2+\sigma_{ps}^2}}{1+\frac{|H_{n,k}^{ss}|^2P_{n,k}^B(\gamma_{n,k}^{ss})}{\sigma_n^2+\sigma_{ps}^2}}\right)+\left(\frac{\mathscr{F}}{\mathscr{T}}\frac{\frac{|H_{n,k}^{ss}|^2}{\sigma_n^2}}{1+\frac{|H_{n,k}^{ss}|^2P_{n,k}^B(\gamma_{n,k}^{ss})}{\sigma_n^2}}\right)\right\}$$
$$\left.-\left\{\eta\frac{\mathscr{B}}{\mathscr{T}}|H_{n,k}^{sp}|^2\right\}-\left\{\mu\left(\frac{\mathscr{B}}{\mathscr{T}}+\frac{\mathscr{F}}{\mathscr{T}}\right)\right\}\right]. \tag{3.22}$$

By applying the Karush-Kuhn-Tucker (KKT) conditions, the following potential optimum power allocation policy when the spectrum is detected idle, $P_{n,k}^{I*}(\gamma_{n,k}^{ss})$, is

obtained

$$P_{n,k}^{I*}(\gamma_{n,k}^{ss}) = \left[\frac{\sqrt{\Delta^I} + \chi^I}{\Pi^I}\right]^+ \tag{3.23}$$

where Δ^I, χ^I , and Π^I are defined in (3.24)-(3.27), respectively.

$$\Delta^I = \left(\frac{|H_{n,k}^{ss}|^4}{(\sigma_n^2+\sigma_{ps}^2)\sigma_n^2}\left\{\frac{\mathscr{M}}{\mathscr{T}} + \frac{\mathscr{I}}{\mathscr{T}}\right\} + G^I\left\{\frac{|H_{n,k}^{ss}|^2}{\sigma_n^2+\sigma_{ps}^2} + \frac{|H_{n,k}^{ss}|^2}{\sigma_n^2}\right\}\right)^2$$
$$- \frac{4G^I|H_{n,k}^{ss}|^4}{(\sigma_n^2+\sigma_{ps}^2)\sigma_n^2}\left(\frac{|H_{n,k}^{ss}|^2}{\sigma_n^2+\sigma_{ps}^2} \times \frac{\mathscr{M}}{\mathscr{T}} + \frac{|H_{n,k}^{ss}|^2}{\sigma_n^2} \times \frac{\mathscr{I}}{\mathscr{T}} + G^I\right) \tag{3.24}$$

$$\chi^I = \frac{|H_{n,k}^{ss}|^4}{(\sigma_n^2+\sigma_{ps}^2)\sigma_n^2}\left\{\frac{\mathscr{M}}{\mathscr{T}} + \frac{\mathscr{I}}{\mathscr{T}}\right\} + G^I\left\{\frac{|H_{n,k}^{ss}|^2}{\sigma_n^2+\sigma_{ps}^2} + \frac{|H_{n,k}^{ss}|^2}{\sigma_n^2}\right\} \tag{3.25}$$

$$\Pi^I = -\frac{2G^I|H_{n,k}^{ss}|^4}{(\sigma_n^2+\sigma_{ps}^2)\sigma_n^2} \tag{3.26}$$

$$G^I = -\eta|H_{n,k}^{sp}|^2\frac{\mathscr{M}}{\mathscr{T}} - \mu\left\{\frac{\mathscr{M}}{\mathscr{T}} + \frac{\mathscr{I}}{\mathscr{T}}\right\}. \tag{3.27}$$

Subsequently, the optimal power allocation policy when the spectrum is detected busy, $P_{n,k}^{B*}(\gamma_{n,k}^{ss})$, is

$$P_{n,k}^{B*}(\gamma_{n,k}^{ss}) = \left[\frac{\sqrt{\Delta^B} + \chi^B}{\Pi^B}\right]^+ \tag{3.28}$$

where Δ^B, χ^B, and Π^B are defined in (3.29)-(3.32), respectively. $P_{n,k}^{I*}(\gamma_{n,k}^{ss})$ and $P_{n,k}^{B*}(\gamma_{n,k}^{ss})$ can be considered as multi-level water-filling algorithms.

$$\Delta^B = \left(\frac{|H_{n,k}^{ss}|^4}{(\sigma_n^2+\sigma_{ps}^2)\sigma_n^2}\left\{\frac{\mathscr{B}}{\mathscr{T}} + \frac{\mathscr{F}}{\mathscr{T}}\right\} + G^B\left\{\frac{|H_{n,k}^{ss}|^2}{\sigma_n^2+\sigma_{ps}^2} + \frac{|H_{n,k}^{ss}|^2}{\sigma_n^2}\right\}\right)^2 -$$
$$\frac{4G^B|H_{n,k}^{ss}|^4}{(\sigma_n^2+\sigma_{ps}^2)\sigma_n^2}\left(\frac{|H_{n,k}^{ss}|^2}{\sigma_n^2+\sigma_{ps}^2} \times \frac{\mathscr{B}}{\mathscr{T}} + \frac{|H_{n,k}^{ss}|^2}{\sigma_n^2} \times \frac{\mathscr{F}}{\mathscr{T}} + G^B\right) \tag{3.29}$$

$$\chi^B = \frac{|H_{n,k}^{ss}|^4}{(\sigma_n^2+\sigma_{ps}^2)\sigma_n^2}\left\{\frac{\mathscr{B}}{\mathscr{T}} + \frac{\mathscr{F}}{\mathscr{T}}\right\} + G^B\left\{\frac{|H_{n,k}^{ss}|^2}{\sigma_n^2+\sigma_{ps}^2} + \frac{|H_{n,k}^{ss}|^2}{\sigma_n^2}\right\} \tag{3.30}$$

$$\Pi^B = -\frac{2G^B|H_{n,k}^{ss}|^4}{(\sigma_n^2+\sigma_{ps}^2)\sigma_n^2} \tag{3.31}$$

$$G^B = -\eta |H^{sp}_{n,k}|^2 \frac{\mathscr{B}}{\mathscr{T}} - \mu \left\{ \frac{\mathscr{B}}{\mathscr{T}} + \frac{\mathscr{F}}{\mathscr{T}} \right\}. \tag{3.32}$$

By differentiating (3.19) with respect to $\varphi^I_{n,k}(\gamma^{ss}_{n,k})$, i.e., $\frac{\partial f^I_n(\lambda^I,\eta,\mu)}{\partial \varphi^I_{n,k}(\gamma^{ss}_{n,k})}$, we obtain

$$\begin{aligned}
&\sum_{m=0}^{K} \sum_{b=0}^{K-m} \sum_{f=0}^{K-(m+f)} \sum_{i=K-(m+b+f)}^{K-(m+b+f)} \mathscr{P}(m,b,f,i) \Bigg[\Bigg\{ \\
&\frac{\mathscr{M}}{\mathscr{T}} \left(\frac{\frac{P^I_{n,k}(\gamma^{ss}_{n,k})}{\sigma^2_n + \sigma^2_{ps}}}{\left(1 + \frac{P^I_{n,k}(\gamma^{ss}_{n,k})}{\sigma^2_n + \sigma^2_{ps}}\right) \ln(2)} + r^{10}_{n,k} \right) + \frac{\mathscr{I}}{\mathscr{T}} \left(\frac{\frac{P^I_{n,k}(\gamma^{ss}_{n,k})}{\sigma^2_n}}{\left(1 + \frac{P^I_{n,k}(\gamma^{ss}_{n,k})}{\sigma^2_n}\right) \ln(2)} + r^{00}_{n,k} \right) \Bigg\} \\
&- \left\{ \eta \frac{\mathscr{M}}{\mathscr{T}} P^I_{n,k}(\gamma^{ss}_{n,k}) |H^{sp}_{n,k}|^2 \right\} - \left\{ \mu P^I_{n,k}(\gamma^{ss}_{n,k}) \left(\frac{\mathscr{M}}{\mathscr{T}} + \frac{\mathscr{I}}{\mathscr{T}} \right) \right\} \Bigg] - \lambda^I_k
\end{aligned} \tag{3.33}$$

and by differentiating (3.20) with respect to $\varphi^B_{n,k}(\gamma^{ss}_{n,k})$, i.e., $\frac{\partial f^B_n(\lambda^B,\eta,\mu)}{\partial \varphi^B_{n,k}(\gamma^{ss}_{n,k})}$, we obtain

$$\begin{aligned}
&\sum_{m=0}^{K} \sum_{b=0}^{K-m} \sum_{f=0}^{K-(m+f)} \sum_{i=K-(m+b+f)}^{K-(m+b+f)} \mathscr{P}(m,b,f,i) \Bigg[\Bigg\{ \\
&\frac{\mathscr{B}}{\mathscr{T}} \left(\frac{\frac{P^B_{n,k}(\gamma^{ss}_{n,k})}{\sigma^2_n + \sigma^2_{ps}}}{\left(1 + \frac{P^B_{n,k}(\gamma^{ss}_{n,k})}{\sigma^2_n + \sigma^2_{ps}}\right) \ln(2)} + r^{11}_{n,k} \right) + \frac{\mathscr{F}}{\mathscr{T}} \left(\frac{\frac{P^B_{n,k}(\gamma^{ss}_{n,k})}{\sigma^2_n}}{\left(1 + \frac{P^B_{n,k}(\gamma^{ss}_{n,k})}{\sigma^2_n}\right) \ln(2)} + r^{01}_{n,k} \right) \Bigg\} \\
&- \left\{ \eta \frac{\mathscr{B}}{\mathscr{T}} P^B_{n,k}(\gamma^{ss}_{n,k}) |H^{sp}_{n,k}|^2 \right\} - \left\{ \mu P^B_{n,k}(\gamma^{ss}_{n,k}) \times \left(\frac{\mathscr{B}}{\mathscr{T}} + \frac{\mathscr{F}}{\mathscr{T}} \right) \right\} \Bigg] - \lambda^B_k .
\end{aligned} \tag{3.34}$$

In order to achieve optimal performance in $f^I_n(\lambda^I, \eta, mu)$, $\varphi^I_{n,k}(\gamma^{ss}_{n,k}) = 0$ and $\varphi^I_{n,k}(\gamma^{ss}_{n,k}) = 1$ are assigned where $\frac{\partial f^I_n(\lambda^I,\eta,\mu)}{\partial \varphi^I_{n,k}(\gamma^{ss}_{n,k})} < 0$ and $\frac{\partial f^I_n(\lambda^I,\eta,\mu)}{\partial \varphi^I_{n,k}(\gamma^{ss}_{n,k})} \geq 0$, respectively. The optimal subcarrier allocation policy is therefore achieved by assigning the k^{th} subcarrier to the user with the highest value of $\Lambda^I_{n,k}$. The problem under consideration is formulated as

$$n^{I*} = argmax(\Lambda^I_{n,k}) \quad \forall n \in \mathcal{N} \ , \ \forall k \in \mathcal{K} \tag{3.35}$$

where $\Lambda^I_{n,k}$ is defined in (3.36).

$$\Lambda^I_{n,k} = \sum_{m=0}^{K} \sum_{b=0}^{K-m} \sum_{f=0}^{K-(m+f)} \sum_{i=K-(m+b+f)}^{K-(m+b+f)} \mathscr{P}(m,b,f,i) \left[\left\{ \frac{\mathscr{M}}{\mathscr{T}} \times \right. \right.$$

$$\left(\frac{\frac{P^I_{n,k}(\gamma^{ss}_{n,k})}{\sigma^2_n+\sigma^2_{ps}}}{\left(1+\frac{P^I_{n,k}(\gamma^{ss}_{n,k})}{\sigma^2_n+\sigma^2_{ps}}\right)\ln(2)}+r^{10}_{n,k}\right)+\frac{\mathscr{I}}{\mathscr{T}}\left(\frac{\frac{P^I_{n,k}(\gamma^{ss}_{n,k})}{\sigma^2_n}}{\left(1+\frac{P^I_{n,k}(\gamma^{ss}_{n,k})}{\sigma^2_n}\right)\ln(2)}+r^{00}_{n,k}\right)\Bigg\}$$
$$-\left\{\eta\frac{\mathscr{M}}{\mathscr{T}}P^I_{n,k}(\gamma^{ss}_{n,k})|H^{sp}_{n,k}|^2\right\}-\left\{\mu P^I_{n,k}(\gamma^{ss}_{n,k})\left(\frac{\mathscr{M}}{\mathscr{T}}+\frac{\mathscr{I}}{\mathscr{T}}\right)\right\}\Bigg]. \tag{3.36}$$

Similarly, to accomplish optimal performance in $f^B_n(\lambda^B,\eta,mu)$, $\varphi^B_{n,k}(\gamma^{ss}_{n,k})=0$ and $\varphi^{BS}_{n,k}(\gamma^{ss}_{n,k})=1$ are assigned where $\frac{\partial f^B_n(\lambda^B,\eta,\mu)}{\partial\varphi^B_{n,k}(\gamma^{ss}_{n,k})}<0$ and $\frac{\partial f^B_n(\lambda^B,\eta,\mu)}{\partial\varphi^B_{n,k}(\gamma^{ss}_{n,k})}\geq 0$, respectively. The optimal subcarrier allocation policy is therefore achieved by assigning the k^{th} subcarrier to the user with the highest value of $\Lambda^B_{n,k}$ (defined in (3.38)). This problem can thus be formulated by

$$n^{B*}=argmax(\Lambda^B_{n,k})\ \ \forall n\in\mathcal{N}\ ,\ \forall k\in\mathcal{K}. \tag{3.37}$$

$$\Lambda^B_{n,k}=\sum_{m=0}^{K}\sum_{b=0}^{K-m}\sum_{f=0}^{K-(m+f)}\sum_{i=K-(m+b+f)}^{K-(m+b+f)}\mathscr{P}(m,b,f,i)\Bigg[\Bigg\{\frac{\mathscr{B}}{\mathscr{T}}\times$$
$$\left(\frac{\frac{P^B_{n,k}(\gamma^{ss}_{n,k})}{\sigma^2_n+\sigma^2_{ps}}}{\left(1+\frac{P^B_{n,k}(\gamma^{ss}_{n,k})}{\sigma^2_n+\sigma^2_{ps}}\right)\ln(2)}+r^{11}_{n,k}\right)+\frac{\mathscr{F}}{\mathscr{T}}\left(\frac{\frac{P^B_{n,k}(\gamma^{ss}_{n,k})}{\sigma^2_n}}{\left(1+\frac{P^B_{n,k}(\gamma^{ss}_{n,k})}{\sigma^2_n}\right)\ln(2)}+r^{01}_{n,k}\right)\Bigg\}$$
$$-\left\{\eta\frac{\mathscr{B}}{\mathscr{T}}P^B_{n,k}(\gamma^{ss}_{n,k})|H^{sp}_{n,k}|^2\right\}-\left\{\mu P^B_{n,k}(\gamma^{ss}_{n,k})\left(\frac{\mathscr{B}}{\mathscr{T}}+\frac{\mathscr{F}}{\mathscr{T}}\right)\right\}\Bigg]. \tag{3.38}$$

3.4.3 Sub-Gradient Method

For any optimal values of $\left(P^{I*}_{n,k}(\gamma^{ss}_{n,k}),P^{B*}_{n,k}(\gamma^{ss}_{n,k}),\varphi^{I*}_{n,k}(\gamma^{ss}_{n,k}),\varphi^{B*}_{n,k}(\gamma^{ss}_{n,k})\right)$, the dual variables are updated as follows

$$\eta(t+1)=\eta(t)-\tau_1(t)\Big(I_{th}-C_{H2}\Big) \tag{3.39}$$

and

$$\mu(t+1)=\mu(t)-\tau_2(t)\Big(P_t-C_{H1}\Big) \tag{3.40}$$

where t is the iteration number, and $\tau_1(t)$ and $\tau_2(t)$ respectively denote the step sizes for the interference and power constraints.

To guarantee optimality, λ_k^I and λ_k^B should be selected between the first and second maxima of $\Lambda_{n,k}^B$ and $\Lambda_{n,k}^B$, respectively. By replacing (3.23) and (3.35) in (3.19), and (3.28) and (3.37) in (3.20), $f_n^I(\lambda^I, \eta, \mu)$ and $f_n^B(\lambda^B, \eta, \mu)$, and ultimately the solution to (3.13) can be obtained.

3.5 Opportunistic Spectrum Access

In the opportunistic spectrum access strategy, the secondary users simultaneously sense all frequency bands and access only those that are detected to be idle. The accuracy of the spectrum sensing mechanism is of great importance towards preserving the QoS of the primary service users. As previously discussed, spectrum sensing mechanism decisions may be erroneous. In the case of detecting the spectrum as idle when it is actually busy, the cognitive operation imposes harmful interference on the primary network. Most of the existing works on opportunistic spectrum access assume perfect sensing and thus employ an aggressive radio resource allocation. In contrast, in this work, resources are allocated within all detected idle channels while possible interference due to mis-detection is not allowed to exceed the interference constraint.

The instantaneous rate of the OFDMA cognitive radio system for user n and subcarrier k, for idle detected and actual spectrum, i.e., S_{00}, and for mis-detection, i.e., S_{01}, scenarios can be respectively expressed as

$$r_{n,k}^0 = \log_2\left(1 + \frac{P_{n,k}(\gamma_{n,k}^{ss})|H_{n,k}^{ss}|^2}{\sigma_n^2}\right) \tag{3.41}$$

$$r_{n,k}^1 = \log_2\left(1 + \frac{P_{n,k}(\gamma_{n,k}^{ss})|H_{n,k}^{ss}|^2}{\sigma_n^2 + \sigma_{ps}^2}\right). \tag{3.42}$$

For the opportunistic spectrum access scenario under consideration, the OFDMA

CR network aggregate instantaneous rate can be formulated as follows

$$R_O = \sum_{m=0}^{K} \sum_{b=0}^{K-m} \sum_{f=0}^{K-(m+f)} \sum_{i=K-(m+b+f)}^{K-(m+b+f)} \mathscr{P}(m,b,f,i) \left(\frac{\mathscr{M}}{\mathscr{T}} \sum_{n=1}^{N} \sum_{k=1}^{K} \varphi_{n,k}(\gamma_{n,k}^{ss}) r_{n,k}^{1} + \frac{\mathscr{I}}{\mathscr{T}} \sum_{n=1}^{N} \sum_{k=1}^{K} \varphi_{n,k}(\gamma_{n,k}^{ss}) r_{n,k}^{0} \right). \tag{3.43}$$

The constraint on the average transmit power can be expressed as

$$C_{O1} : \sum_{m=0}^{K} \sum_{b=0}^{K-m} \sum_{f=0}^{K-(m+f)} \sum_{i=K-(m+b+f)}^{K-(m+b+f)} \mathscr{P}(m,b,f,i) \times \left(\frac{\mathscr{M}}{\mathscr{T}} \sum_{n=1}^{N} \sum_{k=1}^{K} \varphi_{n,k}(\gamma_{n,k}^{ss}) P_{n,k}(\gamma_{n,k}^{ss}) + \frac{\mathscr{I}}{\mathscr{T}} \times \sum_{n=1}^{N} \sum_{k=1}^{K} \varphi_{n,k}(\gamma_{n,k}^{ss}) P_{n,k}(\gamma_{n,k}^{ss}) \right). \tag{3.44}$$

The constraint on the aggregate received interference on the primary network is computed by

$$C_{O2} : \sum_{m=0}^{K} \sum_{b=0}^{K-m} \sum_{f=0}^{K-(m+f)} \sum_{i=K-(m+b+f)}^{K-(m+b+f)} \mathscr{P}(m,b,f,i) \times \left(\frac{\mathscr{M}}{\mathscr{T}} \sum_{n=1}^{N} \sum_{k=1}^{K} \varphi_{n,k}(\gamma_{n,k}^{ss}) P_{n,k}(\gamma_{n,k}^{ss}) |H_{n,k}^{sp}|^2 \right). \tag{3.45}$$

In order to maximize the aggregate instantaneous rate of the OFDMA CR system, we formulate the following optimization problem.

Problem $\mathscr{O}_2$:

$$\max_{P_{n,k}(\gamma_{n,k}^{ss}), \varphi_{n,k}(\gamma_{n,k}^{ss})} R_O \tag{3.46a}$$

$$\text{s. t.:} \quad C_{O1} \leq P_t \tag{3.46b}$$

$$C_{O2} \leq I_{th} \tag{3.46c}$$

$$\sum_{n=1}^{N} \varphi_{n,k}(\gamma_{n,k}^{ss}) = 1 \ , \ k \in \mathcal{K} \tag{3.46d}$$

$$\varphi_{n,k}(\gamma_{n,k}^{ss}) \in \{0,1\} \ , \ n \in \mathcal{N} \ , \ k \in \mathcal{K}. \tag{3.46e}$$

3.5.1 Lagrangian Function

The Lagrangian function for solving Problem $\mathscr{O}_2$ can be expressed as

$$L(\lambda,\eta,\mu) = R_O - \sum_{k=1}^{K}\lambda_k\left(\sum_{n=1}^{N}\varphi_{n,k}(\gamma_{n,k}^{ss}) - 1\right) - \eta\Big(C_{O2} - I_{th}\Big) - \mu\Big(C_{O1} - P_t\Big). \tag{3.47}$$

3.5.2 Lagrangian Dual Problem

The Lagrangian dual function under consideration is therefore

$$\min_{\lambda,\eta,\mu}\Big(F(\lambda,\eta,\mu)\Big)\ ,\ s.t.:\ \lambda,\eta,\mu \geq 0 \tag{3.48}$$

where

$$F(\lambda,\eta,\mu) = \sum_{n=1}^{N} f_n(\lambda,\eta,\mu) + \sum_{k=1}^{K}\lambda_k + \eta I_{th} + \mu P_t \tag{3.49}$$

and

$$f_n(\lambda,\eta,\mu) = \max_{P_{n,k}(\gamma_{n,k}^{ss}),\varphi_{n,k}(\gamma_{n,k}^{ss})}\Bigg(R_O^n - \sum_{k=1}^{K}\lambda_k\varphi_{n,k}(\gamma_{n,k}^{ss}) - \eta C_{O2}^n - \mu C_{O1}^n\Bigg) \tag{3.50}$$

where $\forall n \in \mathcal{N}$, R_O^n is the rate per user, C_{O1}^n denotes the average power per user, and C_{O2}^n is the interference per user, given

$$R_O^n = \sum_{m=0}^{K}\sum_{b=0}^{K-m}\sum_{f=0}^{K-(m+f)}\sum_{i=K-(m+b+f)}^{K-(m+b+f)}\mathscr{P}(m,b,f,i)\times \left(\frac{\mathscr{M}}{\mathscr{T}}\sum_{k=1}^{K}\varphi_{n,k}(\gamma_{n,k}^{ss})r_{n,k}^{1} + \frac{\mathscr{I}}{\mathscr{T}}\sum_{k=1}^{K}\varphi_{n,k}(\gamma_{n,k}^{ss})r_{n,k}^{0}\right), \tag{3.51}$$

$$C_{O1}^{n}: \sum_{m=0}^{K}\sum_{b=0}^{K-m}\sum_{f=0}^{K-(m+f)}\sum_{i=K-(m+b+f)}^{K-(m+b+f)} \mathscr{P}(m,b,f,i)\times$$
$$\left(\frac{\mathscr{M}}{\mathscr{T}}\sum_{k=1}^{K}\varphi_{n,k}(\gamma_{n,k}^{ss})P_{n,k}(\gamma_{n,k}^{ss}) + \frac{\mathscr{I}}{\mathscr{T}}\sum_{k=1}^{K}\varphi_{n,k}(\gamma_{n,k}^{ss})P_{n,k}(\gamma_{n,k}^{ss})\right). \tag{3.52}$$

and

$$C_{O2}^{n}: \sum_{m=0}^{K}\sum_{b=0}^{K-m}\sum_{f=0}^{K-(m+f)}\sum_{i=K-(m+b+f)}^{K-(m+b+f)} \mathscr{P}(m,b,f,i)\times$$
$$\left(\frac{\mathscr{M}}{\mathscr{T}}\sum_{k=1}^{K}\varphi_{n,k}(\gamma_{n,k}^{ss})P_{n,k}(\gamma_{n,k}^{ss})|H_{n,k}^{sp}|^2\right) \tag{3.53}$$

By computing $\frac{\partial f_n(\lambda,\eta,\mu)}{\partial\left(\varphi_{n,k}(\gamma_{n,k}^{ss})P_{n,k}(\gamma_{n,k}^{ss})\right)}$, the following expression is derived

$$\sum_{m=0}^{K}\sum_{b=0}^{K-m}\sum_{f=0}^{K-(m+f)}\sum_{i=K-(m+b+f)}^{K-(m+b+f)} \mathscr{P}(m,b,f,i)\left[\left\{\left(\right.\right.\right.$$
$$\left.\left.\left.\frac{\mathscr{M}}{\mathscr{T}}\frac{\frac{|H_{n,k}^{ss}|^2}{\sigma_n^2+\sigma_{ps}^2}}{1+\frac{|H_{n,k}^{ss}|^2P_{n,k}(\gamma_{n,k}^{ss})}{\sigma_n^2+\sigma_{ps}^2}}\right) + \left(\frac{\mathscr{I}}{\mathscr{T}}\frac{\frac{|H_{n,k}^{ss}|^2}{\sigma_n^2}}{1+\frac{|H_{n,k}^{ss}|^2P_{n,k}(\gamma_{n,k}^{ss})}{\sigma_n^2}}\right)\right\}$$
$$-\left\{\eta\frac{\mathscr{M}}{\mathscr{T}}|H_{n,k}^{sp}|^2\right\} - \left\{\mu\left(\frac{\mathscr{M}}{\mathscr{T}}+\frac{\mathscr{I}}{\mathscr{T}}\right)\right\}\Bigg]. \tag{3.54}$$

Consequently, by applying KKT conditions, the potential optimal power allocation policy, $P_{n,k}^{*}(\gamma_{n,k}^{ss})$, is

$$P_{n,k}^{*}(\gamma_{n,k}^{ss}) = \left[\frac{\sqrt{\Delta}+\chi}{\Pi}\right]^{+} \tag{3.55}$$

where

$$\Delta = \left(\frac{|H_{n,k}^{ss}|^4}{(\sigma_n^2+\sigma_{ps}^2)\sigma_n^2}\left\{\frac{\mathscr{M}}{\mathscr{T}}+\frac{\mathscr{I}}{\mathscr{T}}\right\} + G\left\{\frac{|H_{n,k}^{ss}|^2}{\sigma_n^2+\sigma_{ps}^2}+\frac{|H_{n,k}^{ss}|^2}{\sigma_n^2}\right\}\right)^2$$
$$-\frac{4G|H_{n,k}^{ss}|^4}{(\sigma_n^2+\sigma_{ps}^2)\sigma_n^2}\left(\frac{|H_{n,k}^{ss}|^2}{\sigma_n^2+\sigma_{ps}^2}\frac{\mathscr{M}}{\mathscr{T}}+\frac{|H_{n,k}^{ss}|^2}{\sigma_n^2}\frac{\mathscr{I}}{\mathscr{T}}+G\right) \tag{3.56}$$

$$\chi = \frac{|H_{n,k}^{ss}|^4}{(\sigma_n^2+\sigma_{ps}^2)\sigma_n^2}\left\{\frac{\mathscr{M}}{\mathscr{T}}+\frac{\mathscr{I}}{\mathscr{T}}\right\}+G\left\{\frac{|H_{n,k}^{ss}|^2}{\sigma_n^2+\sigma_{ps}^2}+\frac{|H_{n,k}^{ss}|^2}{\sigma_n^2}\right\} \tag{3.57}$$

$$\Pi = \frac{2G|H_{n,k}^{ss}|^4}{(\sigma_n^2+\sigma_{ps}^2)\sigma_n^2} \tag{3.58}$$

$$G = -\eta|H_{n,k}^{sp}|^2\frac{\mathscr{M}}{\mathscr{T}}-\mu\left\{\frac{\mathscr{M}}{\mathscr{T}}+\frac{\mathscr{I}}{\mathscr{T}}\right\}. \tag{3.59}$$

$P_{n,k}^*(\gamma_{n,k}^{ss})$ can be considered as a multi-level water-filling algorithm. By differentiating (3.50) with respect to $\varphi_{n,k}(\gamma_{n,k}^{ss})$, i.e., $\frac{\partial f_n(\lambda,\eta,\mu)}{\partial\varphi_{n,k}(\gamma_{n,k}^{ss})}$, we obtain

$$\begin{aligned}
&\sum_{m=0}^{K}\sum_{b=0}^{K-m}\sum_{f=0}^{K-(m+f)}\sum_{i=K-(m+b+f)}^{K-(m+b+f)}\mathscr{P}(m,b,f,i)\Bigg[\Bigg\{\\
&\frac{\mathscr{M}}{\mathscr{T}}\left(\frac{\frac{P_{n,k}(\gamma_{n,k}^{ss})}{\sigma_n^2+\sigma_{ps}^2}}{\left(1+\frac{P_{n,k}(\gamma_{n,k}^{ss})}{\sigma_n^2+\sigma_{ps}^2}\right)\ln(2)}+r_{n,k}^1\right)+\frac{\mathscr{I}}{\mathscr{T}}\left(\frac{\frac{P_{n,k}(\gamma_{n,k}^{ss})}{\sigma_n^2}}{\left(1+\frac{P_{n,k}^I(\gamma_{n,k}^{ss})}{\sigma_n^2}\right)\ln(2)}+r_{n,k}^0\right)\Bigg\}\\
&-\left\{\eta\frac{\binom{K-1}{m-1}\binom{K-m}{b}}{\binom{K}{m}\binom{K-m}{b}}\frac{\binom{K-m-b}{f}\binom{K-m-b-f}{i}}{\binom{K-m-b}{f}\binom{K-m-b-f}{i}}P_{n,k}(\gamma_{n,k}^{ss})|H_{n,k}^{sp}|^2\right\}\\
&-\left\{\mu P_{n,k}(\gamma_{n,k}^{ss})\left(\frac{\mathscr{M}}{\mathscr{T}}+\frac{\mathscr{I}}{\mathscr{T}}\right)\right\}\Bigg]-\lambda_k.
\end{aligned} \tag{3.60}$$

In order to achieve optimal performance in $f_n(\lambda,\eta,mu)$, $\varphi_{n,k}(\gamma_{n,k}^{ss})=0$ and $\varphi_{n,k}(\gamma_{n,k}^{ss})=1$ are assigned where $\frac{\partial f_n(\lambda,\eta,\mu)}{\partial\varphi_{n,k}(\gamma_{n,k}^{ss})}<0$ and $\frac{\partial f_n(\lambda,\eta,\mu)}{\partial\varphi_{n,k}(\gamma_{n,k}^{ss})}\geq 0$, respectively. The optimal subcarrier allocation policy is therefore achieved by assigning the k^{th} subcarrier to the user with the highest value of $\Lambda_{n,k}$. The problem under consideration is formulated as

$$n^* = argmax(\Lambda_{n,k}) \quad \forall n\in\mathcal{N}\ ,\ \forall k\in\mathcal{K} \tag{3.61}$$

where

$$\Lambda_{n,k} = \sum_{m=0}^{K}\sum_{b=0}^{K-m}\sum_{f=0}^{K-(m+f)}\sum_{i=K-(m+b+f)}^{K-(m+b+f)}\mathscr{P}(m,b,f,i)\Bigg[\Bigg\{$$

$$\frac{\mathscr{M}}{\mathscr{T}}\left(\frac{\frac{P_{n,k}(\gamma_{n,k}^{ss})}{\sigma_n^2+\sigma_{ps}^2}}{\left(1+\frac{P_{n,k}(\gamma_{n,k}^{ss})}{\sigma_n^2+\sigma_{ps}^2}\right)\ln(2)}+r_{n,k}^1\right)+\frac{\mathscr{I}}{\mathscr{T}}\left(\frac{\frac{P_{n,k}(\gamma_{n,k}^{ss})}{\sigma_n^2}}{\left(1+\frac{P_{n,k}^I(\gamma_{n,k}^{ss})}{\sigma_n^2}\right)\ln(2)}+r_{n,k}^0\right)\Bigg\}$$
$$-\left\{\eta\frac{\binom{K-1}{m-1}\binom{K-m}{b}}{\binom{K}{m}\binom{K-m}{b}}\frac{\binom{K-m-b}{f}\binom{K-m-b-f}{i}}{\binom{K-m-b}{f}\binom{K-m-b-f}{i}}P_{n,k}(\gamma_{n,k}^{ss})|H_{n,k}^{sp}|^2\right\}-$$
$$\left\{\mu P_{n,k}(\gamma_{n,k}^{ss})\left(\frac{\mathscr{M}}{\mathscr{T}}+\frac{\mathscr{I}}{\mathscr{T}}\right)\right\}\Bigg]. \tag{3.62}$$

3.5.3 Sub-Gradient Method

For any optimal pair of $\left(P_{n,k}^*(\gamma_{n,k}^{ss}),\varphi_{n,k}^*(\gamma_{n,k}^{ss})\right)$, the dual variables are updated as follows

$$\eta(t+1)=\left[\eta(t)-\tau_1(t)\left(I_{th}-C_{O2}\right)\right]^+ \tag{3.63}$$

and

$$\mu(t+1)=\left[\mu(t)-\tau_2(t)\left(P_t-C_{O1}\right)\right]^+ \tag{3.64}$$

where, as previously mentioned, t is the iteration number, and $\tau_1(t)$ and $\tau_2(t)$ respectively denote the step sizes for the interference and power constraints. By replacing (3.55) and (3.61) in (3.50), $f_n^I(\lambda^I,\eta,\mu)$, and ultimately the solution to (3.49) can be obtained.

3.6 Performance Evaluation and Discussion

The performance of the downlink OFDMA CR network with hybrid and opportunistic spectrum access scheme using the proposed stochastic RRA algorithm subject to satisfying peak transmit and interference power limits is studied. The total system bandwidth is divided into 8 subcarriers each with 18 kHz. $|H_{n,k}^{ss}|^2$ are assumed to be Exponentially-distributed with mean values taken as Uniformly-distributed random variables within 0 to 1, $\forall n\in\{1,...,N\},\forall k\in\{1,...,K\}$. Further, interfering cross-link power gains, $|g_k^{sp}|^2$ are considered to be Exponentially-distributed with a mean

of 0.5, $\forall k \in \{1, ..., K\}$. Note that equal receiver operating characteristic (ROC) is assumed over all users and subcarriers. All results correspond to an OFDMA CR network with 3 SRxs.

Fig. 3.1, and Fig. 3.2 show the aggregate transmission rate of the OFDMA CR network using the proposed stochastic RRA algorithm versus the spectrum sensing detection probability for the hybrid case and opportunistic case respectively. As expected, a higher probability of detection results in improved R_H performance due to a more reliable detection of the licensed spectrum, resulting in higher probabilities of scenarios $S^{ii}_{n,k}$ and $S^{bb}_{n,k}$ and consequently harmless joint underlay and overlay cognitive communications. Further, the gain in performance increases for higher probabilities of licensed band availability, particularly under accurate sensing information. E.g., for $\mathscr{P}^d_{n,k} = 0.8$, by increasing $\mathscr{P}(\mathscr{H}^i_{n,k})$ from 0.5 to 0.6, the achievable aggregate transmission rate is improved by 36.80%.

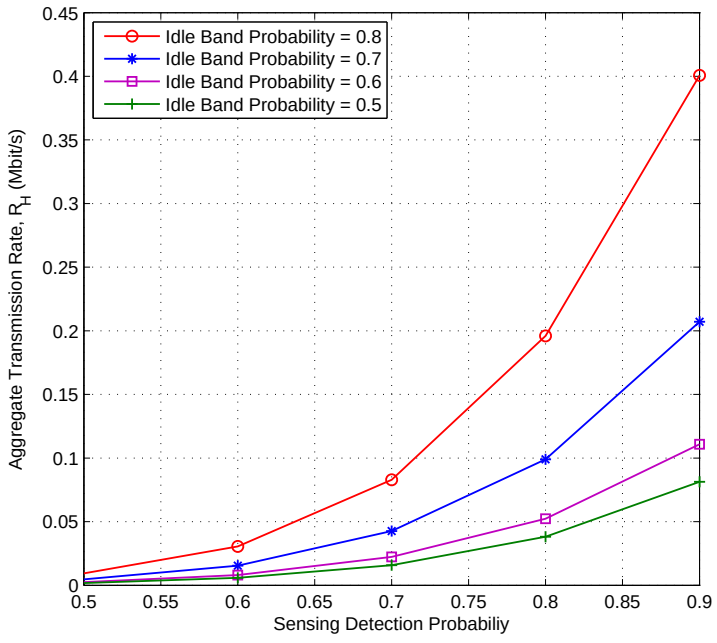

Figure 3.1: Aggregate transmission rate for the hybrid case versus sensing detection probability $\mathscr{P}^d_{n,k}$ with different probabilities of channel availability $\mathscr{P}(\mathscr{H}^i_{n,k})$. System parameters are: $I_{th} = 1$ Watts, $P_t = 5$ Watts, $\sigma^2_{ps} = 0.01$ Watts, $\sigma^2_n = 0.001$ Watts.

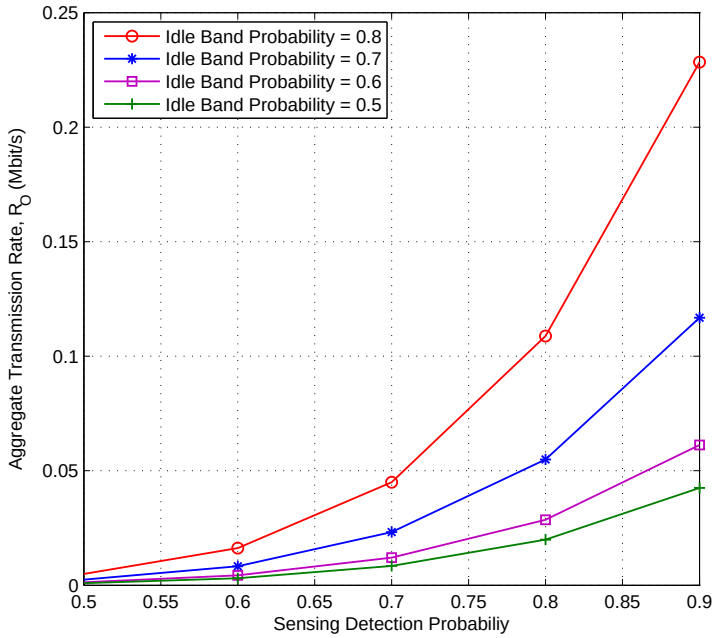

Figure 3.2: Aggregate transmission rate for the opportunistic case versus sensing detection probability $\mathscr{P}^d_{n,k}$ with different probabilities of channel availability $\mathscr{P}(\mathscr{H}^i_{n,k})$. System parameters are: $I_{th} = 1$ Watts, $P_t = 5$ Watts, $\sigma^2_{ps} = 0.01$ Watts, $\sigma^2_n = 0.001$ Watts.

The achievable aggregate transmission rate of the OFDMA CRs against the interference power constraint for different values of transmit power threshold and primary-secondary interference power for hybrid case and opportunistic case are respectively depicted in Fig. 3.3 and Fig. 3.4. Trivially, a higher interference power limit allows for greater transmission power which in turn improves the rate performance. The gain in R_H, however, reaches a plateau in high I_{th} region as P_t becomes the dominant power constraint. In areas where I_{th} is subordinate, a higher P_t and lower σ^2_{ps} setting enhances the CRs uppermost transmission rate performance. In addition, the impact of various primary-secondary interference power values on the attainable number of bits per second are illustrated in Fig. 3.5 for hybrid case and 3.6 for opportunistic case. A higher value of σ^2_{ps} degrades the overall cognitive network performance, especially due to its deteriorating effect in the events of mis-detection.

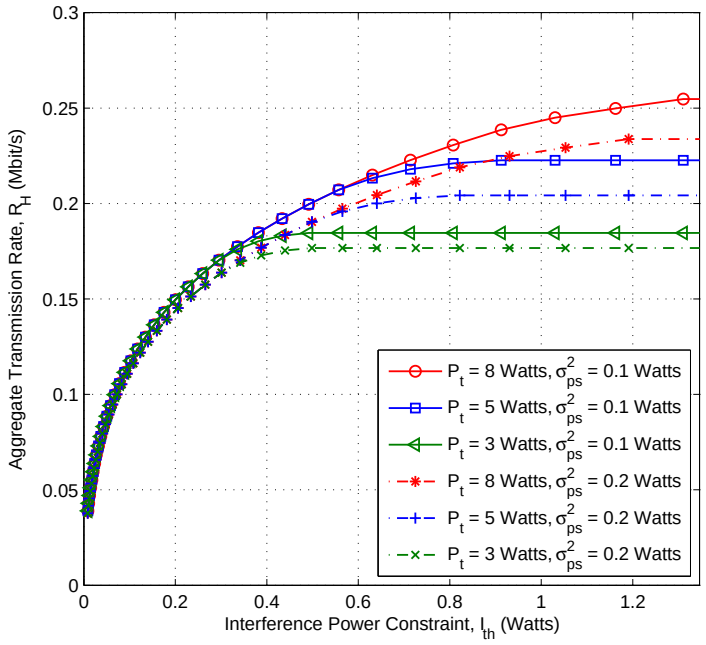

Figure 3.3: Aggregate transmission rate for the hybrid case against interference power thresholds with different transmit power constraints and primary-secondary noise levels. System parameters are: $\sigma_n^2 = 0.002$ Watts, $\mathscr{P}^d_{n,k} = 0.9$, $\mathscr{P}(\mathscr{H}^i_{n,k}) = 0.8$.

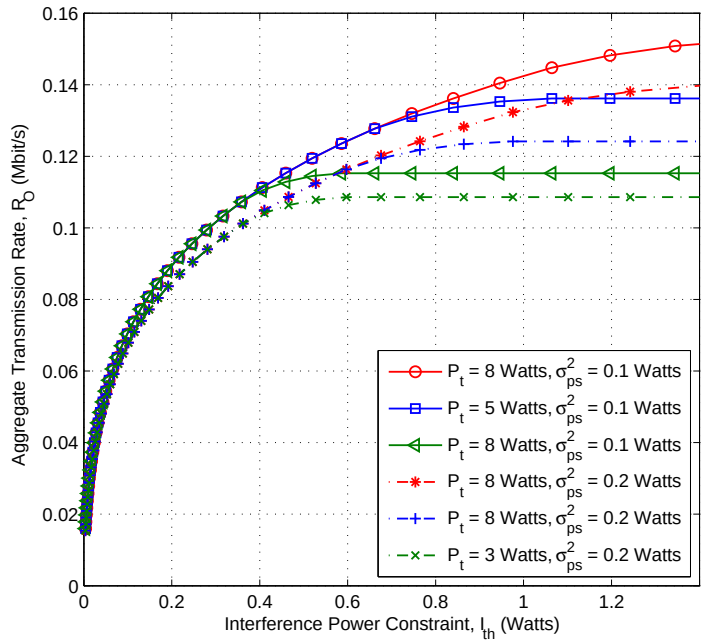

Figure 3.4: Aggregate transmission rate for the opportunistic case against interference power thresholds with different transmit power constraints and primary-secondary noise levels. System parameters are: $\sigma_n^2 = 0.002$ Watts, $\mathscr{P}^d_{n,k} = 0.9$, $\mathscr{P}(\mathscr{H}^i_{n,k}) = 0.8$.

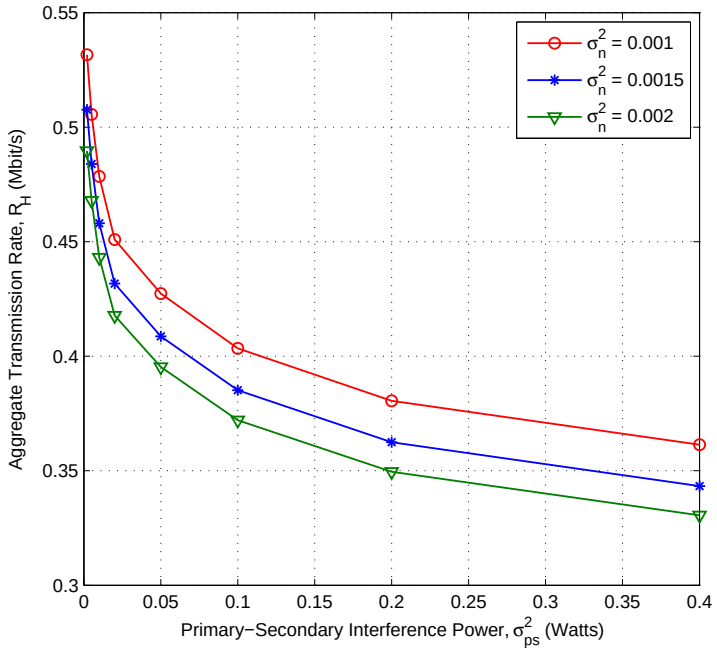

Figure 3.5: Aggregate transmission rate for the hybrid case versus primary-secondary interference power levels with different noise power values. System parameters are: $I_{th} = 5$ Watts, $P_t = 10$ Watts, $\mathscr{P}^d_{n,k} = 0.9$, $\mathscr{P}(\mathscr{H}^i_{n,k}) = 0.8$.

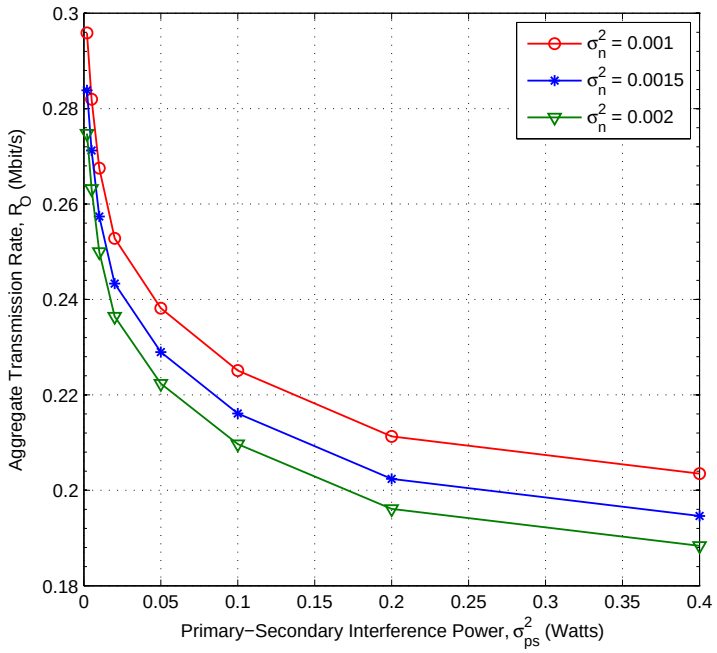

Figure 3.6: Aggregate transmission rate for the opportunistic case versus primary-secondary interference power levels with different noise power values. System parameters are: $I_{th} = 5$ Watts, $P_t = 10$ Watts, $\mathscr{P}^d_{n,k} = 0.9$, $\mathscr{P}(\mathscr{H}^i_{n,k}) = 0.8$.

We compare the performance of the proposed stochastic hybrid RRA algorithm with the stochastic conservative approach where cognitive transmission only commences over idle detected bands. Fig. 3.7, and Fig. 3.8, show that the hybrid solution provides superior performance in comparison through added flexibility on resource allocation decisions. The improvement is particularly significant in the case of inaccurate spectrum sensing information where the hard-decision-based approach severely limits the CRs overall rate performance.

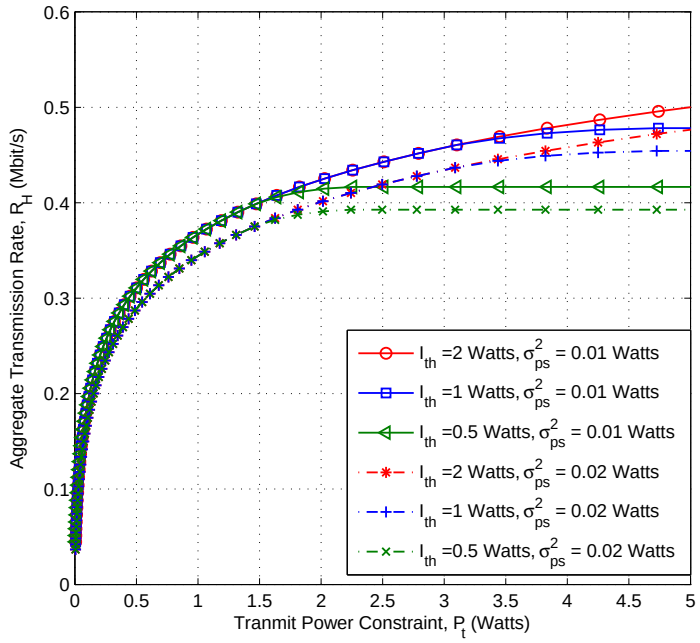

Figure 3.7: Aggregate transmission rate for the Hybrid case against transmit power thresholds using the proposed RRA algorithm with different interference constraints and primary-secondary noise levels. System parameters are: $\sigma^2_{ps} = 0.01$ Watts, $\sigma^2_n = 0.002$ Watts, $\mathscr{P}^d_{n,k} = 0.9$, $\mathscr{P}(\mathscr{H}^i_{n,k}) = 0.8$.

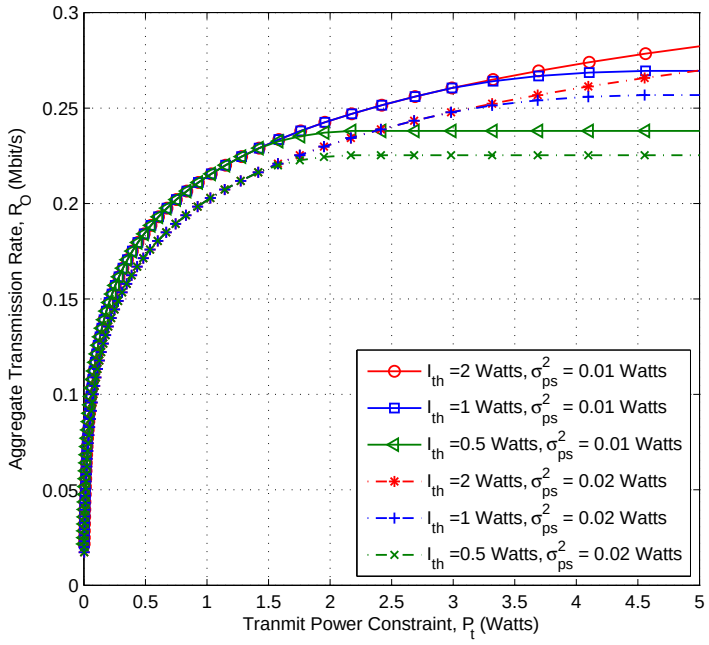

Figure 3.8: Aggregate transmission rate for the opportunistic case versus transmit power thresholds using the proposed RRA algorithm with different interference constraints and primary-secondary noise levels. System parameters are: $\sigma^2_{ps} = 0.01$ Watts, $\sigma^2_n = 0.002$ Watts, $\mathscr{P}^d_{n,k} = 0.9$, $\mathscr{P}(\mathscr{H}^i_{n,k}) = 0.8$.

3.7 Conclusions

In this section, we developed stochastic resource allocation algorithms for multi-user multi-band OFDMA-based CRs with joint underlay and overlay spectrum access mechanism over wireless fading channels. In contrast to the state-of-the-art hard-decision-based methods, our novel solution allocated radio resources based on the collective stochastic information of different number of subcarriers experiencing different idle, false-alarm, mis-detection, and busy scenarios, resulting in improved overall transmission rate performance. At the same time, stochastic transmit and interference power constraints were imposed on the CRs in order to tailor for the imperfectness associated with the spectrum sensing information.

Chapter 4

Quality-Aware Resource Allocation for Scalable Video Transmission over Cognitive Radio Networks

4.1 Introduction

In recent years, due to the advanced development in digital technology and mobile computing, and with the rising number of multimedia mobile terminals, there has been a significant increase in demand for support of multimedia applications over wireless networks. This trend has caused a critical shortage of the radio spectrum resource. Efficient deployment of the available spectrum resources is therefore a top priority. (OFDM) is a potential radio access technology for CR networks due to its flexibility and adaptability in the physical layer [93]. However, video streams are delay-sensitive and bandwidth-intensive [94], hence, transmitting and decoding the video streams is more challenging than generic data and voice. Scalable video codec (SVC) extension of the H.264/AVC standard provides significant benefits for CR applications due to its temporal, spatial, and quality scalability that enables on-the-fly codec reconfiguration based on video quality, required resolution at the terminal, and channel conditions [95]. In this chapter, we propose a quality-aware (QA) flexible

and adaptive cross-layer resource allocation scheme for multi-user video applications over OFDMA-based CR networks with probabilistic interference constraint.

Adaptive resource allocation for OFDMA-based CR networks has been studied extensively in the past few years [96–98]. Suboptimal and optimal power allocation policies are examined in [99], where the total capacity of the CR system is maximized under a primary receiver (PRx) interference limit. In [100], to maximize the system throughput in OFDMA-based CR networks, a fair resource allocation scheme in the physical layer is devised, while ensuring PRx interference limit. The authors in [101] developed an efficient algorithm by jointly considering secondary transmitter (STx) transmission power budget and PRx interference limit. The work in [102] introduces a low-complexity algorithm to maximize CR network total capacity while satisfying secondary receiver (SRx) proportional rate requirements. In [103], an optimal resource allocation scheme is developed to maximize CR network throughput under both imperfect and perfect sensing conditions. The authors in [104] focused on the probabilities of unused sub-channels in an OFDMA-based cognitive wireless network with the objective of optimizing total CR network utility. Quality of service (QoS) support issues in OFDMA-based CR networks have already been investigated in a few studies. The authors in [105] and [106] formulated the joint power and bit allocation problem while considering secondary network QoS constraints. The goal was to maximize the overall secondary network capacity by adjusting STx transmit power, whilst satisfying SRx minimum signal-to-interference-plus-noise ratio (SINR) requirements. The work in [107] developed a strategy for broadcasting scalable H.264 videos over non-cognitive downlink MIMO–OFDM systems. However the adopted technique in this scheme is based on the piecewise linear PSNR-rate model for the layered SVC video streams, which would be considered to be wasteful in terms of bit-rate as the increase in bit-rate does not project the real increment in PSNR for the layered SVC resource adaptation.

To the best of authors' knowledge, there have been few studies on Quality-Aware cross-layer resource allocation in OFDMA-based CR networks. The authors in [108] addressed the resource allocation problem in an OFDMA-based CR system using a cross-layer approach to provide satisfactory QoS to both real-time and non-real-

time video applications. The work in [109] proposed a resource allocation scheme for OFDMA-based CR networks with per-subcarrier power limit. The design in [110] for OFDMA-based CR networks considers the transmission of scalable video over OFDMA-based CR networks and attempts to perform bit, subcarrier, and power allocation for different SRx such that the total rate of the CR network increases, resulting in improved video quality. Although these works have improved the resource allocation of OFDMA-based CR networks, the users' quality-rate (Q-R) model of the video bit stream has not been considered. Furthermore, one of the main challenges associated with CR network design is estimating the channels between the STx and the PRx to ensure that interference is maintained under control. Most of the previous works on CR networks resource allocation, assume perfect channel state information (CSI) between the secondary transmitter (STx) and the PRx, and few have considered imperfect CSI. [111] and [112] considered a spectrum sharing scenario with imperfect cross-link CSI. The authors derived optimal power and ergodic capacity for the secondary network subject to PRx instantaneous interference outage. However, the results correspond to a single cognitive user and a single carrier. Motivated by these results, in this chapter, a cross-layer QA resource allocation algorithm is developed to optimize OFDMA-based CR networks performance, considering imperfect STx to PRx cross-link CSI, whilst satisfying the PRx interfering probability constraint. Thus, the proposed framework incorporates the probabilistic nature of the CSI. One of the most challenging issues associated with implementing probabilistic constrained optimization design is the intensive computational complexity to perform stochastic analysis. We develop an efficient and mathematically accurate approach to replace the probabilistic constraints by deterministic ones. The main contributions of this chapter are:

- Proposing a new low-complexity formulation for the probabilistic imperfect STx to PRx cross-link CSI.

- Developing a new closed-form expression for deterministic approximation of the probabilistic PRx interference constraint, in order to solve the probabilistic constrained mixed discrete-continuous non-linear programing (MDCNLP)

problem.

- Analyzing the problem of maximizing overall SRx quality of multi-user scalable video applications subject to prescribed total transmission power, maximum interference limit on the PRx and minimum acceptable video quality.

The remainder of this chapter is organized as follows: In Section 4.2 we describe the system model and the associated assumptions, including framework structures, network distribution model, primary transmitter (PTx) to SRx interference, and STx to PRx interference limit. In Section 4.4, the Non-linear optimization problem, deterministic constraints, and probabilistic interference conditions are formulated. Section 4.3 briefly describes the scalable video compression structure and video user quality model. In Section 4.5 we present our optimization algorithm in two parts. Performance of the proposed method is evaluated using computer simulations in Section 4.6. Finally, a summary of the main results and contributions is provided in Section 4.7.

4.2 THE NETWORK MODEL

4.2.1 Network Model

We consider a downlink multi-user video streaming scenario for OFDMA-based cognitive radio networks. The proposed model consists of one secondary transmitter (STx), one primary transmitter (PTx), N secondary receivers (SRxs), and M PRxs. It is assumed that each subcarrier experiences frequency-flat fading. The sets of subcarriers, PRx, and SRx are respectively denoted by: $\mathbb{K} = \{1, ..., K\}$, $\mathbb{M} = \{1, ..., M\}$, and $\mathbb{N} = \{1, ..., N\}$. When a cognitive user requests a video, it sends a messages to the STx, the STx then forwards the demand to the video server where the adaptive SVC encoder encodes the video into several layers and delivers the layers to the intermediate control server (ICS). ICS re-packetizes the received packets from the video server in a way that the STx recognizes the layer IDs. The proposed packetization scheme in described in section 4.3.

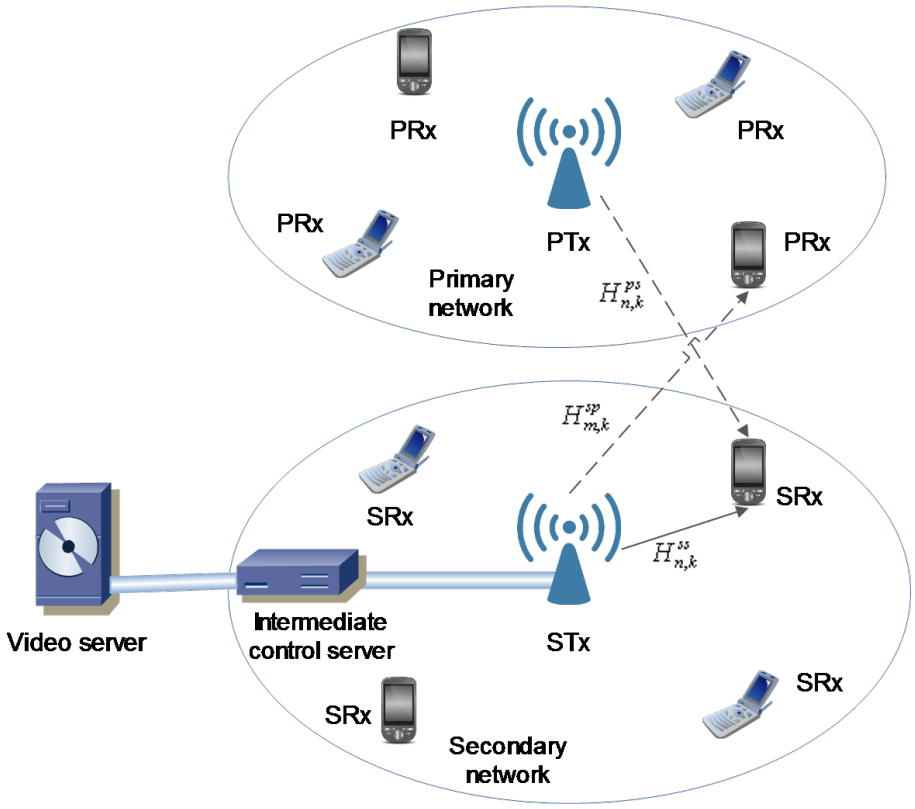

Figure 4.1: Network model, one STx, one PTx, and multiple uniformly distributed PRx and SRx.

In CR networks, where the primary and secondary users are distributed side by side, the mutual interference affects both the primary and the secondary systems. Let B denote the overall available bandwidth for secondary users and we also assume that each sub-channel has an equal bandwidth of $B_s = B/K$. The unit interference caused by the PTx on the SRx n over subcarrier k can be taken as noise and is measured by the SRx. We denote the signal-to-interference-plus-noise ratio (SINR) of the subcarrier k with unit power at SRx as:

$$\gamma_{n,k} = \frac{|H^{ss}_{n,k}|^2}{\sum_{m=1}^{M} J_{m,n,k} + N_0 B}, \tag{4.1}$$

where N_0 is the power spectral density (PSD) of the additive white Gaussian noise (AWGN), $H^{ss}_{n,k}$ is the subcarrier k gain from the STx to the n^{th} SRx, $J_{m,n,k}$ is the interference power imposed by the PTx on the n^{th} SRx over subcarrier k. The interference caused by PTx on the PRx m, which should be no larger than the m^{th}

PRx interference limit, can be denoted as:

$$I_{m,t} = \sum_{k=1}^{K} \sum_{n=1}^{N} \varphi_{n,k}.P_{n,k}.I_{m,k}, \tag{4.2}$$

where $P_{n,k}$ denotes the subcarrier k transmit power allocated to the n^{th} SRx, $\varphi_{n,k}$ is the time-sharing factor for the subcarrier k of the SRx n. In this work, we assume that only one SRx can communicate over each subcarrier at any given time and $\varphi_{n,k}$ can take on either zero or one, when the subcarrier is not allocated or assigned to the user n respectively, and $I_{m,k}$ is equal to $I_{m,k} = V_{m,k}|H^{sp}_{n,k}|^2$, where $H^{sp}_{n,k}$ is the channel gain from STx to the m^{th} PRx, and $V_{m,k} = \int_{d_{m,k}-W_m/2}^{d_{m,k}+W_m/2} T_s((sin\pi fT_s)/\pi fT_s)^2 df$, T_s is the symbol duration, W_m is the m^{th} PRx bandwidth, $d_{m,k} = |f_k - f_m|$ is the spectral distance between the centre frequency of subcarrier k (f_k) and that of the primary user m (f_m). In our imperfect channel modeling, the estimated channel gain between the STx and the m^{th} PRx for any $m \,\epsilon\, \mathbb{M}$ and $k \,\epsilon\, \mathbb{K}$ is denoted by a K-tuple vector, $\hat{G}_m = [\hat{H}^{sp}_{m,k}]^T$ of K sub-channel gain entries $\hat{H}^{sp}_{m,k}$, where,

$$G_m = \hat{G}_m + E_m. \tag{4.3}$$

$G_m = [H^{sp}_{n,k}]^T$ is a K-tuple vector of entries $H^{sp}_{n,k}$ to represent the actual channel gain, and $E_m = [e_{m,k}]^T$ is a vector with entries $e_{m,k}$ to represent the error vector of independent and identically distributed (i.i.d.) complex Gaussian variables ($C\,\mathcal{N}(0, \sigma_e^2)$), with mean of zero and variance of σ_e^2. We propose an effective method to mitigate the impact of channel estimation error on the PRx quality of service (QoS). This method, based on the probabilistic information of interference, aims to enhance primary network robustness against the STx activity. To improve the system performance and to mitigate the impact of the channel estimation errors, we confine the probability of violating the PRx interference limit by STx to be smaller than a maximum acceptable collision probability, i.e.,

$$Pr(f(G_m) > I^m_{th}) \leq \varepsilon^m, \tag{4.4}$$

where $f(G_m)$ is the total interference imposed on the m^{th} PRx, I^m_{th} is the tolerable

interference limit of the m^{th} PRx, and ε^m is the maximum acceptable probability of collision between the STx and the m^{th} PRx. According to the channel estimation error model (4.3), the total interference $I_{m,t}$ is:

$$I_{m,t} = f(\hat{G}_m + E_m) = \sum_{k=1}^{K} \sum_{n=1}^{N} \varphi_{n,k}.P_{n,k}.\sigma_e^2.V_{m,k}Z_{m,k} \tag{4.5}$$

which is, according to equation (4.2), a non-central Chi-square-distributed random variable, where $Z_{m,k}$ is characterized by a non-central Chi-square-distributed random variable with two degrees of freedom, and the corresponding non-centrality parameter, δ_k, is given by, $\delta_k = \frac{|\hat{H}^{sp}_{m,k}|^2}{\sigma_e^2}$. To avoid disruptive inter-cell interference, and to facilitate effective and efficient power consumption, we impose a total transmit power constraint P_t on the cognitive network:

$$\sum_{n=1}^{N} \sum_{k=1}^{K} \varphi_{n,k} P_{n,k} \leq P_t. \tag{4.6}$$

At the physical layer, we focus on M-ary quadrature amplitude modulation (MQAM) and convolutional coding with bit interval coded modulation (BICM) based on the results in [113]. A particular set of MQAM modes is illustrated in Table 4.1.

4.3 MULTIMEDIA QUALITY MODEL

Video transmission over dynamic and error-prone wireless CR networks requires a flexible system to adapt the video source bit rate to the channel condition and the dynamics of the network. To achieve flexibility in variation of bit rate for video transmission, the SVC extension of the H.264/AVC standard is developed by the Joint Video Team (JVT). For the SVC bit-streams, the base layer encodes the lowest spatial (resolution), temporal (frame rate), and quality (signal-to-noise ratio (SNR)) level of the video stream, whilst the enhancement layers can be used to reconstruct a higher level of quality during the decoding process.

In theory, rate adaptation can be conducted to any spatio-temporal-quality resolution under a given bit rate constraint, assuming dyadic spatio-temporal-quality

scaling is used. However, usually only a limited set of spatial, temporal, and quantization parameter levels are permitted at the SVC. In SVC stream layer, spatial and temporal dependency resolution are denoted by s and t, indices of the possible spatial resolutions $S = \{QCIF, CIF, 4CIF, ...\}$, and frame rates $T = \{3.75, 7.5, 15, 30, ...\}$, with cardinality of $|S|$ and $|T|$ respectively. Moreover, SNR refinement layers within each dependency layer are identified by q, the index of the quality layer with quantization step-sizes of $Q = \{64, 40, 25, ...\}$, with cardinality of $|Q|$. In the following, we describe the layer ordering and packet priorities in detail. Assuming (s, t, q) as the 3-dimensional SVC layer index, we map the 3-dimensional coordinates to a one-dimensional index as, $F(s, t, q) = l$, where $F(., ., .)$ represents a particular ordering scheme. We use l to indicate the l^{th} element of $L = |S| \times |T| \times |Q|$ layers ordered by $F(s, t, q)$, where, S, T, and Q represent the sets of spatial, temporal, and SNR resolutions, respectively. It is clear that a convex ordering scheme has to satisfy the criterion: $\text{PSNR}_n^l > \text{PSNR}_n^{l+1}$, where PSNR_n^l is the layer l of the SRx n peak signal-to-noise ratio (PSNR). First, we initialize the lowest layer i.e., $(0, 0, 0)$, as the first point of the ordering path, next, by considering the three possible paths, i.e., $(s + 1, t, q)$, $(s, t + 1, q)$, $(s, t, q + 1)$, we choose the layer with the highest quality improvement, $argmax(\triangle\text{PSNR}/\Delta R)$, where $\triangle$PSNR and $\triangle R$ are respectively the quality and rate increments due to the chosen layer addition. For the packetization scheme, similar to H264/AVC, SVC coded data structure is divided into two parts, namely video coding layer (VCL) and network abstraction layer (NAL) units. To transport from video server to STx, each NAL unit is packetized into one or more real-time transport protocol (RTP) packets. The internet engineering task force (IEFT) [114] specification of RTP payload format, suggests that RTP packet with identical NAL unit times is mandatory for fast and real-time SVC video transport. Moreover, in the unequal error protection (UEP) scheme, NAL units belonging to different SVC priority layers are not loaded in an RTP packet. As a result, the RTP packet could only contains one NAL unit and consequently, contains the decoding deadline information of only one SVC layer. Detailed RTP packetization scheme could be found in [114]. Quality of spatial-temporal-quality layers can be expressed

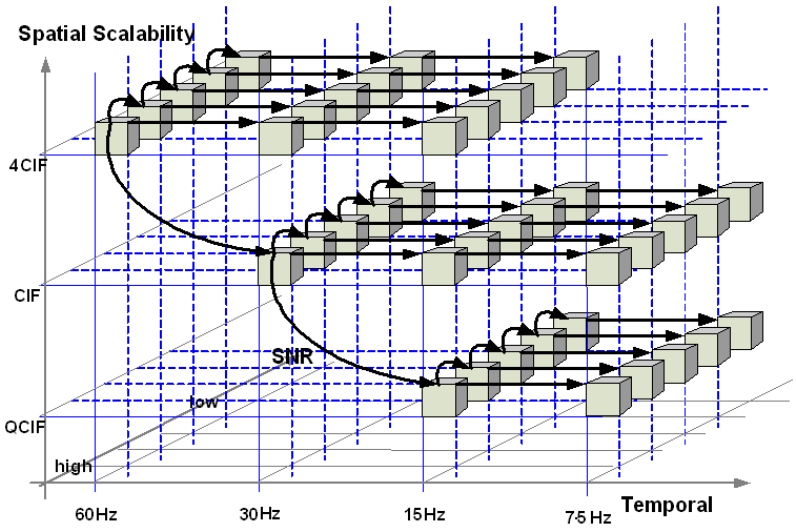

Figure 4.2: Example for decoding structure of the SVC bit stream.

as an aggregate floor function:

$$U_n = \sum_{l \in L} \triangle \mathrm{PSNR}_n^l, \tag{4.7}$$

where U_n denotes the n^{th} user reconstructed video quality, $\triangle \mathrm{PSNR}_n^l$ is the particular layer quality increase as defined below. The quality and rate increase can be expressed as:

$$\triangle \mathrm{PSNR}_n^l = \begin{cases} \mathrm{PSNR}_n^l - \mathrm{PSNR}_n^{l-1} & l \neq 0 \\ \mathrm{PSNR}_n^0 = \mathrm{PSNR}_n(0,0,0) & l = 0 \end{cases} \tag{4.8}$$

$$\Delta R_n^l = \begin{cases} R_n^l - R_n^{l-1}, & l \neq 0 \\ R_n^0 = R_n(0,0,0) & l = 0 \end{cases}. \tag{4.9}$$

In this work we use three video samples: Stefan, Mobile, and Coast guard. The PSNR and rate corresponding to the video sample layers are obtained using the "Joint Scalable Video Model" (JSVM) software [115].

4.4 Problem Formulation

The objective of this chapter is to maximize the overall weighted received quality of SRxs while satisfying the individual users' minimum prescribed quality constraints, subject to a prescribed total transmission power and PRx maximum tolerable interference. Mathematically, the optimization problem can be defined as follows:

$$\max_{\varphi_{n,k},\, P_{n,k}} \sum_{n=1}^{N} w_n U_n \tag{4.10a}$$

$$S.t. : \text{constraints in (4.6) and (4.4)} \tag{4.10b}$$

$$P_{n,k} \geq 0 \;\; \forall n \,\epsilon\, \mathbb{N}, \;\; \forall k \,\epsilon\, K \tag{4.10c}$$

$$\sum_{k=1}^{K} \varphi_{n,k} r_{n,k} \geq R_{n,0} \;\; \forall n \,\epsilon\, \mathbb{N} \tag{4.10d}$$

$$\varphi_{n,k} \,\epsilon\, \{0,1\} \;\; \forall n \,\epsilon\, \mathbb{N}, \;\; \forall k \,\epsilon\, \mathbb{K} \tag{4.10e}$$

$$\sum_{n=1}^{N} \varphi_{n,k} \leq 1 \;\; \forall k \,\epsilon\, \mathbb{K}, \tag{4.10f}$$

where w_n is the n^{th} SR's quality weight $\forall\, n \,\epsilon\, \mathbb{N}$, and represents the user's priority or deadline and can be calculated in different ways. In this work we consider equal weights for all users. U_n is the n^{th} SR's video layered Q-R utility function, $r_{n,k} = B_s.r^c_{n,k} log_2(M_{n,k})$ is the n^{th} SRx rate over the subcarrier k, $r^c_{n,k}$ is the k^{th} subcarrier coding rate and $M_{n,k}$ is the constellation size for a given bit-error-rate (BER) target, P_t is the maximum total transmit power of STx, and $R_{n,0}$ is the minimum required rate to transmit the n^{th} SRx base-layer video content. $\mathbb{N} = \{1, ..., N\}$, $\mathbb{K} = \{1, ..., K\}$ and $\mathbb{M} = \{1, ..., M\}$, are the set of integer numbers, corresponding to the number of possible SRx, sub-channels, and PRx, respectively. I^m_{th} is the m^{th} PRx maximum interference threshold. (4.6) and (4.10c) indicate transmit power constraints. (4.10d) refers to the SRx minimum rate constraint, while (4.4) denotes the PRx interference constraint. The probabilistic inequality in (4.4) is not a convex constraint. In the next section, we reformulate this constraint as a deterministic convex one. (4.10e) and (4.10f) show that every subcarrier can be allocated to at most one SRx. The optimization problem in (4.10a) is a probabilistic constrained

MDCNLP problem, wherein some variables are restricted to taking only discrete or binary values.

4.4.1 Formulation of the Probabilistic constraint

In this subsection, we propose a deterministic approximation for the inequality (4.4). To proceed further we denote the following equality:

$$\sum_{K=1}^{K}\sum_{n=1}^{N}\varphi_{n,k}.P_{n,k}.\sigma_e^2.V_{m,k}Z_{m,k}=\sum_{k=1}^{K}\beta_{m,k}Z_{m,k}, \tag{4.11}$$

where $\beta_{m,k} = \sigma_e^2.\sum_{n=1}^{N}\varphi_{n,k}.P_{n,k}.V_{m,k}$. Eq. (4.11) can be expressed as the sum of weighted Chi-Square random variables over K subcarriers. In general, exact distribution of the linear combination of weighted Chi-Square variables is rather complex. Several approximations of the distribution of sum weighted non-central Chi-square distributed random variables (4.11) have been proposed in literature, e.g. [77,78], and [116], however, they are not easy to implement in the RRA context. We propose a simple approximation based on the moments of (4.11) as the following proposition.The cumulative distribution function (cdf) of the sum of weighted non-central Chi-Square-distributed random variables, $Z_{m,k}$, $k\,\epsilon\,\mathbb{K}$, $m\,\epsilon\,\mathbb{M}$, with 2 degrees of freedom, i.e., $\sum_{k=1}^{K}\beta_{m,k}Z_{m,k}$, is 'similar distributed' to that of the non-central Chi-Square-distributed random variable $\xi\chi_D^2(\delta')$, where δ', D, and ξ are respectively the non-centrality parameter, degree of freedom, and weight of the new distribution, and given by:

$$\delta' = \sum_{k=1}^{K}\delta_k \tag{4.12}$$

$$D = 2K \tag{4.13}$$

$$\xi = \frac{\sum_{k=1}^{K}\beta_{m,k}(2+\delta_k)}{2K+\sum_{k=1}^{K}\delta_k}. \tag{4.14}$$

The similarity of these two distributions, or the accuracy of the proposed approximation, the cdf of the proposed Chi-Square distribution with that of (4.11), using Monte-Carlo simulations were compared in Fig. 2.2. The results show that

the approximation is accurate over a wide range of practical values for K and σ_e^2. Using the this approximation and the theorem in [79], (4.4) can be simplified to:

$$Pr(\sum_{k=1}^{K}\sum_{n=1}^{N}\varphi_{n,k}.P_{n,k}.\sigma_e^2.V_{m,k}Z_{m,k} > I_{th}^m)$$
$$\approx Pr(\xi\chi_D^2(\delta^{'}) > I_{th}^m) \approx Pr(\chi_D^2(0) > \frac{I_{th}^m/\xi}{1+{}^{\delta^{'}}/_D}). \quad (4.15)$$

By some mathematical manipulation and using the Gamma function approximation similar to Proposition 2.5 and the proof in Appendix A, for all integer values $K \neq 1$, and all positive $\frac{I_{th}^m/\xi}{1+{}^{\delta^{'}}/_D}$, (this condition is always true because, I_{th}^m, δ_k, β_k, and K are positive; consequently, ξ, $\delta^{'}$ and D are also positive), the deterministic inequality,

$$\sum_{k=1}^{K}(2+\delta_k).\sigma_e^2.V_{m,k}.\sum_{n=1}^{N}\varphi_{n,k}.P_{n,k} \leq \bar{I}_{th}^m, \quad (4.16)$$

satisfies the probabilistic inequality (4.4), where $\bar{I}_{th}^m = -\frac{K.I_{th}^m}{(K!)^{1/K}.ln(1-(1-\varepsilon^m)^{1/k})}$. Therefore, the constraint (4.4) can be replaced by (4.16).

4.5 Quality-Aware RRA Algorithm

The layered utility-based RRA optimization problem belongs to the group of non-linear combinatorial optimization problems, for which there is no general method to achieve optimality. In this section, a sub-optimal RRA algorithm for downlink MQAM/OFDMA system based on the users' layered SVC video quality, and multi-user resource allocation optimality is presented. The proposed algorithm is formed of two parts. In the first part, we discuss the subcarrier allocation, then, we propose a power allocation algorithm for the obtained subcarrier allocation scheme.

4.5.1 Subcarrier Allocation Algorithm

The proposed subcarrier allocation is detailed in two sub-steps. First, the main purpose is to maximize the number of satisfied users, i.e., those who meet their minimum quality according to the layered Quality model constraint (4.10d). Second,

Table 4.1: SINR limits and transmission modes using adaptive modulation and coding (AMC) [113].

Mode	R_i bit/symb	Coding rate	Modulation	SINR (dB), BER $< 10^{-5}$	SINR (dB), BER $< 10^{-6}$
1	1	1/2	QPSK	4.09	4.65
2	1.33	2/3	QPSK	5.86	6.49
3	1.5	3/4	QPSK	6.84	7.45
4	1.75	7/8	QPSK	8.44	9.05
5	2	1/2	16QAM	10.04	10.93
6	2.66	2/3	16QAM	12.13	12.71
7	3	3/4	16QAM	13.29	14.02
8	3.5	7/8	16QAM	15.01	15.74
9	4	2/3	64QAM	17.70	18.50
10	4.5	3/4	64QAM	18.99	19.88
11	5.25	7/8	64QAM	21.06	21.94

the rest of the remaining subcarriers are allocated to the users with the highest quality improvement based on the layered Quality model. First, to maximize the number of satisfied SRxs, i.e. those who meet their minimum quality according to the layered quality model constraint (4.10d), a maximum power distribution is assumed over all subcarriers. We formulate the equal maximum power as follows:

$$P_{max} = min\{\frac{\bar{I}^m_{th}}{\sum_{k=1}^{K}(2+\delta_k).\sigma^2_e.V^m_{n,k}},\ \frac{P_t}{K}\} \quad \forall m\,\epsilon\,\mathbb{M}. \tag{4.17}$$

The allocated power derived from (4.17), satisfies the power constraint and interference constraints imposed to each PRx individually, i.e., (4.6) and (4.16). In order to achieve the highest possible performance, we denote an ordered normalized minimum rate set as follows:

$$\pi = \{\frac{R^0_{n_1}}{R^t_{n_1}},\ \frac{R^0_{n_2}}{R^t_{n_2}},\ \frac{R^0_{n_3}}{R^t_{n_3}},\ \dots \mid \frac{R^0_{n_1}}{R^t_{n_1}} < \frac{R^0_{n_2}}{R^t_{n_2}} < \frac{R^0_{n_3}}{R^t_{n_3}},\ \dots\} \tag{4.18}$$

$$\mathbb{N} = \{1,\ 2,\ 3,\ ...N\},\ n_1,\ n_2,\ n_3,\ \dots\ \in \mathbb{N}, \tag{4.19}$$

where π is the ordered normalized minimum rate set for N SRxs, and

$$R^t_n = \sum_{k=1}^{K} r_{n,k} \tag{4.20}$$

is the n^{th} SRx maximum achievable rate over K subcarriers when P_{max} allocated to all subcarriers. In the first sub-step, in order to allocate a minimum set of subcarriers to each SRx, in each iteration a subcarrier with highest $\gamma_{n,k}$ from the feasible set of subcarriers is assigned to the user with the lowest normalized minimum rate. This is repeated until all users have been allocated their minimum number of subcarriers to fulfill the minimum required rate. Once a subcarrier is assigned, it will not be considered in further subcarrier allocation operations. In other words, each subcarrier can be allocated to just one SRx. In the second sub-step, the remaining subcarriers are assigned to the users according to the layered quality model. In this stage, the cognitive users' normalized quality level improvement are formulated as flows:

$$\Re_n = \{\Phi_n^1,\ \Phi_n^2,\ \Phi_n^3,\ ...,\ \Phi_n^L\},\ \forall n \,\epsilon\, \mathbb{N} \tag{4.21}$$

$$\Phi_n^l = \frac{\triangle PSNR_n^l}{\Delta R_n^l}.R_n^t, \tag{4.22}$$

where $\Re_n$ is the set of L levels of n^{th} SRx's normalized quality improvement, Φ_l^n is the l^{th} level of the n^{th} SRx's normalized quality improvement. The sorted set of all SRx normalized quality improvements in descending order, is denoted as:

$$\mathbb{E} = \{\Phi_{n_1}^{l_1},\ \Phi_{n_2}^{l_2},\ \Phi_{n_3}^{l_3},\ ...,\ \Phi_{n_n}^{l_n}\}$$

$$\Phi_{n_1}^{l_1} \geq \Phi_{n_2}^{l_2} \geq \Phi_{n_3}^{l_3} \geq ... \geq \Phi_{n_n}^{l_n},\ \forall n \,\epsilon\, \mathbb{N},\ \forall l \,\epsilon\, \mathbb{L}. \tag{4.23}$$

In this sub-step, subcarrier is allocated to the users according to their levels' ordering in (4.23) iteratively, until reaches the corresponding quality level. Similar to the previous sub-step, once a subcarrier is assigned, it will not be considered in further subcarrier allocation process. The algorithm continues until all subcarriers are allocated.

4.5.2 Power Allocation Algorithm

As previously mentioned, each user requires a minimum rate to guarantee the base layer transmission; below this minimum rate, there is no layered quality characteri-

zation to allocate the power according to this model. In the first sub-step of power allocation, the multi-level water-filling power allocation policy is used to distribute the power between the users' assigned subcarriers to meet the required minimum rate. However, because of the interference constraints in CR networks, the classical water-filling method is not applicable. Any power allocation scheme in CR, must not only maximize the utility function, but also satisfies the maximum total transmit and interference power threshold constraints. Starting with the user with highest priority in the ordered normalized minimum rate set (π), in each bit loading iteration, power is allocated to the user's assigned subcarrier with the highest rate enhancement. When the users' minimum required rates is satisfied, or the total transmission power or interference constraints are reached, the iteration process stops. This water-filling process is repeated for N users according to the ordered normalized minimum rate set order (4.18). By the end of this process, we can move to allocate the rest of available power according to the layered quality model. In second sub-step, the power allocation to the subcarriers is similar to the previous sub-step, but in a different order. The power is allocated according to the SRx's normalized quality level improvement set (4.23). Furthermore, the power level is set to satisfy the upper-bound of the layers' required rate corresponding to the chosen level as:

$$\sum_{k \in \mathbb{Z}_n} B_s . r^c_{n,k} log_2(M_{n,k}) = R^l_n,\ n \in \{n_1,\ n_2, ..,\ n_N\}$$
$$l \in \{l_1,\ l_2, ...,\ l_L\}. \tag{4.24}$$

4.6 PERFORMANCE ANALYSIS

In this section we examine the performance of the QA algorithm and compare it to the non-quality-aware (NQA) algorithm used in the literature, e.g., [108], [68], under total transmit power and probabilistic peak aggregate interference constraints with imperfect cross-channel estimation using the respective optimal resource allocation solutions. For the simulations, the video content and the model parameters are

Algorithm 2: Quality-aware subcarrier allocation

Minimum subcarrier allocation

1. Set the initial value to each user's subcarriers vector $\mathbb{Z}_1$, $\mathbb{Z}_2$, $\mathbb{Z}_3$ ... and $\mathbb{Z}_N = 0$
2. Calculate P_{max} and R_n^t according to (4.17) and (4.20) respectively
3. Select the first available normalized minimum rate from the set π based on (4.18)
4. Allocate the selected user i a subcarrier with highest $\gamma_{n,k}$ from the set of available subcarriers $\mathbb{K}$
5. Update $\mathbb{Z}_n$ and $\mathbb{K}$, Remove the allocated subcarrier from $\mathbb{K}$ and add it to $\mathbb{Z}_n$
6. Repeat steps 4 and 5 until $\sum_{k \in \mathbb{Z}_n} B.r_{n,k}^c log_2(M_{n,k}) \geq R_n^0$, in the case of $\mathbb{K}$ is empty go to sub-step minimum power allocation in the algorithm 3
7. Remove the $\frac{R_n^0}{R_n^t}$ from the set π
8. Repeat steps 3 to 7 until all users rate limits are reached

Quality-based subcarrier allocation

1. Set the initial vale for the new $\mathbb{Z}_1$, $\mathbb{Z}_2$, $\mathbb{Z}_3$...,$\mathbb{Z}_N$ and $\mathbb{K}$ achieved from the previous sub-step
2. Find the SRx normalized quality levels improvement sets according to (**??**)
3. Determine the sorted set of all SRx normalized quality improvement $\mathbb{E}$ from (4.23)
4. Select the first available member of set $\mathbb{E}$ and determine the corresponding user n and level l
5. Allocate the selected user n the subcarrier with highest $\gamma_{n,k}$, from the available subcarriers $\mathbb{K}$
6. Update $\mathbb{Z}_n$ and $\mathbb{K}$, Remove the allocated subcarrier from $\mathbb{K}$ and add it to $\mathbb{Z}_n$
7. Repeat steps 4 to 6 until $\sum_{k \in \mathbb{Z}_n} B.r_{n,k}^c log_2(M_{n,k}) \geq R_n^l$, in the case of $\mathbb{K}$ is empty go to minimum power allocation step
8. Remove the Φ_n^l from the set $\mathbb{E}$
9. Repeat step 3 to 7 until all users' rate limits are reached or $\mathbb{E}$ is empty.

Algorithm 3: Quality-aware power allocation

Minimum power allocation

1. Set the initial value of the new $\mathbb{Z}_1$, $\mathbb{Z}_2$, $\mathbb{Z}_3$..., and $\mathbb{Z}_N$ from Algorithm.2
2. Set the initial value of ΔP
3. Set the initial value of $\mathbb{PZ}_1$, $\mathbb{PZ}_2$, $\mathbb{PZ}_3$...,$\mathbb{PZ}_N$=0, which are the subcarriers power set
4. Select the first available normalized minimum rate from the set π based on (4.18)
5. If $\sum_{n \in \mathbb{N}} \sum_{k \in \mathbb{Z}} (2+\delta_k).\sigma_e^2.V_{n,k}^m.P_{n,k} \leq \bar{I}_{th}^m$ and $\sum_{n \in \mathbb{N}} \sum_{k \in \mathbb{Z}} P_{n,k} \leq P_t$, select the user subcarrier with highest rate enhancement, i.e, $\Delta r_{n,k}$, and increase the rate by $P_{n,k} = P_{n,k} + \Delta P$, and update $\mathbb{PZ}_n$
6. Repeat step 3 and 4 until $\sum_{k \in \mathbb{Z}_i} B.r_{n,k}^c log_2(M_{n,k}) \geq R_n^0$
7. Remove the $\frac{R_n^0}{R_n^t}$ from the set π
8. Repeat step 3 to 6 until all users rate limits are reached

Quality-based power allocation

1. Set the initial value$\mathbb{PZ}_1$, $\mathbb{PZ}_2$, $\mathbb{PZ}_3$...,$\mathbb{PZ}_N$ from minimum power allocation sub-step
2. Determine the sorted set of all SUs' normalized quality improvement $\mathbb{E}$ from (4.23)
3. Select the first available member of set $\mathbb{E}$ and determine the corresponding user n and level l .
4. select the user subcarrier with highest rate enhancement, i.e, $\Delta r_{n,k}$, and increase the rate by $P_{n,k} = P_{n,k} + \Delta P$, and update $\mathbb{PZ}_n$
5. Repeat step 3 and 4 until $\sum_{k \in \mathbb{Z}_i} B.r_{n,k}^c log_2(M_{n,k}) \geq R_n^l$
6. Remove Φ_n^l from the set $\mathbb{E}$
7. Repeat step 3 to 6 until all users' rate limits are reached or $\mathbb{E}$ is empty.

derived by the video server. We assume that the connection between the video server, ICS, and STx is error free. Three cognitive users respectively, receiving the standard video samples, Stefan, Mobile, and Coast guard, in CIF (352 × 288) resolution, are

assumed for the simulations. The video streams are encoded using JSVM 9.15 reference software into two SNR layers: one base layer and an enhancement layer, and five temporal layers (with the same resolution). The wireless network is modeled as a three-user Rayleigh fading symmetric/asymmetric channel and $w_n = 1$ for all users. For simplicity, we consider a single PRx. In our simulations, we assumed 32 OFDM subcarriers, with total bandwidth, 1.6 MHz. In addition, the AWGN PSD is set to -110 dBm. The PSD of the PTx interferences to all SRxs are equal and are set to $10^{-8}W/Hz$. Discrete-rate cases with real-valued MQAM signal constellations with BICM are also considered for practical scenarios as listed in Table 4.1, for different values of BER [113]. It is further assumed that every SRx has a minimum quality threshold requirement to receive the base layer corresponding to the scalable video streams. Sufficient buffer time is assumed to be available for the reliable transmission of the base layer for each user. In the case where the packet that belongs to the user's base layer is not received at the decoder by the deadline, a simple intra-layer frame copy (FC)technique is used for error correction.

Fig. 4.3 and Fig. 4.4 show the achievable PSNR values for the adaptive MQAM /OFDMA CR system versus STx-PRx interference power threshold levels with, respectively, 1% and 5% collision probability. As expected, greater PSNR values are achieved for higher maximum tolerable interference since I_{th} limits the cognitive users' transmit power. The results show that the proposed algorithm outperforms the conventional NQA scenario under similar probabilistic interference power threshold and collision probability. However, as shown in Fig. 4.5 and Fig. 4.6, the NQA algorithm achieves a higher total rate than the QA algorithm. NQA always operates at the most extreme point, where users compete for the maximum rate. This "quality-blind" RRA algorithm allocates the most resources to the user with better channel regardless of the user's contribution to the overall system quality enhancement.

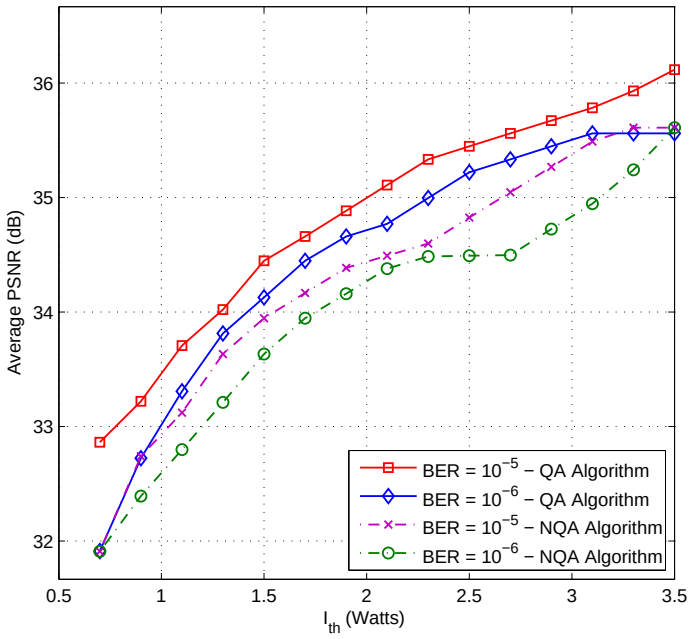

Figure 4.3: Average PSNR performance using the proposed quality-aware RRA and non-quality-aware RRA algorithms versus I_{th} constraint of three symmetrically distributed video users and different BER target. System parameters are: K = 32, N=3, P_t = 30 Watts, σ_e^2 =1, and $\varepsilon^m = 1\%$.

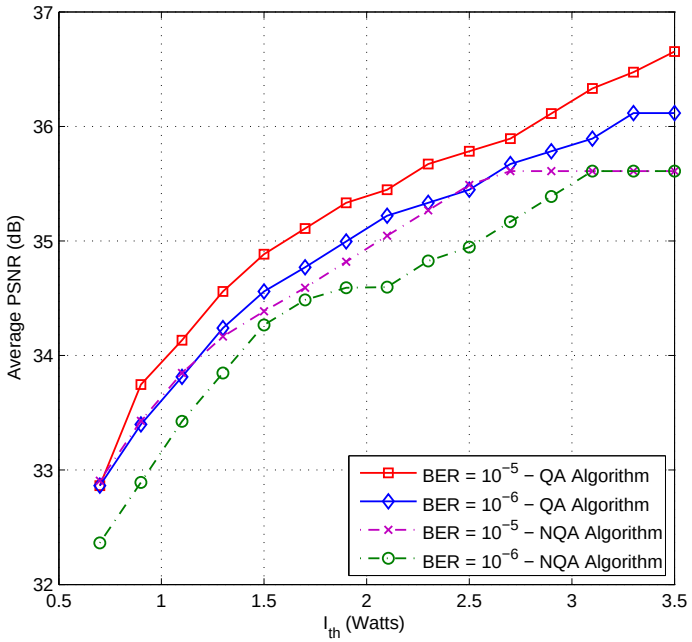

Figure 4.4: Average PSNR performance using the proposed quality-aware RRA and non-quality-aware RRA algorithms versus I_{th} constraint of three symmetrically distributed video users and different BER target. System parameters are: K = 32, N=3, P_t = 30 Watts, σ_e^2 =1, and $\varepsilon^m = 5\%$.

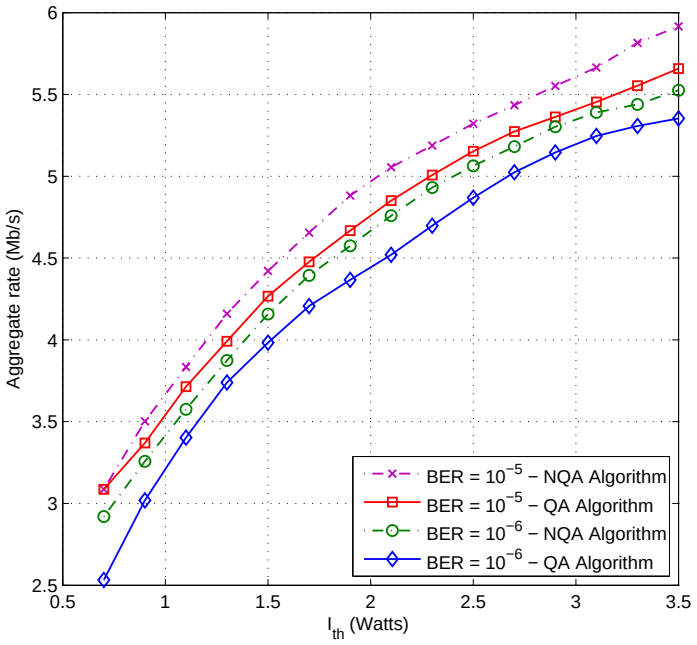

Figure 4.5: Aggregate rate performance using the proposed quality-aware RRA and non-quality-aware RRA algorithms versus I_{th} constraint of three symmetrically distributed video users and different BER target. System parameters are: K = 32, N=3, P_t = 30 Watts, σ_e^2 =1, and $\varepsilon^m = 1\%$.

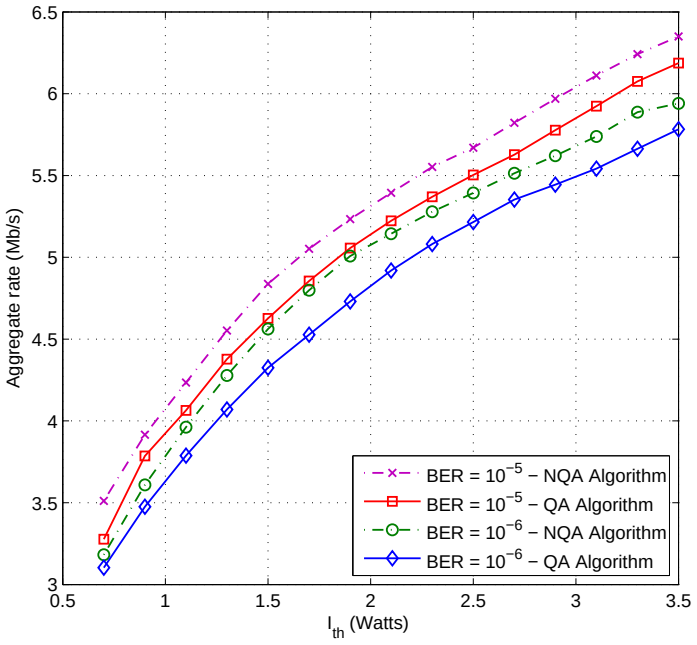

Figure 4.6: Aggregate rate performance using the proposed quality-aware RRA and non-quality-aware RRA algorithms versus I_{th} constraint of three symmetrically distributed video users and different BER target. System parameters are: K = 32, N=3, P_t = 30 Watts, σ_e^2 =1, and $\varepsilon^m = 5\%$.

Fig. 4.7 and Fig. 4.8 illustrate the average PSNR, versus channel estimation error variance for three video users symmetrically located within a 1 km radius from the STx. Simulation results show that, for both considered RRA schemes, the average PSNR decreases with increasing the variance of the cross-channel estimation error. The proposed probabilistic interference approach, however, keeps the probability of meeting the target primary user QoS larger than $1-\varepsilon^m$. Apart from the impact of I_{th} on the performance, lower values of collision probability increase the robustness of the interference management scheme, but this comes at the cost of lower achievable average PSNRs.

In the second scenario, we consider the same parameters as before, except that the PRx channels are asymmetric. We assume that, the PRxs' distances to the cognitive base-station are 0.6, 1.3, and 0.8 km, respectively. Fig. 4.9 and Fig. 4.10 illustrate evolution of the maximum achievable average PSNR under different maximum tolerable interference thresholds for 1% and 5% collision probability respectively. For example, the proposed algorithm achieves a 3.8 dB increase in the average PSNR over the NQA algorithm where $I_{th} = 1.5$ watt, $\sigma_e^2 = 1$, $BER = 10^{-5}$, and $\varepsilon^m = 5\%$. It can be observed that the advantage of using the QA algorithm is even greater under the asymmetric scenario. The plausible justification for this can be explained as the user with the better channel conditions in NQA algorithm, receives higher resources, the quality improvement is low or negligible due to the user quality saturation. It is notable that the advantage of the proposed QA algorithm is even more when the difference between the users' videos quality is considerable.

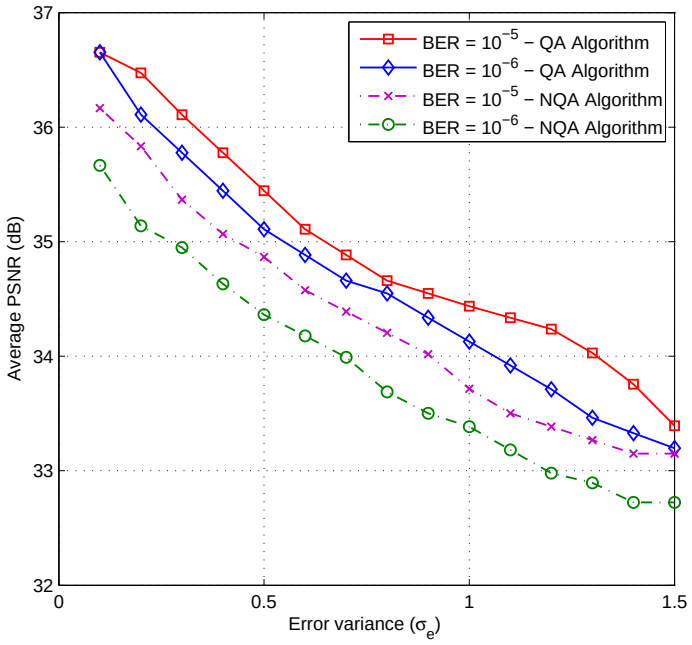

Figure 4.7: Average PSNR versus Error variance of three symmetrically distributed video users using the proposed quality-aware RRA and non-quality-aware RRA algorithms with different values of collision probability. System parameters are: $I_{th} = 1.5$ Watts, K = 32, N=3, $P_t = 30$ Watts, and $\varepsilon^m = 1\%$.

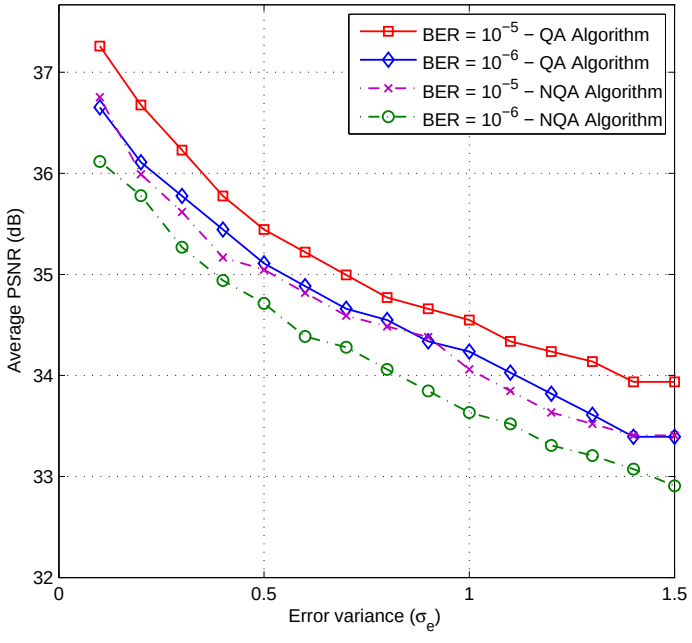

Figure 4.8: Average PSNR versus Error variance of three symmetrically distributed video users using the proposed quality-aware RRA and non-quality-aware RRA algorithms with different values of collision probability. System parameters are: $I_{th} = 1.5$ Watts, K = 32, N=3, $P_t = 30$ Watts, and $\varepsilon^m = 5\%$.

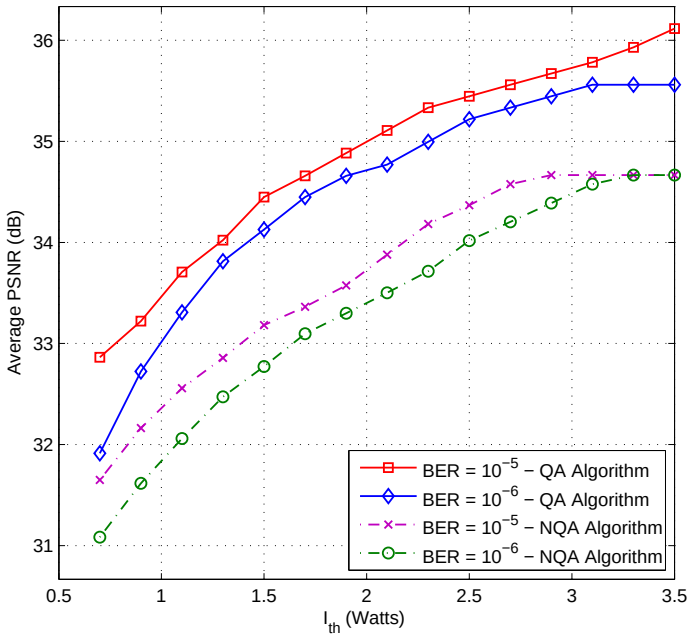

Figure 4.9: Average PSNR performance using the proposed quality-aware RRA and non-quality-aware RRA algorithms versus I_{th} constraint of three asymmetrically distributed video users with different BER target value. System parameters are: K = 32, N=3, P_t = 30 Watts, σ_e^2 =1, and $\varepsilon^m = 1\%$.

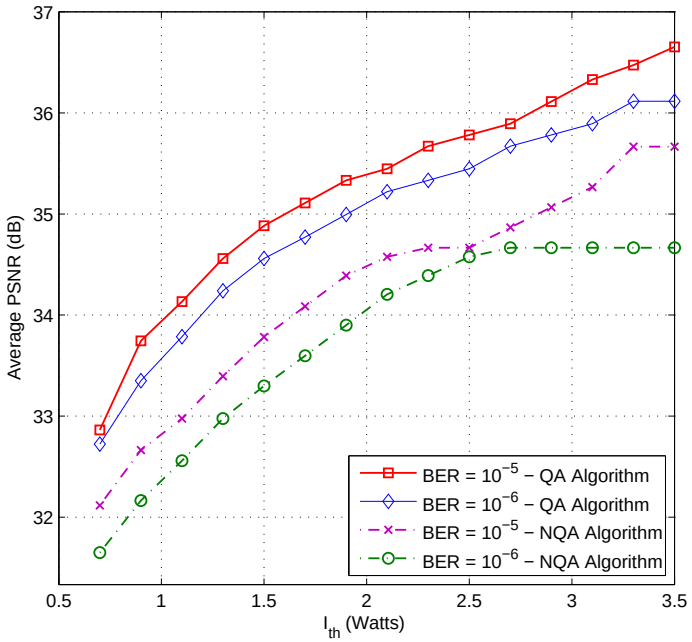

Figure 4.10: Average PSNR performance using the proposed quality-aware RRA and non-quality-aware RRA algorithms versus I_{th} constraint of three asymmetrically distributed video users with different BER target value. System parameters are: K = 32, N=3, P_t = 30 Watts, σ_e^2 =1, and $\varepsilon^m = 5\%$.

4.7 CONCLUSION

In this chapter, cross-layer RRA algorithms for scalable multi-user video streams in MQAM/OFDMA-based CR networks have been developed. We proposed a novel framework to maximize SRxs' average PSNR whilst guaranteeing the PRx interference limit under imperfect cross-link information. To characterize the relationship between the transmit rate and the average PSNR of the scalable video streams, a simple layer ordering model was proposed. We formulated a probabilistic constrained optimization problem to restrict the probability of violating the tolerable interference limit on the PRx by the STx to a predetermined limit. We have shown that the use of distribution approximation provides an accurate estimation of the actual probabilistic constraint for a wide range of practical error variance and number of subcarriers. Simulation results illustrated that the cross-layer RRA can significantly improve the aggregate quality of the SRx video streams in an error-prone environment over the state-of-the-art rate maximization algorithms in the literature.

Chapter 5

Conclusions and Future Research Proposals

5.1 Conclusions

The growth in demand for various wireless applications requires extremely intelligent systems capable of making appropriate decision and efficiently adapting parameters based on the observation of their surroundings. In addition, the network design should be in a acceptable complexity level to be implemented in practical scenarios. In such a system, OFDM has been regarded as a promising PHY layer transmission technique because of the flexibility it provides to schedule and allocate the resources and also the simplicity of implementation. Furthermore, radio resource management is of great importance in efficient wireless communication systems design. However the radio resource allocation in OFDM systems can not be efficient and optimal if conducted by considering only the PHY layer, due to the interdependence among the different layers parameters. To this end, cross-layer design offers considerable potential to achieve global optimum performance and to guarantee the QoS requirements in the application layer. Moreover, in the past decade, cognitive radio is considered to be a prominent candidate for be towards improving wireless network capacity. Further, cognitive radio is regarded as an effective way to address the problem of spectrum crunch, by means of intelligent and efficient usage of the available radio spectrum. Inspired by these challenges, this thesis focused on cross-layer design and

optimization in OFDMA- base CR networks, involving the parameters from PHY layer, MAC layer and the application layer, with the goal of maximizing different metric parameters, in particular the total deliverable throughput, total rate, and total achievable application layer video streams PSNR.

In Chapter 1, a brief survey on the current and emerging cellular mobile networks was provided. Following a brief history of wireless communication, an overview of basics of OFDM technology, performance and implementation were given. General idea of CR networks and different spectrum access strategies were studied. Particular emphasis was placed on functionalities and associated challenges of OFDM based CR networks. Cross-layer design concept and different implementation strategies including, backward and forward information flow cross-layer, design coupling without new interfaces, merging of adjacent layers, and vertical calibration concept were studied. Finally the wireless video communications and the video scalability are discussed in brief.

In Chapter 2 the comprehensive problem of joint power, subcarrier, and rate allocation, together with interference mitigation in downlink OFDMA CR networks was tackled. The spectral efficiency performance of adaptive MQAM/OFDMA underlay CR networks with certain/uncertain interfering channel information were studied. A novel RRA algorithms to improve the overall cognitive system performance subject to satisfying total average power and peak aggregate interference constraints. In the proposed framework we considered both cases of perfect and imperfect cross-link CSI at the cognitive transmitter. In the latter, different 'average case', 'worst case', and 'probabilistic case' scenarios of channel estimation error were modeled and analysed. To compute the aggregate average spectral efficiency, we developed unique approximated distributions of the received SINR for given users over different sub-channels in the respective cases under consideration (i.e., average case, worst case and probabilistic case). The performance of the proposed RRA algorithm and interference management techniques under various sets of system settings was examined. We have shown that by incorporating the proposed joint resource allocation and interference management design framework, a higher overall system performance in the OFDMA CR network can be realized over the conventional optimization methods.

In Chapter 3, a stochastic resource allocation algorithms for multi-user multi-band OFDMA-based CRs with joint underlay and overlay spectrum access strategies over wireless fading channels was developed. In order to protect the primary users QoS from destructive interference imposed by the CRs in underlay spectrum access strategy and the miss-detection scenarios due to the imperfect sensing information, we considered stochastic total transmit and interference power constraints, where the number of subcarriers in each scenario (Idle, false-alarm, miss-detection, and busy) is Binomially-distributed. At the same time, we developed the total transmission rate objective function based on the collective stochastic information of different number of subcarriers experiencing different idle, false-alarm, miss-detection, and busy scenarios, resulting in improved overall transmission rate performance. In contrast to the state-of-the-art hard-decision-based methods, although separate transmit power and subcarrier allocation policies based on the stochastic information of different number of subcarriers experiencing different scenarios is derived, we have developed an exclusive final optimum soft-decision-based power and subcarrier assignment for the proposed OFDMA CR network.

Chapter 4 proposed a cross-layer design technique to maximize the total PSNR and the number of satisfied secondary users of multi-user scalable video streams in MQAM/OFDMA-based CR networks by jointly considering the application layer and the physical layer, and by utilising the probabilistic information about secondary-primary cross channels. We first developed the 3-dimensional scalable video quality of the H.264/SVC video transmission over an OFDMA-based CR networks. An ordered expression for the layers PSNR improvement of the scalable video applications and the layered utility-based RRA optimization problem were derived. The total user's quality is expressed following four physical layer parameters: subcarrier allocation, modulation spectral efficiency, power allocation, and probabilistic interference limitation. Furthermore to solve the probabilistic constrained mixed discrete-continuous non-linear programing (MDCNLP) problem, we proposed an efficient suboptimal algorithm is in two steps. Adaptive MQAM/OFDMA systems under imperfect channel information at the transmitter are shown to have substantial gain in aggregate PSNR compared to conventional quality blind OFDMA-based

CR RRA algorithms.

5.2 Future Research Proposals

In this section, additional research ideas for future work are outlined. Specifically, different potential improvements to the proposed works are suggested. An immediate extension to enhance the work carried out in chapter 2, is to incorporate the number of automatic repeat request (ARQ) retransmissions in the optimization problem. It would be interesting to determine the level of interference on the primary users and develop the algorithms to achieve an efficient control over the throughput-interference-delay trade-off.

Throughout the work in Chapter 3, to simplify the analysis, the ROC was assumed to be equal over all subcarriers and users. However, in practical systems with different sensing environment, optimum ROC selection is a crucial parameter affecting the imposed interference and consequently , the total achievable primary and secondary users performance. Hence, taking different ROC into consideration would be an interesting research undertaking. It would be also be beneficial to extend and analyse the proposed stochastic framework with a more practical distribution for modelling the number of subcarrier arability in each scenario.

Cross-layer design proposed in chapter 4 did not consider the layers' play back deadline. Also, queuing delay is an important QoS parameter affecting the overall performance of the system. A cross-layer framework designed to serve multiple primary and secondary users by incorporating the application layer, physical and data link layer, and considering the layers play back deadline and queuing delay can be an exciting research topic. Forward error correction (FEC) is one technique of error correction schemes which is largely has been employed in communication systems. However, due to the hierarchical structure and the dependence between the SVC video stream layers, it is important consider this inter-dependence between layers in the FEC design. Therefore, In this sense, there is still large room for enhancing the current unequal error protection (UEP) FEC design, as such protection are expected to incorporate the inter-layer dependence with the emerging UEP technologies. Fur-

thermore, to enhance the practical feasibility of the proposed cross-layer algorithms, for the cooperative CR networks, analysis can be extended to a quality-aware multi-relay selection for multi-stream cooperative CR systems with relay nodes and/or base station.

Appendix A

Proof of Proposition 4

For a Chi-Square random variable χ^2_D, with a degree of freedom $2K$, the probability

$$\mathscr{P}(\xi\chi^2_D(\delta^{'}) > I^m_{th}) \approx \mathscr{P}(\xi\chi^2_D(0) > \frac{I^m_{th}/\xi}{1+{\delta^{'}}/{D}}), \tag{A.1}$$

can be formulated using the upper gamma function [117] as

$$Pr(\chi^2_D(0) > \frac{I^m_{th}/\xi}{1+{\delta^{'}}/{D}}) = \frac{\Gamma(K\,,\,\frac{I^m_{th}}{2\xi(1+{\delta^{'}}/{D})})}{\Gamma(K)}. \tag{A.2}$$

By defining

$$x^y = \frac{I^m_{th}}{2\xi(1+{\delta^{'}}/{D})}, \tag{A.3}$$

and using the results from [117], we have

$$\Gamma(K\,,\,x^y) = y\int_x^\infty e^{-t^y}dt, \tag{A.4}$$

where $y = 1/K$. Given $1/(K\Gamma(K)) = 1/\Gamma(K+1)$, and using the corollary of [117], we can derive the following equalities

$$\frac{\Gamma(K\,,\,x^y)}{\Gamma(K)} = \frac{y\int_x^\infty e^{-t^y}dt}{\Gamma(K)} = \frac{\int_x^\infty e^{-t^y}dt}{\Gamma(K+1)}. \tag{A.5}$$

The upper-bound of (A.5) can be expressed as

$$\frac{\Gamma(K\,,\,x^y)}{\Gamma(K)} = \frac{\int_x^\infty e^{-t^y}dt}{\Gamma(K+1)} \leq 1-[1-e^{-\vartheta x^y}]^{1/y}. \tag{A.6}$$

The expression in (A.6) is valid for all positive x, if and only if,

$$0 \leq \vartheta \leq \min\{1, [\Gamma(K+1)]^{-1/K}\}. \tag{A.7}$$

Thus, for all $K \geq 1$,

$$\vartheta = (\Gamma(K+1))^{-1/K}. \tag{A.8}$$

Subsequently, from (2.65), (A.6), and (A.8),

$$\frac{\Gamma(K\,,\,x^y)}{\Gamma(K)} \leq \varepsilon^m \tag{A.9}$$

and by replacing (A.5) in (A.9), we have

$$1-[1-e^{-\vartheta x^y}]^{1/y} \leq \varepsilon^m. \tag{A.10}$$

With further manipulation, it can be shown that

$$x^y = -\frac{\ln(1-\sqrt[K]{1-\varepsilon^m})}{(\Gamma(K+1))^{-1/K}}. \tag{A.11}$$

Replacing (A.3) in (A.11) we have:

$$\frac{I_{th}^m}{2\xi(1+{}^{\delta'}\!/_D)} \leq -\frac{\ln(1-\sqrt[K]{1-\varepsilon^m})}{(\Gamma(K+1))^{-1/K}}, \tag{A.12}$$

Finally, by replacing (2.68), (2.69), and (2.70) in (A.12), we have:

$$\begin{aligned}\delta^2_{H^{sp}_{m,k}|\hat{H}^{sp}_{m,k}} \sum_{k=1}^{K}(2+\mu_{\Xi^m[k]}) \sum_{n=1}^{N} \varphi_{n,k}(\Upsilon)P_{n,k}(\Upsilon) \\ \leq \frac{K\,I_{th}^m}{(K!)^{1/K}\ln\left(1-(1-\varepsilon^m)^{1/K}\right)}.\end{aligned} \tag{A.13}$$

Appendix B

Received SINR cdf Derivation

Deriving cdf of the received SINR given the estimation, $F_{\gamma_{n,k}|\hat{H}^{sp}_{m,k}}(\gamma_{n,k}|\hat{H}^{sp}_{m,k})$, for different 'average case', 'worst case', and 'probabilistic case', scenarios are as follows:

B.0.1 'Average Case'

The random variable $H^{sp}_{m,k}|\hat{H}^{sp}_{m,k}$, given the 'average case' of estimation error, is a complex Gaussian random variable with mean zero and variance $\delta^2_{\hat{H}^{sp}_{m,k}}(1+\rho^2)^2$. Using Lemma 1, $N^{sp}_m = \sum_{k=1}^{K}|H^{sp}_{m,k}|\hat{H}^{sp}_{m,k}|^2$ can be approximated by

$$N^{sp}_m = \sum_{k=1}^{K}|H^{sp}_{m,k}|^2 \sim N\left(\mu_{N^{sp}_m}, \delta^2_{N^{sp}_m}\right) \tag{B.1}$$

where $\mu_{N^{sp}_m} = 2K\delta^2_{\hat{H}^{sp}_{m,k}}(1+\rho^2)^2$ and $\delta^2_{N^{sp}_m} = 4K\delta^4_{\hat{H}^{sp}_{m,k}}(1+\rho^2)^4$. By replacing these new parameters in (2.22), $F_{\gamma_{n,k}|\hat{H}^{sp}_{m,k}}(\gamma_{n,k}|\hat{H}^{sp}_{m,k})$ can be obtained under the 'average case' of estimation error.

B.0.2 'Worst Case'

To derive the distribution of the received SINR given the estimation, for the 'worst case' of estimation error, we invoke Lemma 1. In this case, the random variable $H^{sp}_{m,k}|\hat{H}^{sp}_{m,k}$ is a complex Gaussian random variable with mean $\sqrt{\frac{\delta^2_{\Delta H^{sp}_{m,k}}(1-\rho^2)}{1-pr}}$ and variance $\delta^2_{\hat{H}^{sp}_{m,k}}(1+\rho^2)^2$. Hence, the random variable $N^{sp}_m = \sum_{k=1}^{K}|H^{sp}_{m,k}|\hat{H}^{sp}_{m,k}|^2$ can

be estimated as

$$N_m^{sp} = \sum_{k=1}^{K} |H_{m,k}^{sp}|\hat{H}_{m,k}^{sp}|^2 \sim N\left(\mu_{N_m^{sp}}, \delta_{N_m^{sp}}^2\right) \tag{B.2}$$

where $\mu_{N_m^{sp}} = \delta_{\hat{H}_{m,k}^{sp}}^2 (1+\rho^2)^2\left[2K + \mu^{'}\right]$ and $\delta_{N_m^{sp}}^2 = \delta_{\hat{H}_{m,k}^{sp}}^4 (1+\rho^2)^4\left[4K + 4\mu^{'}\right]$ and $\mu^{'} = \sum_{k=1}^{K} |\delta_{\Delta H_{m,k}^{sp}}^2 (1-\rho^2)/(1-pr)\delta_{\hat{H}_{m,k}^{sp}}^2 (1+\rho^2)^2|$. Using the parameters of N_m^{sp} in (2.22) yields the distribution of the received SINR given the estimation for this case.

B.0.3 'Probabilistic Case'

For the 'probabilistic case' of estimation error, invoking Lemma 1 and using (2.74),

$$\begin{aligned}\hat{N}_{sp}^m &= \sum_{k=1}^{K} \delta_{H_{m,k}^{sp}|\hat{H}_{m,k}^{sp}}^2 \left(2 + \left|\frac{\mu_{H_{m,k}^{sp}|\hat{H}_{m,k}^{sp}}}{\delta_{H_{m,k}^{sp}|\hat{H}_{m,k}^{sp}}}\right|^2\right) \\ &= \sum_{k=1}^{K} (1-\rho^2)\delta_{\Delta H_{m,k}^{sp}}^2 \left(2 + \left|\frac{(1+\rho^2)\hat{H}_{m,k}^{sp}}{\sqrt{(1-\rho^2)}\delta_{\Delta H_{m,k}^{sp}}}\right|^2\right)\end{aligned} \tag{B.3}$$

is a Normally-distributed random variable with mean $\mu_{\hat{N}_{sp}^m} = 2K\delta_{\hat{H}_{m,k}^{sp}}^2 \left(1+\rho^2\right)^2 + 2K\left(1-\rho^2\right)^2 \delta_{\Delta H_{m,k}^{sp}}^2$ and variance $\delta_{\hat{N}_{sp}^m}^2 = 4K\delta_{\hat{H}_{m,k}^{sp}}^4 \left(1+\rho^2\right)^4$. Hence, by replacing $\hat{N}_{sp}^m$ and $\overline{I_{th}^m}$ with N_m^{sp} and I_{th}^m, respectively, and applying the analysis in (11)-(20), $F_{\gamma_{n,k}|\hat{H}_{m,k}^{sp}}(\gamma_{n,k}|\hat{H}_{m,k}^{sp})$ can be developed for the collision probability constraint with 'probabilistic case' of estimation error.

References

[1] T. K. Sarkar, R. Mailloux, A. A. Oliner, M. Salazar-Palma, and D. L. Sengupta, *History of wireless.* John Wiley & Sons, 2006, vol. 177. 1.1

[2] F. Woolley, "International frequency regulation and planning," *EBU Technical Review*, pp. 45–62, 1995. 1.1

[3] H.-H. Chen and M. Guizani, *Next generation wireless systems and networks.* John Wiley & Sons, 2006. 1.2

[4] D. Tse and P. Viswanath, *Fundamentals of wireless communication.* Cambridge University Press, 2005. 1.2

[5] C. Fortuna and M. Mohorcic, "Trends in the development of communication networks: Cognitive networks," *Computer Networks*, vol. 53, no. 9, pp. 1354–1376, 2009. 1.2

[6] Q. H. Mahmoud, "Cognitive networks," *John Wiley& Sons Ltd*, pp. 57–71, 2007. 1.2

[7] J. Heiskala and J. Terry, Ph.D., *OFDM Wireless LANs: A Theoretical and Practical Guide.* Indianapolis, IN, USA: Sams, 2001. 1.3.1

[8] H. Rohling, *OFDM: Concepts for Future Communication Systems*, ser. Signals and communication technology. Springer, 2011. [Online]. Available: http://books.google.co.uk/books?id=r3oD87z4E7UC 1.3.1, 1.3.2

[9] L. Hanzo and T. Keller, *OFDM and MC-CDMA: A Primer.* Wiley, 2007. [Online]. Available: http://books.google.co.uk/books?id=CWmDlCxFpAMC 1.3.1

[10] R. Short, *Ofdm: Theory and Practice.* John Wiley & Sons Canada, Limited, 2010. [Online]. Available: http://books.google.co.uk/books?id=dCi3cQAACAAJ 1.3.1, 1.3.2, 1.3.3

[11] H. Liu and G. Li, *OFDM-Based Broadband Wireless Networks: Design and Optimization.* Wiley, 2005. [Online]. Available: http://books.google.co.uk/books?id=mPkcadmRSvAC 1.3.1

[12] T.-D. Chiueh and P.-Y. Tsai, *OFDM baseband receiver design for wireless communications.* John Wiley & Sons, 2008. 1.3.2

[13] S. Yang, *OFDMA System Analysis and Design*, ser. Artech House telecommunications library. Artech House, 2010. [Online]. Available: http://books.google.co.uk/books?id=TiYxUy7LnRsC 1.3.4, 1.3.4

[14] M. Simon and M. Alouini, *Digital Communication Over Fading Channels.* Wiley-Interscience, 2005. 1.3.5

[15] T. Rappaport, *Wireless Communications: Principles and Practice.* Prentice Hall PTR, 2001. 1.3.5.1

[16] R. Bernhardt, "Macroscopic diversity in frequency reuse radio systems," *Selected Areas in Communications, IEEE Journal on*, vol. 5, no. 5, pp. 862–870, Jun. 1987. 1.3.5.1

[17] R. H. Clarke, "A statistical theory of mobile-radio reception," *Bell Systems Technical Journal*, vol. 47, no. 5, pp. 957–1000, 1968. 1.3.5.1

[18] S. Fischer, S. Kudras, V. Kuhn, and K. Kammeyer, "Analysis of diversity effects for satellite communication systems," in *Global Telecommunications Conference, 2001. GLOBECOM '01. IEEE*, vol. 4, 2001, pp. 2759–2763 vol.4. 1.3.5.1

[19] A. Coulson, A. Williamson, and R. Vaughan, "A statistical basis for lognormal shadowing effects in multipath fading channels," *IEEE Trans. Commun.*, vol. 46, no. 4, pp. 494–502, Apr. 1998. 1.3.5.1

[20] J. Salo, L. Vuokko, H. M. El-Sallabi, and P. Vainikainen, "An additive model as a physical basis for shadow fading," *IEEE Trans. Veh. Technol.*, vol. 56, no. 1, pp. 13–26, Jan. 2007. 1.3.5.1

[21] I. Abou-Faycal, M. Trott, and S. Shamai, "The capacity of discrete-time memoryless rayleigh-fading channels," *IEEE Trans. Inf. Theory*, vol. 47, no. 4, pp. 1290–1301, may 2001. 1.3.5.1

[22] A. Saleh and R. Valenzuela, "A statistical model for indoor multipath propagation," *Selected Areas in Communications, IEEE Journal on*, vol. 5, no. 2, pp. 128–137, feb. 1987. 1.3.5.1

[23] L. Greenstein, D. Michelson, and V. Erceg, "Moment-method estimation of the ricean k-factor," *Communications Letters, IEEE*, vol. 3, no. 6, pp. 175–176, Jun. 1999. 1.3.5.1

[24] C. Tepedelenlioglu, A. Abdi, and G. Giannakis, "The ricean k factor: estimation and performance analysis," *IEEE Trans. Wireless Commun.*, vol. 2, no. 4, pp. 799–810, Jul. 2003. 1.3.5.1

[25] R. Bultitude, S. Mahmoud, and W. Sullivan, "A comparison of indoor radio propagation characteristics at 910 MHz and 1.75 ghz," *Selected Areas in Communications, IEEE Journal on*, vol. 7, no. 1, pp. 20–30, Jan. 1989. 1.3.5.1

[26] P. Shaft, "On the relationship between scintillation index and rician fading," *IEEE Trans. Commun.*, vol. 22, no. 5, pp. 731–732, may 1974. 1.3.5.1

[27] A. Abu-Dayya and N. Beaulieu, "Switched diversity on microcellular ricean channels," *IEEE Trans. Veh. Technol.*, vol. 43, no. 4, pp. 970–976, Nov. 1994. 1.3.5.1

[28] M. Nakagami, "The m-distribution- a general formula of intensity distribution of rapid fading," in *Statistical Methods in Radio Wave Propagation.* OXFORD, UK.: Pergamon Press, 1960, pp. 3–36. 1.3.5.1, 1.3.5.1

[29] L.-L. Yang and L. Hanzo, "Performance of generalized multicarrier DS-CDMA over Nakagami-m fading channels," *IEEE Trans. Commun.*, vol. 50, no. 6, pp. 956–966, Jun. 2002. 1.3.5.1

[30] T. Eng and L. Milstein, "Coherent DS-CDMA performance in Nakagami multipath fading," *IEEE Trans. Commun.*, vol. 43, no. 234, pp. 1134–1143, Apr. 1995. 1.3.5.1

[31] M.-S. Alouini and A. J. Goldsmith, "Adaptive modulation over Nakagami fading channels," *Wireless Personal Communications*, vol. 13, pp. 119–143, 2000. 1.3.5.1

[32] U. Charash, "Reception through Nakagami fading multipath channels with random delays," *IEEE Trans. Commun.*, vol. 27, no. 4, pp. 657–670, Apr. 1979. 1.3.5.1

[33] S. Abbas and A. Sheikh, "A geometric theory of Nakagami fading multipath mobile radio channel with physical interpretations," in *Vehicular Technology Conference, 1996. Mobile Technology for the Human Race., IEEE 46th*, vol. 2, Apr. 1996, pp. 637–641 vol. 2. 1.3.5.1

[34] "Spectrum framework review, a consultation on ofcom's views as to how radio spectrum should be managed," Tech. Rep., Nov. 2004. [Online]. Available: http://stakeholders.ofcom.org.uk/binaries/consultations/sfr/summary/sfr.pdf 1.4

[35] J. Mitola and G. Q. Maguire Jr, "Cognitive radio: making software radios more personal," *Personal Communications, IEEE*, vol. 6, no. 4, pp. 13–18, 1999. 1.4

[36] S. Haykin, "Cognitive radio: brain-empowered wireless communications," *Selected Areas in Communications, IEEE Journal on*, vol. 23, no. 2, pp. 201 – 220, Feb. 2005. 1.4

[37] I. Akyildiz, W. Lee, M. Vuran, and S. Mohanty, "Next generation/dynamic spectrum access/cognitive radio wireless networks: a survey," *Computer Networks*, vol. 50, no. 13, pp. 2127–2159, 2006. 1.4.1.1, 1.4.1.4

[38] A. H. Yucek, T., "A survey of spectrum sensing algorithms for cognitive radio applications," *Communications Surveys Tutorials, IEEE*, vol. 11, no. 1, pp. 116 –130, Quarter 2009. 1.4.1.1

[39] H. J. Zhu Han, Rongfei Fan, "Replacement of spectrum sensing in cognitive radio," *IEEE Trans. Wireless Commun.*, vol. 8, no. 6, pp. 2819 –2826, Jun. 2009. 1.4.1.1

[40] A. Ghasemi and E. Sousa, "Collaborative spectrum sensing for opportunistic access in fading environments," in *New Frontiers in Dynamic Spectrum Access Networks, 2005. DySPAN 2005. 2005 First IEEE International Symposium on*, Nov. 2005, pp. 131 –136. 1.4.1.1

[41] C. Tekin, S. Hong, and W. Stark, "Enhancing cognitive radio dynamic spectrum sensing through adaptive learning," in *Military Communications Conference, 2009. MILCOM 2009. IEEE*, Oct. 2009, pp. 1 –7. 1.4.1.1

[42] Y.-C. Liang, Y. Zeng, E. C. Peh, and A. T. Hoang, "Sensing-throughput tradeoff for cognitive radio networks," *IEEE Trans. Wireless Commun.*, vol. 7, no. 4, pp. 1326–1337, 2008. 1.4.1.1

[43] K. Hamdi and K. Ben Letaief, "Power, sensing time, and throughput tradeoffs in cognitive radio systems: a cross-layer approach," in *Wireless Communications and Networking Conference, 2009. WCNC 2009. IEEE.* IEEE, 2009, pp. 1–5. 1.4.1.1

[44] C.-W. Wang and L.-C. Wang, "Modeling and analysis for proactive-decision spectrum handoff in cognitive radio networks," in *Communications, 2009. ICC '09. IEEE International Conference on*, Jun. 2009, pp. 1 –6. 1.4.1.3

[45] A. Ghasemi and E. Sousa, "Capacity of fading channels under spectrum-sharing constraints," in *Communications, 2006. ICC '06. IEEE International Conference on*, vol. 10, Jun. 2006, pp. 4373–4378. 1.4.1.4

[46] J. S. Srinivasa, S., "How much spectrum sharing is optimal in cognitive radio networks?" *IEEE Trans. Wireless Commun.*, vol. 7, no. 10, pp. 4010 –4018, October 2008. 1.4.1.4

[47] Etkin, R., Parekh, A., and Tse, D., , "Spectrum sharing for unlicensed bands," *Selected Areas in Communications, IEEE Journal on*, vol. 25, no. 3, pp. 517 –528, Apr. 2007. 1.4.1.4

[48] F. Digham, "Joint power and channel allocation for cognitive radios," *Wireless Communications and Networking Conference, 2008. WCNC 2008. IEEE*, pp. 882 –887, Apr. 2008. 1.4.2

[49] M. Vu, N. Devroye, M. Sharif, and V. Tarokh, "Scaling laws of cognitive networks," in *Cognitive Radio Oriented Wireless Networks and Communications, 2007. CrownCom 2007. 2nd International Conference on*, Aug. 2007, pp. 2 –8. 1.4.2

[50] H. Asrslan and S. Yarkan, "Cross-layer adaptation and optimization for cognitive radio," *Cognitive Radio, Software Defined Radio, and Adaptive Wireless Systems*, pp. 421–452, 2007. 1.5

[51] F. Foukalas, V. Gazis, and N. Alonistioti, "Cross-layer design proposals for wireless mobile networks: a survey and taxonomy," *Communications Surveys & Tutorials, IEEE*, vol. 10, no. 1, pp. 70–85, 2008. 1.5

[52] S. Shakkottai, T. Rappaport, and P. Karlsson, "Cross-layer design for wireless networks," *IEEE Commun. Mag.*, vol. 41, no. 10, pp. 74–80, Oct. 2003. (document), 1.5, 1.8

[53] V. Srivastava and M. Motani, "Cross-layer design: a survey and the road ahead," *Communications Magazine, IEEE*, vol. 43, no. 12, pp. 112–119, Dec. 2005. (document), 1.5, 1.8

[54] I. E. Richardson, "The H.264 advanced video compression standard, 2nd ed," p. 346, 2010. 1.7

[55] L. Hanzo, P. Cherriman, and J. Streit, *Video Compression and Communications: From Basics to H.261, H.263, H.264, MPEG4 for DVB and HSDPA-Style Adaptive Turbo-Transceivers*. Wiley, 2007. [Online]. Available: http://books.google.co.uk/books?id=-Ex49cxyvmQC 1.7

[56] J. Woods, *Multidimensional Signal, Image, and Video Processing and Coding*, ser. Academic Press. Academic Press, 2012. [Online]. Available: http://books.google.co.uk/books?id=7xpTOYzhseEC 1.7

[57] H. Wang, L. Kondi, A. Luthra, and S. Ci, *4G Wireless Video Communications*, ser. Wireless Communications and Mobile Computing. Wiley, 2009. [Online]. Available: http://books.google.co.uk/books?id=a0tV8jUqAmQC 1.7

[58] C. Zhu and Y. Li, *Advanced Video Communications over Wireless Networks*. Taylor & Francis, 2013. [Online]. Available: http://books.google.co.uk/books?id=nqcMwoyfQ0UC 1.7, 1.7.1.3

[59] L. Hanzo, H. Haas, S. Imre, D. O'Brien, M. Rupp, and L. Gyongyosi, "Wireless myths, realities, and futures: From 3G/4G to optical and quantum wireless," *Proceedings of the IEEE*, vol. 100, no. Special Centennial Issue, pp. 1853 –1888, 13 2012. 2.1

[60] I. Koffman and V. Roman, "Broadband wireless access solutions based on OFDM access in ieee 802.16," *IEEE Commun. Mag.*, vol. 40, no. 4, pp. 96–103, Apr. 2002. 2.1, 3.1

[61] G. Li and H. Liu, "Downlink radio resource allocation for multi-cell OFDMA system," *IEEE Trans. Wireless Commun.*, vol. 5, no. 12, pp. 3451–3459, Dec. 2006. 2.1, 3.1

[62] X. Zhou, G. Li, D. Li, D. Wang, and A. Soong, "Probabilistic resource allocation for opportunistic spectrum access," *IEEE Trans. Wireless Commun.*, vol. 9, no. 9, pp. 2870–2879, Sep. 2010. 2.1, 3.1, 3.2.1

[63] M. Sternad, T. Svensson, T. Ottosson, A. Ahlen, A. Svensson, and A. Brunstrom, "Towards systems beyond 3G based on adaptive OFDMA transmission," *Proc. IEEE*, vol. 95, no. 12, pp. 2432–2455, Dec. 2007. 2.1, 3.1

[64] G. Bansal, J. Hossain, and V. Bhargava, "Optimal and suboptimal power allocation schemes for OFDM-Based cognitive radio systems," *IEEE Trans. Wireless Commun.*, vol. 7, no. 11, pp. 4710–4718, Nov. 2008. 2.1, 3.1

[65] P. Mitran, L. B. Le, and C. Rosenberg, "Queue-aware resource allocation for downlink OFDMA cognitive radio networks," *IEEE Trans. Wireless Commun.*, vol. 9, no. 10, pp. 3100–3111, Oct. 2010. 2.1, 3.1

[66] H. Suraweera, P. Smith, and M. Shafi, "Capacity limits and performance analysis of cognitive radio with imperfect channel knowledge," *IEEE Trans. Veh. Technol.*, vol. 59, no. 4, pp. 1811–1822, May 2010. 2.1, 2.2.1

[67] Z. Rezki and M.-S. Alouini, "Ergodic capacity of cognitive radio under imperfect channel-state information," *IEEE Trans. Veh. Technol.*, vol. 61, no. 5, pp. 2108–2119, Jun. 2012. 2.1, 2.2.1

[68] N. Mokari, K. Navaie, and M. Khoshkholgh, "Downlink radio resource allocation in OFDMA spectrum sharing environment with partial channel state information," *IEEE Trans. Wireless Commun.*, vol. 10, no. 10, pp. 3482–3495, Oct. 2011. 2.1, 4.6

[69] C. Zarakovitis, Q. Ni, D. Skordoulis, and M. Hadjinicolaou, "Power-efficient cross-layer design for OFDMA systems with heterogeneous QoS, imperfect CSI, and outage considerations," *IEEE Trans. Veh. Technol.*, vol. 61, no. 2, pp. 781–798, Feb. 2012. 2.2.1

[70] K. Nehra and M. Shikh-Bahaei, "Spectral efficiency of adaptive MQAM/OFDM systems with CFO over fading channels," *IEEE Trans. Veh. Technol.*, vol. 60, no. 3, pp. 1240–1247, Mar. 2011. 2.2.1, 2.2.3

[71] R. Zhang, S. Cui, and Y.-C. Liang, "On ergodic sum capacity of fading cognitive multiple-access and broadcast channels," *IEEE Trans. Inf. Theory*, vol. 55, no. 11, pp. 5161–5178, Nov. 2009. 2.2.1, 3.2.1

[72] X. Gong, S. Vorobyov, and C. Tellambura, "Optimal bandwidth and power allocation for sum ergodic capacity under fading channels in cognitive radio networks," *IEEE Trans. Signal Process.*, vol. 59, no. 4, pp. 1814–1826, Apr. 2011. 2.2.1

[73] K.-S. Ahn and R. Heath, "Performance analysis of maximum ratio combining with imperfect channel estimation in the presence of cochannel interferences," *IEEE Trans. Wireless Commun.*, vol. 8, no. 3, pp. 1080–1085, Mar. 2009. 2.2.1

[74] H. Zhang, L. Venturino, N. Prasad, P. Li, S. Rangarajan, and X. Wang, "Weighted sum-rate maximization in multi-cell networks via coordinated scheduling and discrete power control," *IEEE J. Sel. Areas Commun.*, vol. 29, no. 6, pp. 1214–1224, Jun. 2011. 2.2.2

[75] J. Luo, R. Yates, and P. Spasojevic, "Service outage based power and rate allocation for parallel fading channels," *IEEE Trans. Inf. Theory*, vol. 51, no. 7, pp. 2594–2611, Jul. 2005. 2.3.2

[76] S. Boyd and L. Vandenberghe, *Convex Optimization*. New York, NY, USA: Cambridge University Press, 2004. 2.3.2

[77] S. Gabler and C. Wolff, "A quick and easy approximation to the distribution of a sum of weighted Chi-square variables," *Statistical Papers*, vol. 28, pp. 317–325, 1987, 10.1007/BF02932611. 2.5, 4.4.1

[78] A. Castaño-Martínez and F. López-Blázquez, "Distribution of a sum of weighted noncentral Chi-square variables," *TEST*, vol. 14, pp. 397–415, 2005, 10.1007/BF02595410. 2.5, 4.4.1

[79] D. R. Cox and N. Reid, "Approximations to noncentral distributions," *The Canadian Journal of Statistics / La Revue Canadienne de Statistique*, vol. 15, no. 2, pp. pp. 105–114, 1987. 2.5, 2.5, 4.4.1

[80] I. Daubechies, "Time-frequency localization operators: a geometric phase space approach," *IEEE Trans. Inf. Theory*, vol. 34, no. 4, pp. 605–612, 1988. 2.5

[81] M. Fitch, M. Nekovee, S. Kawade, K. Briggs, and R. MacKenzie, "Wireless service provision in tv white space with cognitive radio technology: A telecom operator's perspective and experience," *IEEE Commun. Mag.*, vol. 49, no. 3, pp. 64–73, Mar. 2011. 3.1

[82] H. Karimi, "Geolocation databases for white space devices in the UHF TV bands: Specification of maximum permitted emission levels," in *New Frontiers in Dynamic Spectrum Access Networks (DySPAN), 2011 IEEE Symposium on*, May 2011, pp. 443–454. 3.1

[83] I. Akyildiz, W.-Y. Lee, M. C. Vuran, and S. Mohanty, "A survey on spectrum management in cognitive radio networks," *IEEE Commun. Mag.*, vol. 46, no. 4, pp. 40–48, Apr. 2008. 3.1

[84] A. Ghasemi and E. Sousa, "Interference aggregation in spectrum-sensing cognitive wireless networks," *Selected Topics in Signal Processing, IEEE Journal of*, vol. 2, no. 1, pp. 41 –56, Feb. 2008. 3.1

[85] S. Boyd, J. Frye, M. Pursley, and T. Royster, "Spectrum monitoring during reception in dynamic spectrum access cognitive radio networks," *IEEE Trans. Commun.*, vol. 60, no. 2, pp. 547–558, Feb. 2012. 3.1

[86] P. Cheraghi, Y. Ma, R. Tafazolli, and Z. Lu, "Cluster-based differential energy detection for spectrum sensing in multi-carrier systems," *IEEE Trans. Signal Process.*, vol. 60, no. 12, pp. 6450–6464, Dec. 2012. 3.1

[87] S. Akin and M. Gursoy, "Performance analysis of cognitive radio systems under qos constraints and channel uncertainty," *IEEE Trans. Wireless Commun.*, vol. 10, no. 9, pp. 2883–2895, Sep. 2011. 3.1

[88] H. Mu and J. Tugnait, "Joint soft-decision cooperative spectrum sensing and power control in multiband cognitive radios," *IEEE Trans. Signal Process.*, vol. 60, no. 10, pp. 5334–5346, Oct. 2012. 3.1

[89] A. Shojaeifard, F. Zarringhalam, and M. Shikh-Bahaei, "Joint physical layer and data link layer optimization of CDMA-Based networks," *IEEE Trans. Wireless Commun.*, vol. 10, no. 10, pp. 3278–3287, Oct. 2011. 3.2.1

[90] L. Zhang, Y.-C. Liang, and Y. Xin, "Joint beamforming and power allocation for multiple access channels in cognitive radio networks," *IEEE J. Sel. Areas Commun.*, vol. 26, no. 1, pp. 38–51, Jan. 2008. 3.2.1

[91] Y.-C. Liang, Y. Zeng, E. Peh, and A. T. Hoang, "Sensing-throughput tradeoff for cognitive radio networks," *IEEE Trans. Wireless Commun.*, vol. 7, no. 4, pp. 1326–1337, Apr. 2008. 3.2.2

[92] S. Stotas and A. Nallanathan, "Optimal sensing time and power allocation in multiband cognitive radio networks," *IEEE Trans. Commun.*, vol. 59, no. 1, pp. 226–235, Jan. 2011. 3.2.2

[93] A.-E. M. Taha, N. A. Ali, and H. S. Hassanein, *LTE, LTE-Advanced and WiMAX: Towards IMT-advanced Networks.* John Wiley & Sons, 2011. 4.1

[94] H. Bobarshad, M. van der Schaar, and M. Shikh-Bahaei, "A low-complexity analytical modeling for cross-layer adaptive error protection in video over WLAN," *IEEE Trans. Multimedia*, vol. 12, no. 5, pp. 427–438, Aug. 2010. 4.1

[95] L. Hanzo, P. J. Cherriman, and J. Streit, *Voice Compression and Communications*. John Wiley and Sons, Ltd, 2007. 4.1

[96] D. Ngo, C. Tellambura, and H. Nguyen, "Resource allocation for OFDMA-Based cognitive radio multicast networks with primary user activity consideration," *IEEE Trans. Veh. Technol.*, vol. 59, no. 4, pp. 1668–1679, May 2010. 4.1

[97] R. Wang, V. Lau, L. Lv, and B. Chen, "Joint cross-layer scheduling and spectrum sensing for OFDMA cognitive radio systems," *IEEE Trans. Wireless Commun.*, vol. 8, no. 5, pp. 2410–2416, May 2009. 4.1

[98] M. Dashti, P. Azmi, and K. Navaie, "Radio resource allocation for orthogonal frequency division multiple access-based underlay cognitive radio networks utilising weighted ergodic rates," *Communications, IET*, vol. 6, no. 16, pp. 2543–2552, 6 2012. 4.1

[99] G. Bansal, M. Hossain, and V. Bhargava, "Optimal and suboptimal power allocation schemes for OFDM-Based cognitive radio systems," *IEEE Trans. Wireless Commun.*, vol. 7, no. 11, pp. 4710–4718, Nov. 2008. 4.1

[100] C. Tan, T. Chuah, and S. Tan, "Fair subcarrier and power allocation for multiuser orthogonal frequency-division multiple access cognitive radio networks using a colonel blotto game," *Communications, IET*, vol. 5, no. 11, pp. 1607–1618, 22 2011. 4.1

[101] S. Wang, "Efficient resource allocation algorithm for cognitive OFDM systems," *IEEE Commun. Lett.*, vol. 14, no. 8, pp. 725–727, Aug. 2010. 4.1

[102] Y. Zhang and C. Leung, "Resource allocation for non-real-time services in OFDM-Based cognitive radio systems," *IEEE Commun. Lett.*, vol. 13, no. 1, pp. 16–18, Jan. 2009. 4.1

[103] S. Srinivasa and S. Jafar, "How much spectrum sharing is optimal in cognitive radio networks?" *IEEE Trans. Wireless Commun.*, vol. 7, no. 10, pp. 4010–4018, Oct. 2008. 4.1

[104] X. Zhou, G. Li, D. Li, D. Wang, and A. Soong, "Probabilistic resource allocation for opportunistic spectrum access," *IEEE Trans. Wireless Commun.*, vol. 9, no. 9, pp. 2870–2879, Sep. 2010. 4.1

[105] I. Atta-ur Rahman and A. Malik, "Adaptive resource allocation in OFDM systems using GA and fuzzy rule base system," *World Applied Sciences Journal*, vol. 18, no. 6, pp. 836–844, 2012. 4.1

[106] J. Huang, V. Subramanian, R. Agrawal, and R. Berry, "Downlink scheduling and resource allocation for OFDM systems," *IEEE Trans. Wireless Commun.*, vol. 8, no. 1, pp. 288–296, Jan. 2009. 4.1

[107] Z. Yang and X. Wang, "Scalable video broadcast over downlink MIMO-OFDM systems," *IEEE Trans. Circuits Syst. Video Technol.*, vol. 23, no. 2, pp. 212–223, Feb. 2013. 4.1

[108] Y. Zhang and C. Leung, "Cross-layer resource allocation for mixed services in multiuser OFDMA-Based cognitive radio systems," *IEEE Trans. Veh. Technol.*, vol. 58, no. 8, pp. 4605–4619, Oct. 2009. 4.1, 4.6

[109] Z. Yang and X. Wang, "Scalable video broadcast over downlink MIMO OFDM systems," *IEEE Trans. Circuits Syst. Video Technol.*, vol. 23, no. 2, pp. 212–223, Feb. 2013. 4.1

[110] M. Bocus, J. Coon, C. Canagarajah, J. McGeehan, Armour, and A. Doufexi, "Resource allocation for OFDMA-Based cognitive radio networks with application to h.264 scalable video transmission," *EURASIP Journal on Wireless Communications and Networking*, vol. 2011, no. 1, p. 245673, 2011. 4.1

[111] Z. Rezki and M.-S. Alouini, "Ergodic capacity of cognitive radio under imperfect channel-state information," *IEEE Trans. Veh. Technol.*, vol. 61, no. 5, pp. 2108–2119, Jun. 2012. 4.1

[112] H. Suraweera, P. Smith, and M. Shafi, "Capacity limits and performance analysis of cognitive radio with imperfect channel knowledge," *IEEE Trans. Veh. Technol.*, vol. 59, no. 4, pp. 1811–1822, May 2010. 4.1

[113] G.-M. Su, Z. Han, M. Wu, and K. Liu, "A scalable multiuser framework for video over OFDM networks: Fairness and efficiency," *IEEE Trans. Circuits Syst. Video Technol.*, vol. 16, no. 10, pp. 1217–1231, Oct. 2006. 4.2.1, 4.1, 4.6

[114] Y.-K. Wang and R. Even, "FRTP payload format for H.264 video," *IEEE Commun. Lett.*, May 2011. 4.3

[115] *JSVM Software Manual*, JSVM. [Online]. Available: ube.ege.edu.tr/~boztok/JSVM/SoftwareManual.pdf 4.3

[116] H. Solomon and M. A. Stephens, "Distribution of a sum of weighted Chi-square variables," *Journal of the American Statistical Association*, vol. 72, no. 360, pp. pp. 881–885, 1977. 4.4.1

[117] H. Alzer, "On some inequalities for the incomplete Gamma function," *Math. Comp*, vol. 66, pp. 771–778, 1997. A, A, A